ESD-TR-66-429

FIRST QUARTERLY TECHNICAL REPORT

ON

LARGE APERTURE SEISMIC ARRAYS

CONTRACT AF 19(628)-5981

SUBMITTED TO
ELECTRONICS SYSTEMS DIVISION (ESL)
UNITED STATES AIR FORCE

BY
GENERAL ATRONICS CORPORATION
JULY 1966

SPONSORED BY
ADVANCED RESEARCH PROJECTS AGENCY
ARPA ORDER NO. 800

FIRST QUARTERLY TECHNICAL REPORT

ON

LARGE APERTURE SEISMIC ARRAYS

CONTRACT AF 19(628)-5981

SUBMITTED TO
ELECTRONICS SYSTEMS DIVISION (ESL)
UNITED STATES AIR FORCE

BY
GENERAL ATRONICS CORPORATION
JULY 1966

SPONSORED BY
ADVANCED RESEARCH PROJECTS AGENCY
ARPA ORDER NO. 800

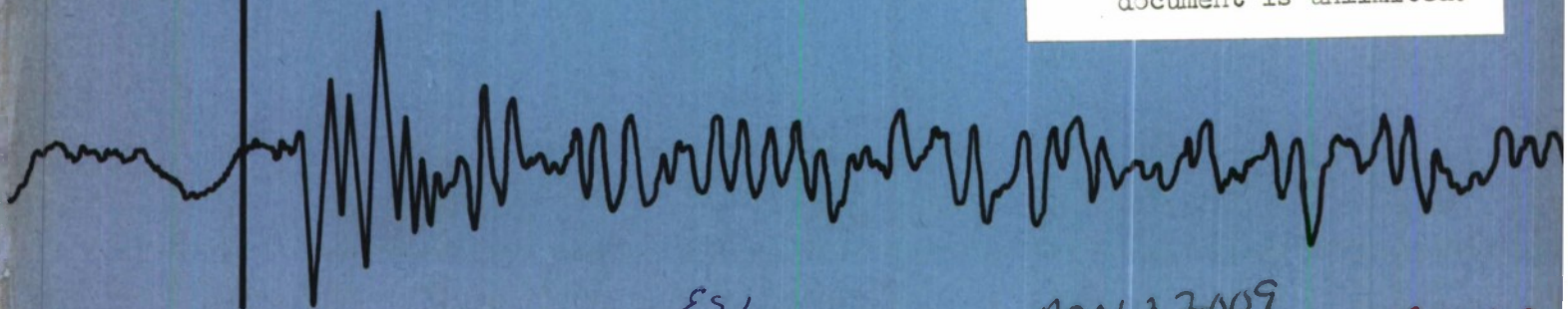

First Quarterly Technical Report
Contract AF 19(628)-5981

LARGE APERTURE SEISMIC ARRAYS

Sponsored by:
Advanced Research Projects Agency
ARPA Order No. 800

GENERAL ATRONICS CORPORATION

5 July 1966

Security Classification

DOCUMENT CONTROL DATA - R&D

(Security classification of title, body of abstract and indexing annotation must be entered when the overall report is classified)

1. ORIGINATING ACTIVITY (Corporate author) General Atronics Corporation	2a. REPORT SECURITY CLASSIFICATION Unclassified 2b GROUP

3. REPORT TITLE
First Quarterly Technical Report on Large Aperture Seismic Arrays

4. DESCRIPTIVE NOTES (Type of report and inclusive dates)

5. AUTHOR(S) (Last name, first name, initial)

6. REPORT DATE	7a TOTAL NO. OF PAGES	7b NO. OF REFS
July 1966	73	14

8a. CONTRACT OR GRANT NO.	9a. ORIGINATOR'S REPORT NUMBER(S)
AF19(628)-5981	1531-2033-7
b. PROJECT NO.	
c. ARPA ORDER NO. 800	9b. OTHER REPORT NO(S) (Any other numbers that may be assigned this report)
d.	ESD-TR-66-489

10. AVAILABILITY/LIMITATION NOTICES
This document is unlimited

11. SUPPLEMENTARY NOTES	12. SPONSORING MILITARY ACTIVITY
	Advanced Research Projects Agency

13. ABSTRACT

The work to date has dealt with the effect of seismometer placement on array sidelobes, the performance to be expected with arrays using one bit signals, from the seismometer, the coherence of signals, noise, and coda across LASA, P-coda correlation as a discriminant, and the frequency dependence of attenuation in the earth's upper mantle.

A randomized array, as opposed to one with clustered elements has shown isdelobes some 14 dB lower than those of the current LASA design. The one bit array (DIMUS) has shown a processing gain of 2 dB less than that for an analog array, as predicted by theory. The same array with the addition of a single analog channel offers good possibilities of proving as useful in identification as a conventional array.

Main P, and noise correlations observed across LASA Montanna from LONGSHOT showed signal correlation to be high, 0.97, and noise quite low for spacings equal to those of the clusters. P-coda correlation decreased to a value near zero for seismometer spacings on the order of 150 km.

Study of P-coda correlation coefficients for widely spaced seismometers fell into two distinct distributions with an equivalent S/N of 16 DB.

A method was developed for estimating the Q of the upper mantle using the P and pP phases of deep earthquakes. First test of the method indicate an average Q of approximately 200 for the upper 500 Km of the mantle in the Fiji Islands Region.

DD FORM 1 JAN 64 1473

Security Classification

SYNOPSIS

This report covers the work performed during the first quarter of Contract AF19(628)-5981, Large Aperture Seismic Arrays. The work to date has dealt with the effect of seismometer placement on array sidelobes, the performance to be expected with arrays using one bit signals from the seismometers, the coherence of signals, noise, and coda across LASA, P-coda correlation as a discriminant and the frequency dependence of attenuation in the earth's upper mantle.

A randomized array, as opposed to one with clustered elements, has shown sidelobes some 14 dB lower than those of the current LASA design. The one bit array (DIMUS) has shown a processing gain of 2 dB less than that for an analog array, as predicted by theory. The same array with the addition of a single analog channel offers good possibilities of proving as useful in identification as a conventional array.

Main P, and noise correlations observed across LASA Montanna from LONGSHOT showed signal correlation to be high, 0.97, and noise quite low for spacings equal to those of the clusters. P-coda correlation decreased to a value near zero for seismometer spacings on the order of 150 km.

Study of P-coda correlation coefficients for widely spaced seismometers fell into two distinct distributions with an equivalent S/N of 16 dB.

A method was developed for estimating the Q of the upper mantle using the P and pP phases of deep earthquakes. First test of the method indicate an average Q of approximately 200 for the upper 500 km of the mantle in the Fiji Islands Region.

This research was sponsored by the Advanced Research Projects Agency and was monitored by ESD (ESL) under Contract Number AF19(628)-5981.

GENERAL ATRONICS CORPORATION

CONTENTS

FIGURES

FIGURES

FIGURES

Section I Introduction

This is the first quarterly technical report on Contract AF19 (628)-5961, Large Aperture Seismic Arrays. The subject matter of this program represents extensions to earlier work in connection with the systems aspects of the detection and identification of underground explosions performed under Contracts SD 251 and SD 283. Work on the current program deals with five general topics:

1) Array Theory
2) Enhancement of pP in coda
3) Application of linear discriminant analysis to short range discriminants
4) High frequency content of seismograms
5) Utility of signal processing against tests conducted so as to resemble or be masked by natural events.

Included in the first topic are not only theoretical determination of beam properties, but also measurements of signal and noise properties which affect beam formation.

Work during this first quarter was concentrated on the first and fourth topics, with most emphasis placed on the first. Here the effects of the distributions of sensors on array performance for teleseismic signals was considered - particularly with respect to the possibilities of control of array sidelobes. Also studied were the correlation of signals, noise, and P-coda with distance in so far as they would affect performance of arrays. An offshoot of this work was the discovery that the zero offset coda correlation coefficient is a potentially good discriminant for separation of shallow earthquakes and underground explosions. Finally, investigation was made of the effects of array performance when only the zero crossings of the individual instrument outputs is retained. Here, potentially large savings in data storage and transmission equipment may be realizable. Simpler signal processing equipment may also be possible where these simpler representations of the signals can be used. Moreover, it may be

possible to avoid clustering of seismometers - thereby improving the sidelobe characterisitcs of arrays, if it is possible to use hard limited signals from the individual seismometers. To date, this investigation shows promise.

Work on the high frequency aspect of seismic signals has been limited to development of a method of determining attenuation in the upper mantle. Results of further work with this method should enable choice of those sites particularly suited to reception of high frequency signals, should they exist.

Section II Beam Theory

Section II-A DERIVATION OF THE DIMENSIONS OF THE TELESEISMIC BEAM OF A LARGE APERTURE ARRAY

In earlier reports a presentation of teleseismic beam theory was given.[1,2] Among the subjects discussed were the cross-sectional properties of a teleseismic beam, the depth of field of the array and a comparison of array properties for several seismic phases. Given also were a radial pattern showing side lobes from about 40° to 100° and the effects upon the sidelobe structure of a transient waveform.

Omitted at that time were the derivations of the three dimensions of a teleseismic beam. These derivations are the subject of this section of the report.

Figure 132 shows an array located at the pole of a spherical earth. Two perpendicular meridians are drawn. The beam is focussed at point P which is located on one of the meridians at latitude $\pi/2 - \Delta_0$. This means that the elements in the array have time delays built into them which exactly correct for the differential travel times from P to the array elements. The meridian containing P is called the radial meridian. The other meridian is called the transverse meridian.

Shown also is a distorted ellipse containing P. This ellipse is an array gain contour. The radial extent of the beam is twice PR, the size of the ellipse on the radial meridian. The transverse extent of the beam is twice PT, the size of the ellipse on the latitude line containing P.

This constant gain contour is the intersection of a distorted constant gain ellipsoid with the surface. The "vertical" axis is along the seismic path. The depth of field of the array is twice PZ, the extent of the beam from the focal point to the constant gain contour along the seismic ray path.

For a surface focus half of the distance covered by the depth of field is outside the earth and therefore not pertinent. Thus the depth of field could be very sensibly defined as the distance PZ, rather than twice it. However, for deep focal points the alternate argument would prevail. For generality, therefore, the depth of field is taken as twice PZ.*

Parameters

τ = dominant period of the seismic signal (sec)

γ_t = transverse extent of the array (radians)

γ_r = radial extent of the array (radians)

η = aperture efficiency

θ_t = transverse extent of beam within 3 db contour (radians)

θ_r = radial extent of beam within 3 db contour (radians)

Δx = transverse extent of the beam within 3 db contour (km)

$$= \frac{2 \times 10^4 \theta_t}{\pi}$$

Δy = radial extent of the beam within 3 db contour (km)

$$= \frac{2 \times 10^4 \theta_t}{\pi}$$

Δh = 3 db depth of field (km)

T = travel time (sec)

Δ = great circle distance variable (radians)

Δ_o = value of Δ from array center to beam focal point (radians)

h = depth variable (km)

h_o = depth of focal point (km)

$$T_\Delta = \left.\frac{\partial T}{\partial \Delta}\right|_{\Delta_o} \quad \text{(sec/rad)}$$

.....

*The above four paragraphs are quoted from Reference 1, pp. 140-141.

$$T_{\Delta\Delta} = \left.\frac{\partial^2 T}{\partial \Delta^2}\right|_{\Delta_o} \qquad (\text{sec/rad}^2)$$

$$T_{h\Delta} = \left.\frac{\partial^2 T}{\partial \Delta \partial h}\right|_{\Delta_o, h_o} \qquad (\text{sec/rad km})$$

Summary

$$\theta_t = \frac{\tau \sin\Delta_o}{\gamma_t \eta T_\Delta} \quad (\text{rad}) \tag{9}$$

$$\theta_r = \frac{\tau}{\gamma_r \eta T_{\Delta\Delta}} \quad (\text{rad}) \tag{13}$$

$$\Delta h = \frac{\tau}{\gamma_r \eta T_{h\Delta}} \quad (\text{km}) \tag{15}$$

Dependence of Beam Dimensions Upon Array Dimensions

The width of the main lobe of the radiation pattern in any plane containing the beam axis is dictated by the length of the projection of the array onto the plane. By analogy with the case of the homogeneous medium, imagine that the beam path shown in Figure 1 is straightened so that the beam cross-section to be derived (containing P, R and T) falls in the plane of the equator. Then from the previous statement it may be seen that the transverse extent in the beam $2\overline{PT}$ is dictated by the transverse size of the array $2\overline{OA}$, which is the extent of the array along the transverse meridian. Similarly, the radial size of the array, $2\overline{OB}$, dictates the radial dimension of the beam $2\overline{PR}$. Less obvious is the fact that the radial extent of the array also dictates the depth of field, $2\overline{PZ}$.

Transverse Beamwidth

Figure 2 shows the pertinent geometry. The angular distance Δ between point A, an angular distance γ from array center in the transverse direction, and point Q, an angular distance θ from beam axis along the transverse dimension of the beam cross-section, is given by

$$\cos\Delta = \cos\alpha\cos\beta\cos\ell + \sin\alpha\sin\beta$$

$$= \sin\gamma\sin\Delta_o\sin\theta + \cos\gamma\cos\Delta. \qquad (1)$$

α and β are the latitudes of array point A and beam point Q. ℓ is the difference in longitude. Δ_o is the distance from array center 0 to beam center P.

Subtraction of $\cos\Delta_o$ from both sides gives

$$\cos\Delta-\cos\Delta_o = \sin\gamma\sin\Delta_o\sin\theta - \cos\Delta_o(1-\cos\gamma) \qquad (2)$$

The difference of two cosines where the angular difference is small is well approximated by

$$\cos\Delta-\cos\Delta_o \simeq \sin\Delta_o\cdot\delta\Delta \qquad (3)$$

from which

$$\delta\Delta \simeq \sin\gamma\sin\theta - \mathrm{ctn}\Delta_o(1-\cos\gamma) \qquad (4)$$

(4) represents the differential distance between array center to beam center (Δ_o) and the distance from point A in the array to point Q in the beam (Δ). The corresponding differential arrival time is

$$\delta T = \delta\Delta \frac{\partial T}{\partial \Delta} \qquad (5)$$

where $\partial T/\partial\Delta$ is the first partial derivative of travel time with respect to distance. If the outputs of the seismometers at all points of the array were added simultaneously, signals arriving from Q would be separated in time by δT.

To form a beam focussed at P it is necessary to add (or subtract) a time delay at each array element equal and opposite

to (5), so that the seismic energy from P would appear simultaneously at the output of each array element. The correction is exactly the second term in (4), since the first term is zero for $\theta=0$. This correction is a function only of the focal distance Δ_o and the transverse distance λ of the seismometer from the array center. It is thus a permissable correction which may be built into a beamforming network. Assuming that this static correction is made, the corrected differential distance becomes

$$\delta\Delta = \sin\gamma\sin\theta \qquad (6)$$

Combining (5) and (6), and replacing the sine by the angle, yields the very simple first order residual differential time delay after correction

$$\delta T \simeq \gamma\theta \left.\frac{\partial T}{\partial \Delta}\right|_{\Delta_o} ; \quad \gamma,\theta<1/2 \qquad (7)$$

Let τ be the dominant period of the seismic signal. Define the transverse beamwidth θ_t as the range in θ over which δT varies from $+\tau/4$ to $-\tau/4$. This definition is consistent with the usual beamwidth definition of a uniformly illuminated array. The first step is (8) in which the notation for the partial derivative has been changed to that given in the glossary.

$$\tilde{\theta}_t \simeq \frac{\tau}{2\gamma T_\Delta} \qquad (8)$$

(8) gives the transverse extent of the beam in angular longitude units along latitude β. To convert this quantity to the distance or angular measure on the surface of the earth, (8) must be multiplied by $\sin\Delta_o$. Two other alterations to (8) are worth making. First, the quantity 2γ in the denominator may be identified with the transverse extent of the array, for which the simpler quantity γ_t is substituted. Secondly, the beamwidth will normally be larger than (8) due either to amplitude weighting or spatial taper in the aperture, normally dictated by sidelobe tolerance or by economics. This factor is usually identified

with aperture efficiency η, a quantity typically on the order of 2/3 to 3/4. The final expression is

$$\theta_t \simeq \frac{\tau \sin\Delta_o}{\gamma_t \eta T_\Delta} \quad \text{(rad)} \tag{9}$$

All angles are in radians and all time quantities are in seconds.

Radial Beamwidth

Figure 3 shows the relevant geometry. A point in the array is shown a distance γ from array center along the radial meridian. The axis of the seismic beam is shown as a solid line. The focal point of the beam is a distance h_o below the surface of the earth. A point in the radial pattern of the beam a distance θ from the focal point is shown. The great circle distances to the array center from this point and from the focal point are $\Delta_o-\theta$ and Δ_o, respectively. Let $T(\Delta_o,h_o)$ be the travel time from array center to the focal point Δ_o,h_o of the beam. Let $T(\Delta_o-\gamma,h_o)$ be the travel time from the point in the array, which is a radial distance γ from the array center, to the focal point. The difference is exactly the static correction for the seismometer at distance γ when the array is focussed at Δ_o,h_o. This quantity is (10).

$$\begin{aligned}\delta T(\gamma,\Delta_o,h_o) &= T(\Delta_o,h_o) - T(\Delta_o-\gamma,h_o) \\ &\simeq \gamma \left.\frac{\partial T}{\partial \Delta}\right|_{\Delta_o,h_o}\end{aligned} \tag{10}$$

For a point in the beam a distance θ from beam axis along the radial direction, the differential travel time is

$$\delta T(\gamma,\Delta_o-\theta,h_o) = T(\Delta_o-\theta,h_o) - T(\Delta_o-\gamma-\theta,h_o) \tag{11}$$

A large portion of the differential travel time, however, is removed by delay correction (10). Thus the residual differential travel time is (11)-(10):

$$\delta T(\gamma,\Delta_o-\theta,h_o) = T(\Delta_o-\theta,h_o) - T(\Delta_o-\gamma-\theta,h_o) - \gamma \left.\frac{\partial T}{\partial \Delta}\right|_{\Delta_o,h_o}$$

$$= \gamma \left.\frac{\partial T}{\partial \Delta}\right|_{\Delta_o,h_o} - \gamma \left.\frac{\partial T}{\partial \Delta}\right|_{\Delta_o,h_o}$$

$$\simeq \gamma\theta \left.\frac{\partial^2 T}{\partial \Delta^2}\right|_{\Delta_o,h_o} \qquad (12)$$

Again, identifying the radial beamwidth θ_r with that range in beam angle θ for which the uncorrected differential travel time varies by $\tau/2$, identifying 2γ as the radial extent of the array γ_r, and introducing the aperture efficiency factor η, gives the radial beamwidth.

$$\theta_r \simeq \frac{\tau}{\gamma_r \eta T_{\Delta\Delta}} \quad \text{(rad)} \qquad (13)$$

Depth of Field

The geometry of Figure 3 suffices for this derivation. The residual differential travel time after delay correction (10) is

$$\delta T(\gamma,\Delta_o,h) \simeq T(\Delta_o,h) - T(\Delta_o-\gamma,h) - \gamma \left.\frac{\partial T}{\partial \Delta}\right|_{\Delta_o,h_o}$$

$$\simeq \gamma \left.\frac{\partial T}{\partial \Delta}\right|_{\Delta_o,h} - \gamma \left.\frac{\partial T}{\partial \Delta}\right|_{\Delta_o,h_o}$$

$$\simeq \gamma(h-h_o) \left.\frac{\partial^2 T}{\partial \Delta \partial h}\right|_{\Delta_o,h_o} \qquad (14)$$

Folowing the earlier procedure, the variation in depth around the focal depth h_o over which the residual differential travel time varies by 1/2 the dominant period of the seismic event is taken as the depth of field. Thus, the depth of field due to a radial array of length γ_r having aperture efficiency η is

$$\Delta h \simeq \frac{\tau}{\gamma_r \eta T_{h\Delta}} \quad \text{(km)} \tag{15}$$

The derivation of (15) involved only the radial extent of the array. Although it is not immediately obvious it is only the radial length which has significant influence upon the depth of field. Hence it is adequate to calculate depth of field in terms of the radial extent only.

To demonstrate this fact attention is called to (14). The quantity γ in that expression represents the differential distance between a point in the beam and the two array points along the radial direction in the array. The generalized statement equivalent to (14) is as follows: given any two points in the array γ in (14) is replaced by the distance between a point in the beam and the two array points. In particular, if the array points are on the transverse meridian, it is necessary to return to (4), evaluated for $\theta = 0$. Thus the differential distance

$$\delta\Delta = \text{ctn}\Delta_o(1-\cos\gamma) \tag{16}$$

Since $\gamma << 1$

$$\delta\Delta \simeq (\gamma^2/2)\ \text{ctn}\Delta_o \tag{17}$$

the transverse equivalent of (14) becomes

$$\delta T_\theta(\gamma, \Delta_o, h) = \frac{\gamma^2}{2}\ \text{ctn}\Delta_o(h-h_o)T_{h\Delta} \tag{18}$$

Identifying $2\gamma = \gamma_\theta$ = transverse extent of the array, and following the same procedure as before, the depth of field due to the transverse extent is

$$\Delta h_\theta = \frac{4\tau\ \tan\Delta_o}{\gamma_\theta^2 \eta T_{h\Delta}} \tag{19}$$

If the array is symmetrical, such that $\gamma_\theta = \gamma_r$, the depth of field due to the transverse extent is greater than that due to the radial extent by the ratio of (19) to (15), or

$$\frac{\Delta h_\theta}{\Delta h_r} = \frac{4\tan\Delta_o}{\gamma_r} >> 1 \tag{20}$$

Thus the depth of field of the array is dictated by its radial size.

As an example consider a 200 km symmetrical aperture focussed at $\Delta_o = 70^o$, an aperture efficiency of 3/4 and a dominant seismic period of one second. The depth of field due to the radial dimension is 3060 km. If the array were collapsed to a line array in the transverse direction, the depth of field would increase to more than 10^6 km. Even for very large arrays and shorter ranges the focal point remains in the far field. Thus the transverse extent of the array does not measurably contribute to its depth of field.

The three beam dimensions, (9), (13), and (15), are plotted in Figure 4 for the P-wave. This figure is taken from Reference 1, Figure 2. Travel time data are from Jeffreys and Bullen[3]. In the figure Δ is the independent variable. The dependent variable contains the beam size, the effective array size $\gamma\eta$ and the dominant period τ. For convenience the vertical scale is in terms of km degrees rather than square radians. Its units are km deg/sec. To obtain beam size in km multiply the ordinate by the dominant period in seconds and divide by the effective array size in degrees. For a one degree array and one second instruments, the vertical scale gives the beam dimensions directly in km. The depth of field curve pertains to a surface focus, $h_o = 0$. Because of the manner in which the depth of field is defined the 3 dB contour extends below the surface only to one-half the depth of field. Corresponding curves for any other seismic phase may be made by using the travel time derivatives for that phase.

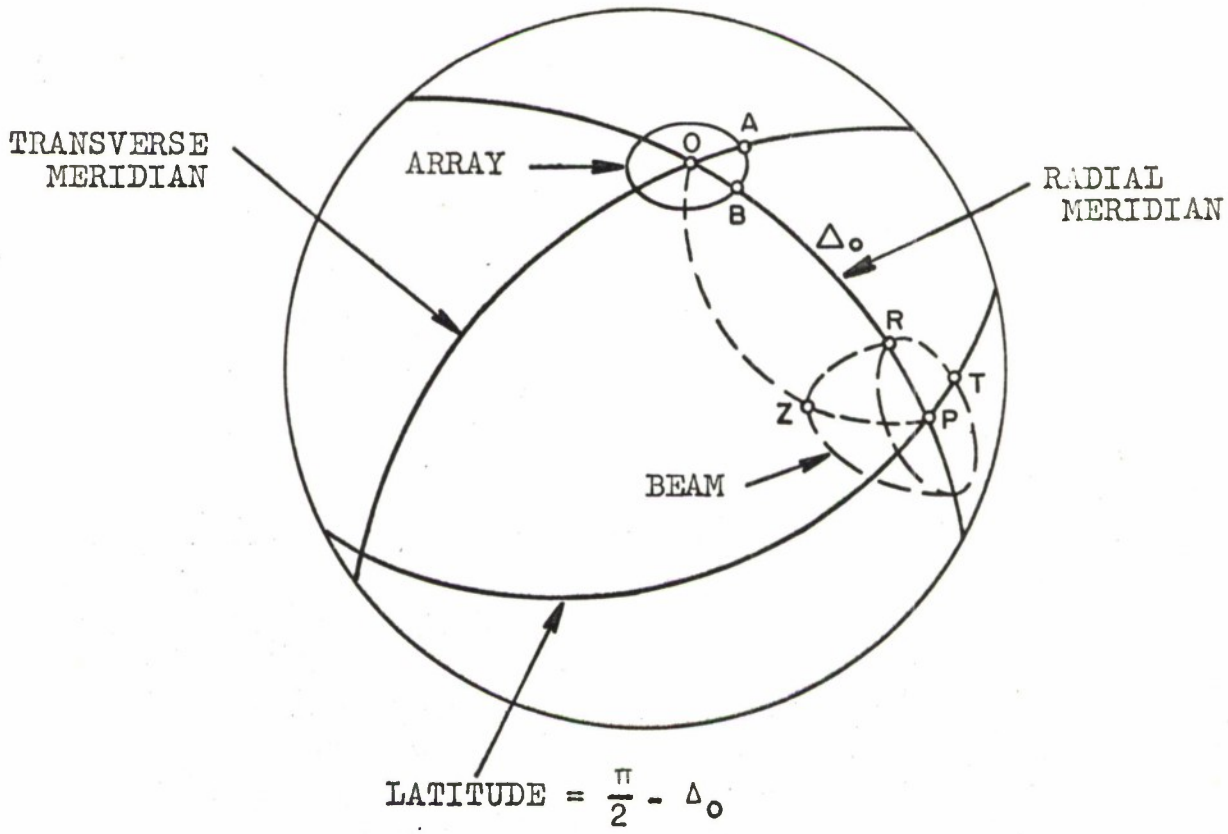

FIGURE 1
GEOMETRY OF TELESEISMIC ARRAY AND BEAM

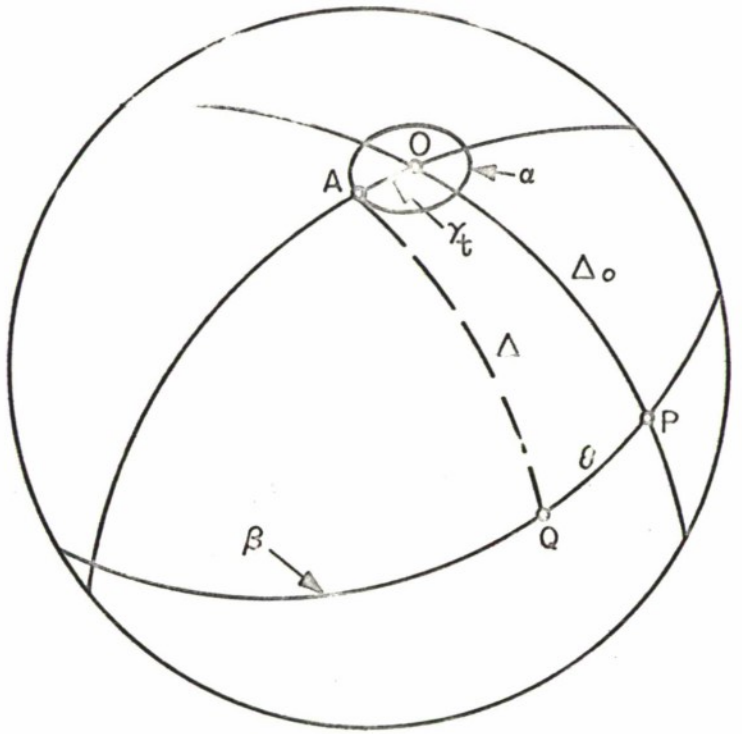

TRANSVERSE

$$\theta_t \approx \frac{\tau \sin \Delta_o}{2\gamma_t T_\Delta}$$

FIGURE 2
TRANSVERSE ARRAY GEOMETRY

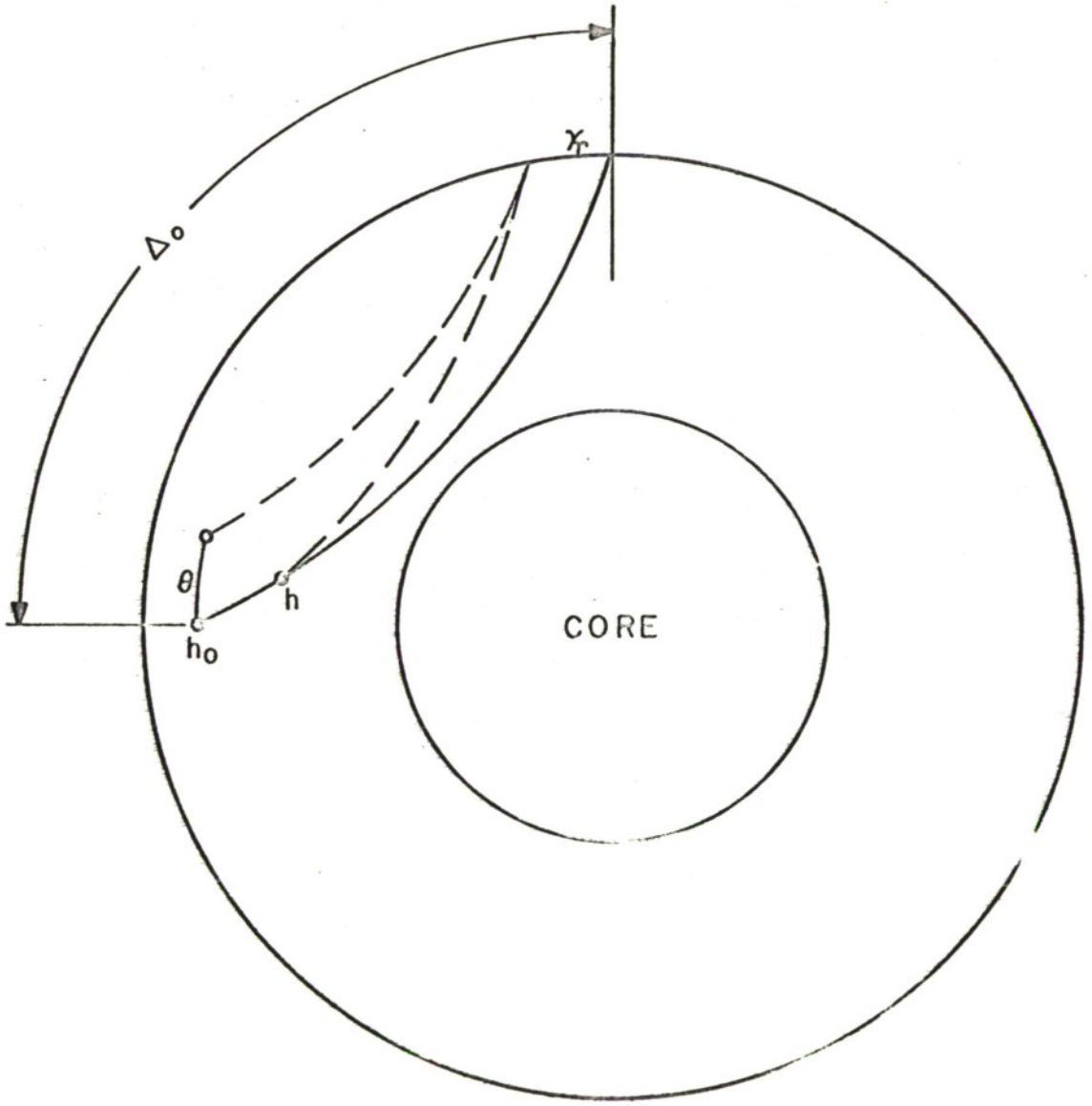

RADIAL AND DEPTH

$$\theta_r \approx \frac{\tau}{2\gamma_r T_{\Delta\Delta}}$$

$$\Delta h \approx \frac{\tau}{2\gamma_r T_{h\Delta}}$$

FIGURE 3

RADIAL AND DEPTH ARRAY GEOMETRY

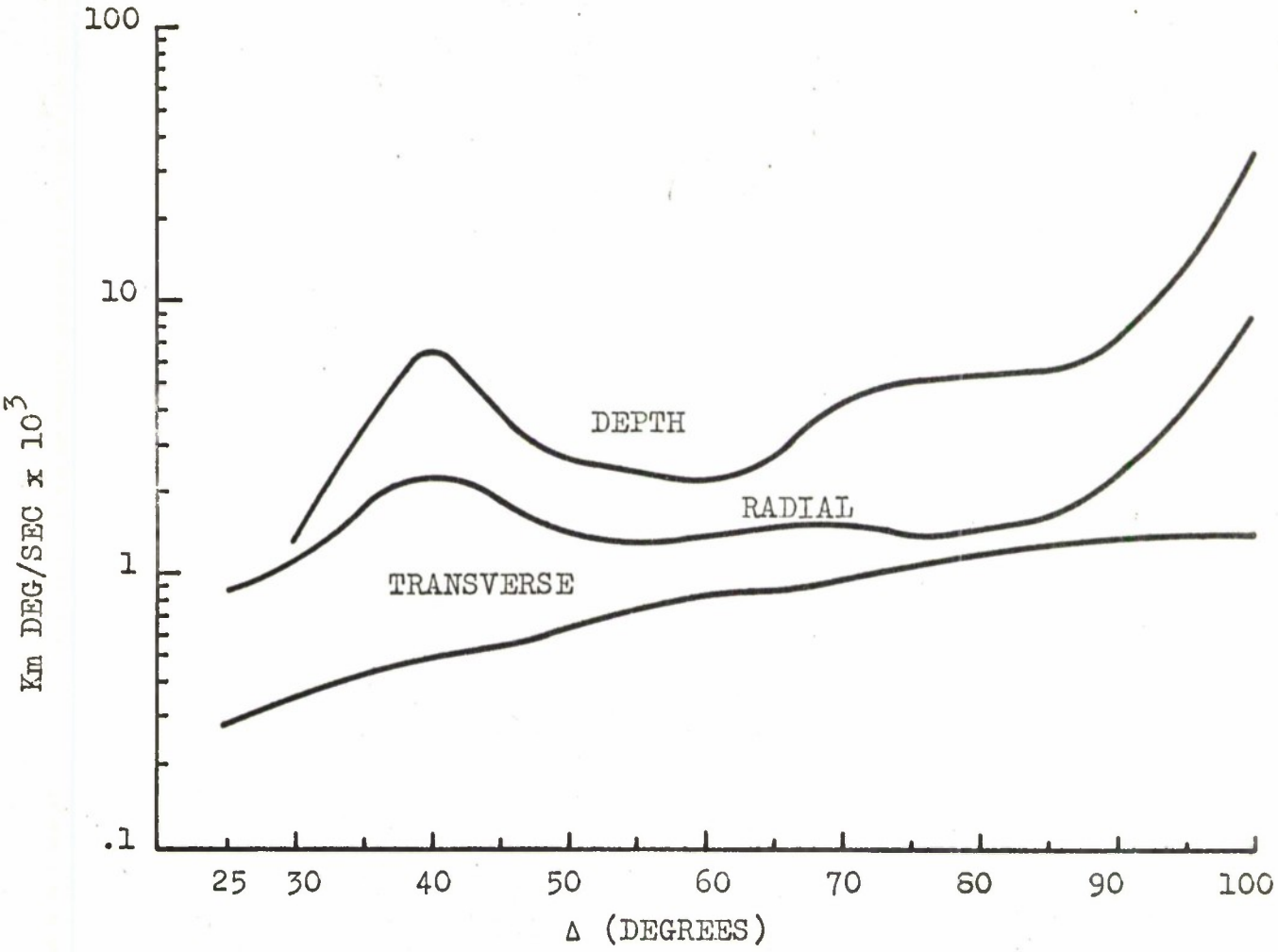

FIGURE 4
DIMENSIONS OF P-WAVE BEAM OF TELESEISMIC ARRAY

Section II-B ARRAY PATTERN COMPUTATIONS

General

Previously reported studies of array patterns for large seismic arrays have been primarily concerned with the performance of such arrays against noise. This work has been principally performed in "k" space, and as a result, does not completely describe the array performance with respect to teleseismic signals. Those areas where additional information can be usefully introduced have to do with the spreading loss and attenuation of seismic propagation, and also with the transient nature of seismic signals. Inclusion of these effects in array pattern calculations give rise to better prediction of the array sidelobes structure. While sidelobes may previously have been of little interest, the increased signal-to-noise gain achievable with arrays such as LASA may convert the teleseismic noise source from an homogeneous one to several moving and time varying "hot spots" representing small events from seismically active regions of the earth. Hence, it becomes important to achieve good control of the sidelobe structure of these large arrays.

Results to date do not take station correction factors into account, particularly, the dependence of these factors on range. It is believed, however, that it is instructive to first study the case where such corrections are assumed to be constant. Later work can extend the analysis to observed variations.

A computer program taking these phenomena into account, was developed to find the radial and transverse beam patterns of seismic arrays for P wave signals. The mathematical model used is the following:

a) The array seismometers are identical and are situated in a horizontal plane.

b) A single signal is present and has the form of a plane wave traveling through an homogeneous, linear and nondispersive medium.

c) The seismometer outputs are identical except for a time delay due to the finite phase velocity of the wave.

The signal used: P phase of LONGSHOT recorded at the center element of the LASA A_o cluster.

The patterns were corrected to include the effects of the attenuation of the signal during the path from the hypocenter to the array, and the effect of the geometric spreading.

Suppose that the array is formed by N seismometers and let their locations defined by the vectors $\vec{r}_k$, k = 1..., N

The output of the k^{th} seismometer will be:

$$X_k(t) = S\ (t - \vec{\alpha}.\vec{r}_k)$$

where S(t) is the transient used

$\vec{\alpha}(t)$ is the delay vector per unit distance

For a given array location, every point of the earth not situated in the core-shadow region is characterized by a vector $\vec{\alpha}$. Let $\vec{\alpha}_o$ be the vector associated with a particular point of the earth that we shall call "Focus" of the array. A beam output is then formed by delaying all seismometer outputs by $\vec{\alpha}_o \cdot \vec{r}_k$, k = 1..., N and summing these delayed signals.

The Focus is characterized by two coordinates with respect to the center of the array:

Δ_o = Range to the center of the array

Az_o = Az of the great circle that joins the Focus with the center of the array

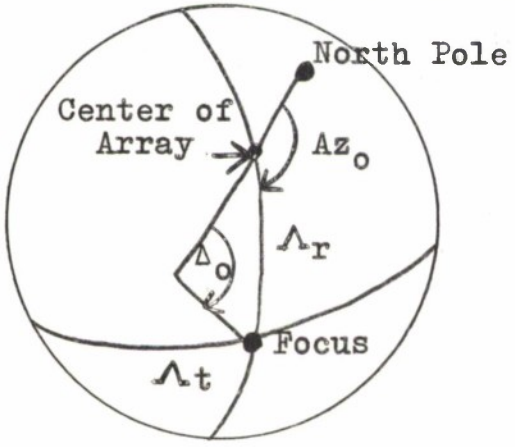

A P-wave signal that reaches the array coming from Δ_o and Az_o (The Focus) will produce the maximum output of the array, with this processing scheme. The same delays $(\vec{\alpha}_o \cdot \vec{r}_k)$ acting on a signal created by an event of the same magnitude but whose hypocenter is not located at the focus of the array will produce an output that is distorted and smaller in amplitude.

The Radial beam pattern computed shows how the maximum amplitude of the delayed-sum varies as the event's hypocenter moves away from the focus, over the great circle Λ_r. As expected, effect of the attenuation and the geometric spreading acts to increase the sidelobes at ranges smaller than the focus and their effect is the opposite for ranges greater than Δ_o.

The transverse pattern computed is a plot of the maximum amplitude of the delayed-sum as we place events at different points on Λ_t.

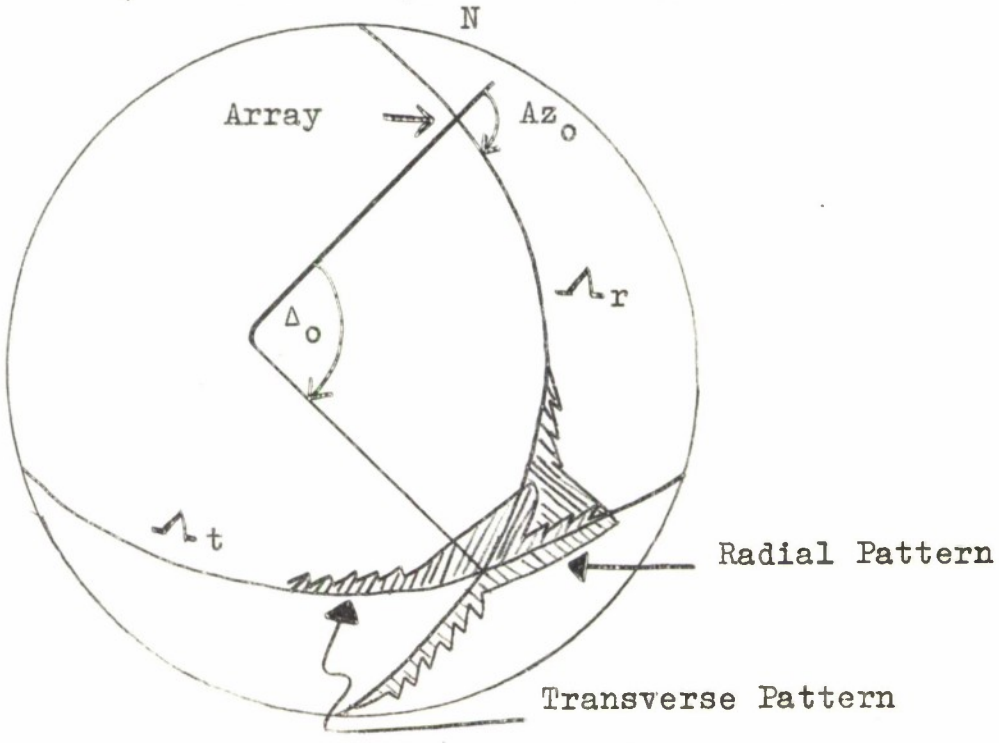

One output of the program is the transient formed by the delayed sum of the seismometer recordings for every point where the beam pattern was computed. Figures 5-a to 5-e show these transients for ranges varying from 20° to 96° and a focal range of 82°.

Correction for Attenuation and Geometric Spreading

Geometric Spreading:

C_1 = Correction factor (amplitude) $= \frac{\Delta_o}{\Delta}$ Δ_o = focus range, Δ = range

This correction is valid for a spherically symmetric traveling wave.

Attenuation loss correction:

The amplitude of seismic signals is assumed to have the following range and frequency dependence, Ref. 4 (after removal of geometric spreading);

$$A(\omega, \Delta) = e^{-\frac{\omega}{2cQ}\Delta}$$

where:

A is the amplitude of the wave.

ω is the angular frequency of the wave.

Δ is the distance (central angle) between source and receiver.

c is the velocity of propagation.

Q is the ratio of energy stored to energy lost per cycle in the earth.

Beam Patterns for LASA

The program discussed above was then used to compute several patterns for LASA - at different focal ranges and different bearings from the array. For these computations, it is first noted that LASA is formed of clusters of seismometers. The dimensions of these clusters are approximately one wavelength at the predominant frequency of teleseismic signals. Thus, the pattern for this array can be found by multiplying the pattern obtained using each cluster as a single element of

an array with the patterns of a single cluster. Since the size of the clusters is small compared to the wavelength of the signals received, the beamwidth of these subarrays is such as to include all teleseismic arrival angles. Thus the pattern for the whole array can differ at most by a few dB from that computed for the center elements of the clusters alone, and thus the patterns given are for a 21 element array with the elements located at the positions of the center of the clusters. The following three foci have been chosen as representative of LASA patterns:

1. $\Delta_o = 82^\circ$, $Az_o = 277^\circ$ — Figures 6 and 7
2. $\Delta_o = 56^\circ$, $Az_o = 264^\circ$ — Figures 8 and 9
3. $\Delta_o = 84^\circ$, $Az_o = 215^\circ$ — Figures 10 and 11

Plots of the radial beam patterns (Figures 6 , 8 , and 10) show the effect of the attenuation and geometric spreading on the pattern. The mainlobe is not strongly affected but the sidelobes change appreciably.

Plots of the transverse beam patterns (Figures 7 , 9 , 11) of LASA center elements do not show such strong effects.

The 3-dB beamwidths obtained are the following:

	with attenuation and geometric spreading	without attenuation and geometric spreading
$\Delta_o = 82^\circ$	$\Theta_r = 13^\circ$	$\Theta_r = 13^\circ$
$Az_o = 277^\circ$	$\Theta_t = 8.5^\circ$	
$\Delta_o = 56^\circ$	$\Theta_r = 10.5^\circ$	$\Theta_r = 10.0^\circ$
$Az_o = 264^\circ$	$\Theta_t = 5.7^\circ$	

	with attenuation and geometric spreading	without attenuation and geometric spreading
$\Delta_o = 84^o$	$\theta_r = 13.75^o$	$\theta_r = 17{,}00^o$
$Az_o = 215^o$	$\theta_t = 12.5^o$	

Because of the poor sidelobes of the LASA patterns, particularly in the radial direction, an experiment was performed to determine the degree to which sidelobes could be controlled if one were not restricted to clustering of elements. Such an array is not proposed at this time for a number of reasons, however, the patterns it could produce are instructive.

The array chosen for this experiment was one whose elements (525) were distributed randomly (normal distribution in both x and y coordinates) over a circle of radius 1^o.

Random Distribution of Seismometers

It will be assumed that the coordinates which locate the array elements are independent, zero mean, normal random variables. In the following, the density function of a zero mean, normal, random variable with variance σ^2 will be denoted by $N(o,\sigma)$. In practice, due to the finite size of the array, the elements will follow a truncated normal distribution rather than a true normal distribution. Two parameters define a symmetric truncated zero mean normal distribution:

σ^2 = variance

R_{max} = maximum value (truncation point)

In our case R_{max} corresponds to the maximum distance from the array center at which an array element can be located.

In determining the array pattern for a radial cut at an angle θ (see Figure below) it is first necessary to project the array elements onto the radial line. Hence the projection of the array element with coordinates (x,y) is given by

$$R = x\sin\theta + y\cos\theta$$

If x and y are independent, random normal, variables with

zero means, then R will also be a zero mean, normal, random variable since it is a linear combination of normal random variables. Also, because of the sine-cosine coeffecients, the variance of R will be the same as those of x and y.

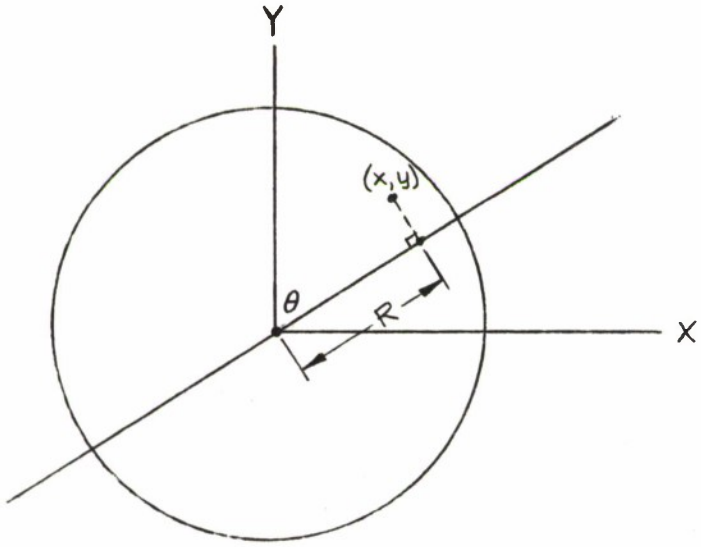

Hence for normally distributed elements, we expect array patterns that are independent of Az_o, the azimuth of the focus.

The use of randomly distributed elements as discussed above will result in an amplitude taper for any radial cut and hence a lower sidelobe level (compared to the clustered array) should be obtained. Figure 12 shows such a distribution, with $\sigma = 0.5$ degrees and $R_{max} = 1$ degree. The relation between σ and R_{max} was chosen to be $\sigma = \frac{1}{2} R_{max}$ in order to avoid strong sidelobe generation due to truncation of the density function. For $\sigma > \frac{1}{2} R_{max}$ the actual array beamwidth will be smaller than computed, but the truncation effect will start to become important. No attempt has been made to find an optimization criterion. Figures 13 and 14 show the computed transient patterns for the random array of Figure 11 when focussed at a range of 58^o at an azimuth of 264^o. Also shown in these figures are the comparable patterns for the present LASA configuration.

Radial Beam Pattern for Randomly Distributed Elements

In analyzing the beam pattern of a random LASA array, a number of simplifying assumptions will be made. The array will be treated as a continuous distribution rather than discrete, truncation effects will be ignored, and the incoming wave will be assumed to be monochromatic rather than broadband. With the above simplifications it will be shown that the resulting array pattern of the random array is essentially the Fourier transform of the probability density function of the random variable R. Hence, for the assumed normal distribution of array elements, the resulting array pattern will have a Gaussian shape.

As discussed previously if the coordinates x, y of an array element are independent random variables with normal distributions $N(o,\sigma)$, the projection R of the element R on a radial line will also have a normal distribution $N(o,\sigma)$. For a monochromatic signal the radial pattern $\varphi(\alpha)$ is given by

$$\varphi(\alpha) = \left| \frac{1}{N} \sum_{i=1}^{N} e^{j2\pi f \alpha R_i} \right|$$

where

f = frequency of the incoming wave
N = number of array elements
α = relative delay per unit distance along the radial
R_i = the projection of the i^{th} element onto the radial.

It should be noted that α the relative delay will be a function of Θ, the angle of the radial, and the phase velocity of the incoming signal. Now since the R_i are random variables, it is the average array pattern $\overline{\varphi(\alpha)}$ that is of interest. Hence

$$\overline{\varphi(\alpha)} = \left| \frac{1}{N} \sum_{i=1}^{N} e^{j2\pi f \alpha R_i} \right|$$

$$= \left| \frac{1}{N} \sum_{i=1}^{N} \frac{1}{\sqrt{2\pi}\sigma} \int_{-\infty}^{\infty} e^{j2\pi f \alpha R_i} \; e^{-\frac{R_i^2}{2\sigma^2}} \, dR_i \right|$$

Thus:

$$\overline{\varphi(\alpha)} = \left| \int_{-\infty}^{\infty} e^{j2\pi f\alpha R} \frac{1}{\sqrt{2\pi}\sigma} e^{-\frac{R^2}{2\sigma^2}} dR \right| = \left| \overline{e^{j2\pi\alpha fR}} \right|$$

Hence $\overline{\varphi(\alpha)}$ is given by the magnitude of the characteristic function of the probability density function of the random variable R. The characteristic function of a Gaussian random variable has a Gaussian form. Hence

$$\overline{\varphi(\alpha)} = e^{2\pi^2\alpha^2 f^2\sigma^2} = k \frac{1}{\sqrt{2\pi}} e^{-\frac{\alpha^2}{2\left(\frac{1}{2\pi\sigma f}\right)^2}}$$

where

$$k = \frac{2\pi}{\sigma}$$

Hence $\overline{\varphi(\alpha)}$ is equal to k N $\left(o, \frac{1}{2\pi\sigma f}\right)$. Due to the reciprocal properties of the Fourier transform the beamwidth of the random array is inversely proportional to the standard deviation of the element locations.

For the expected LASA signals, the received energy will be concentrated in the vicinity of one cycle. Hence for illustration, the array pattern has been calculated on the basis of a received signal frequency of 1 Hz . Results of the computation (See Figure 13) show that the assumptions made above were valid.

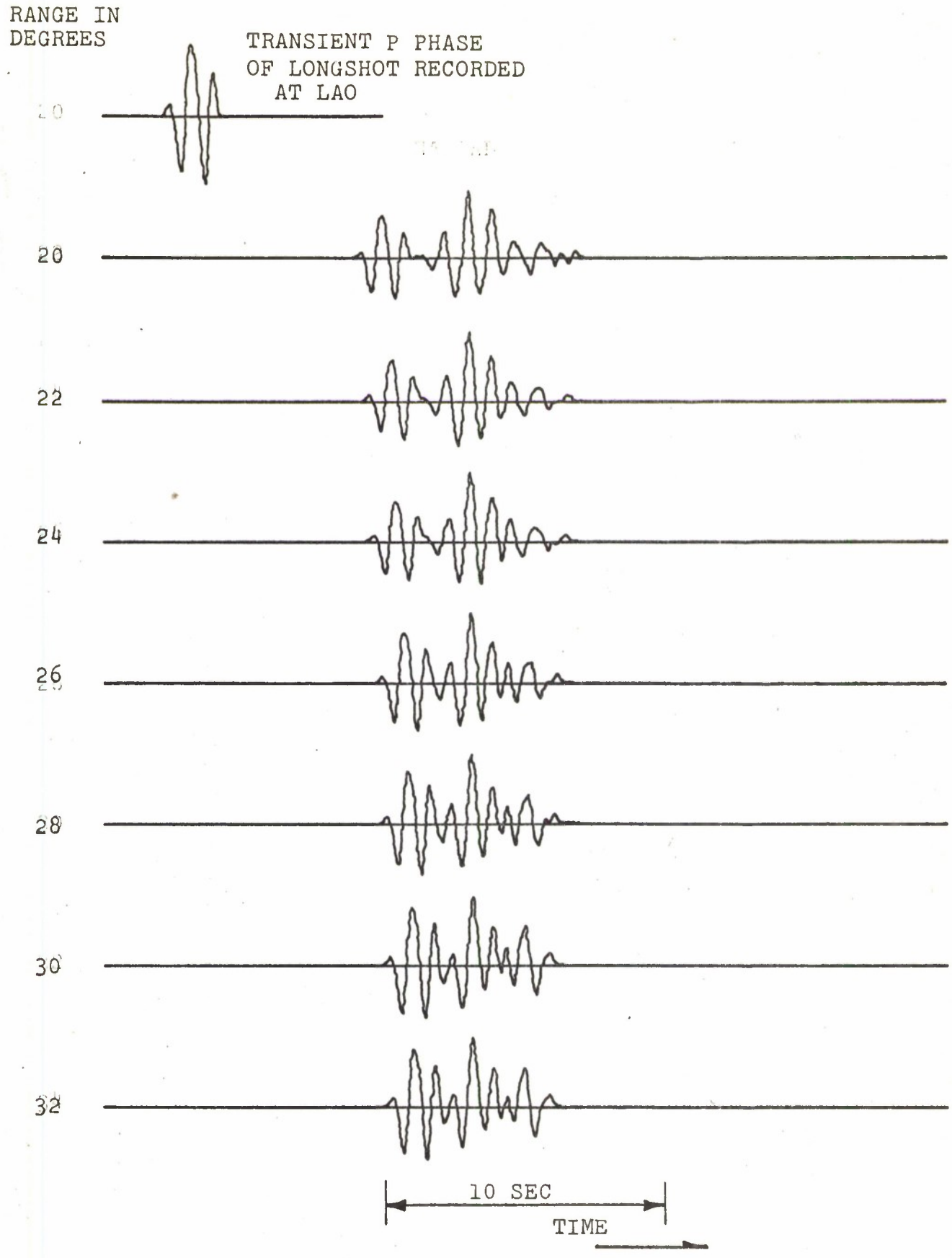

FIGURE 5A - DELAYED SUMS (RADIAL PATTERN) LASA CENTER ELEMENTS (PLOTS NOT ON SCALE)

FOCUS Δ_o = 82°; AZ = 277°

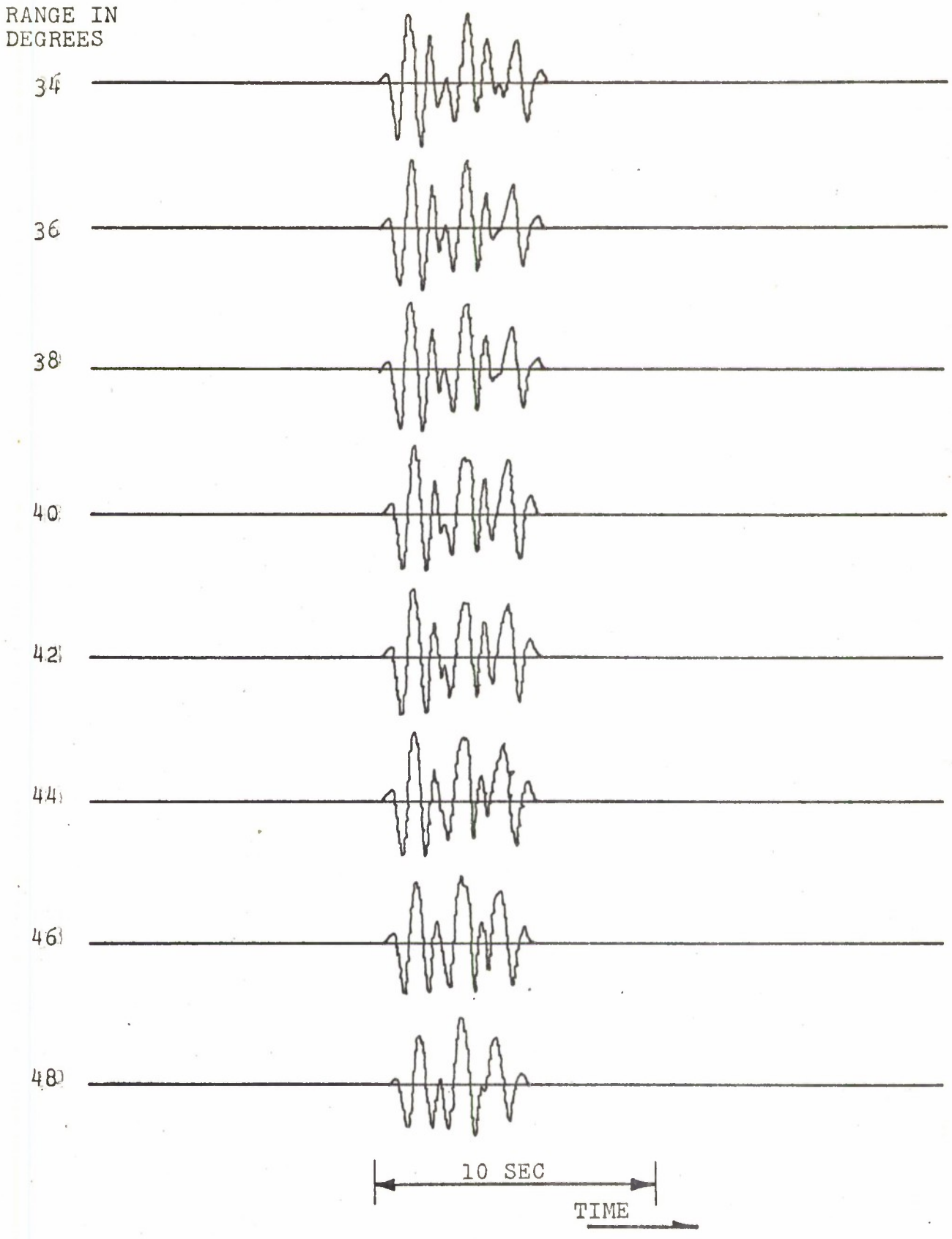

FIGURE 5B

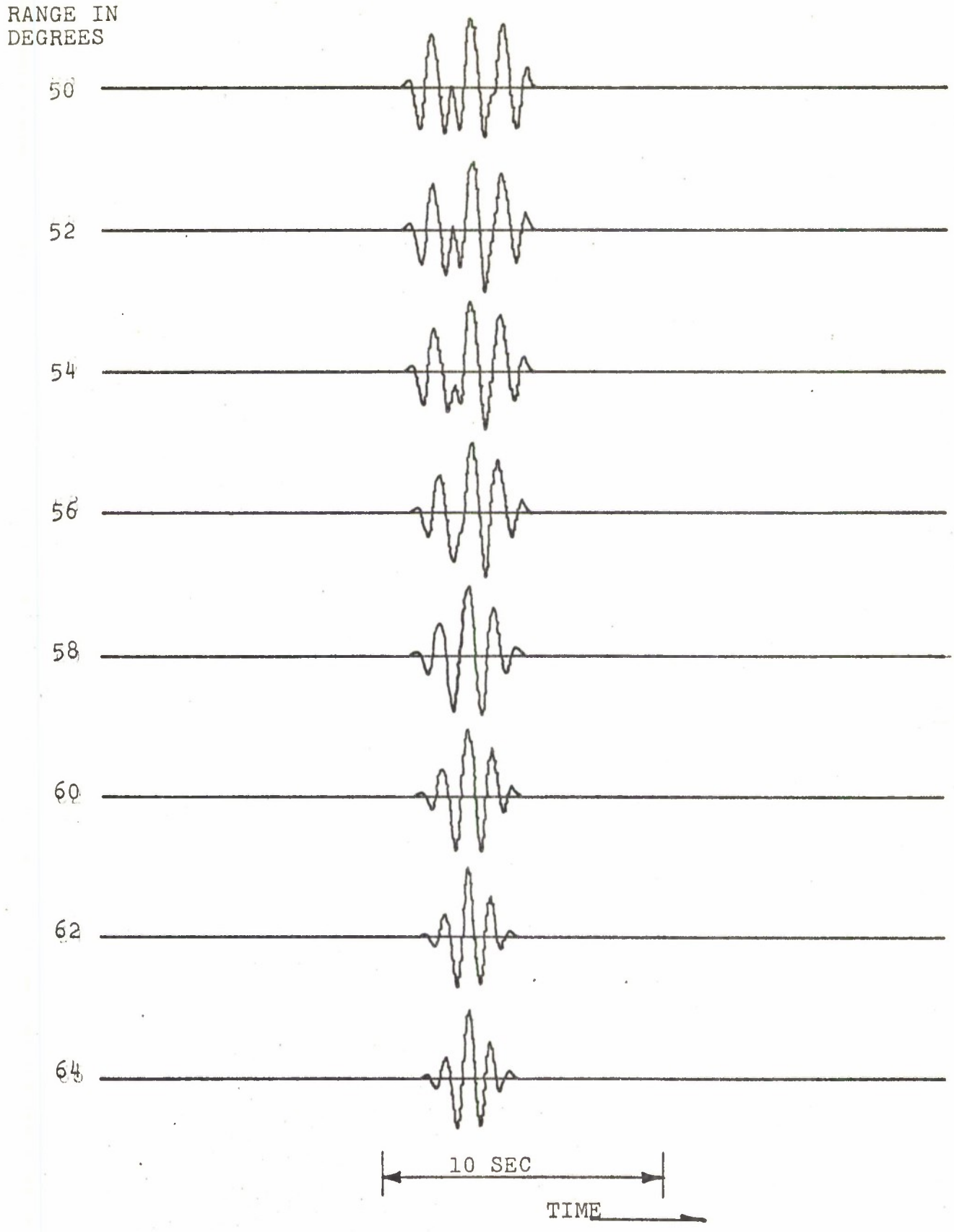

FIGURE 5C

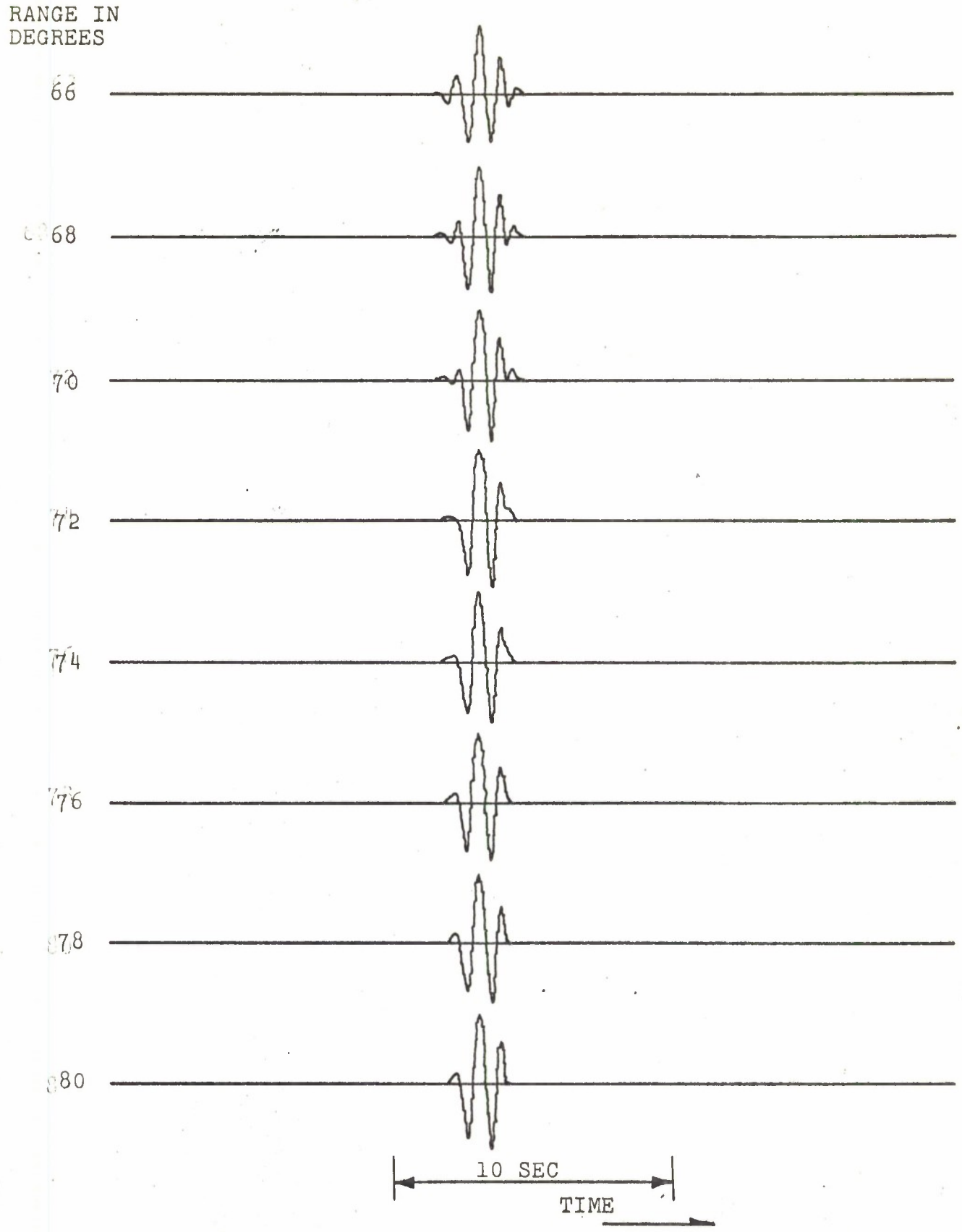

FIGURE 5D

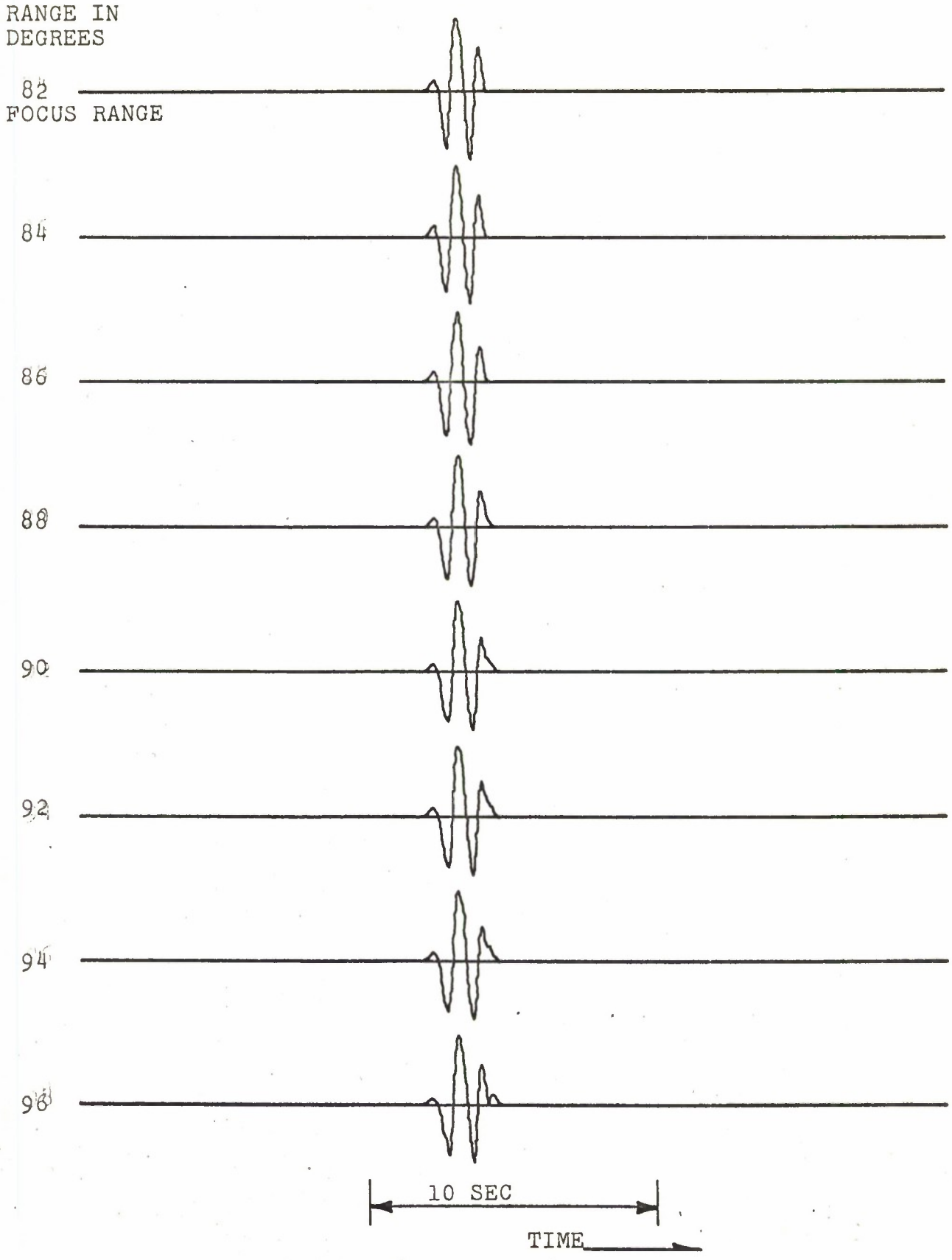

FIGURE 5E

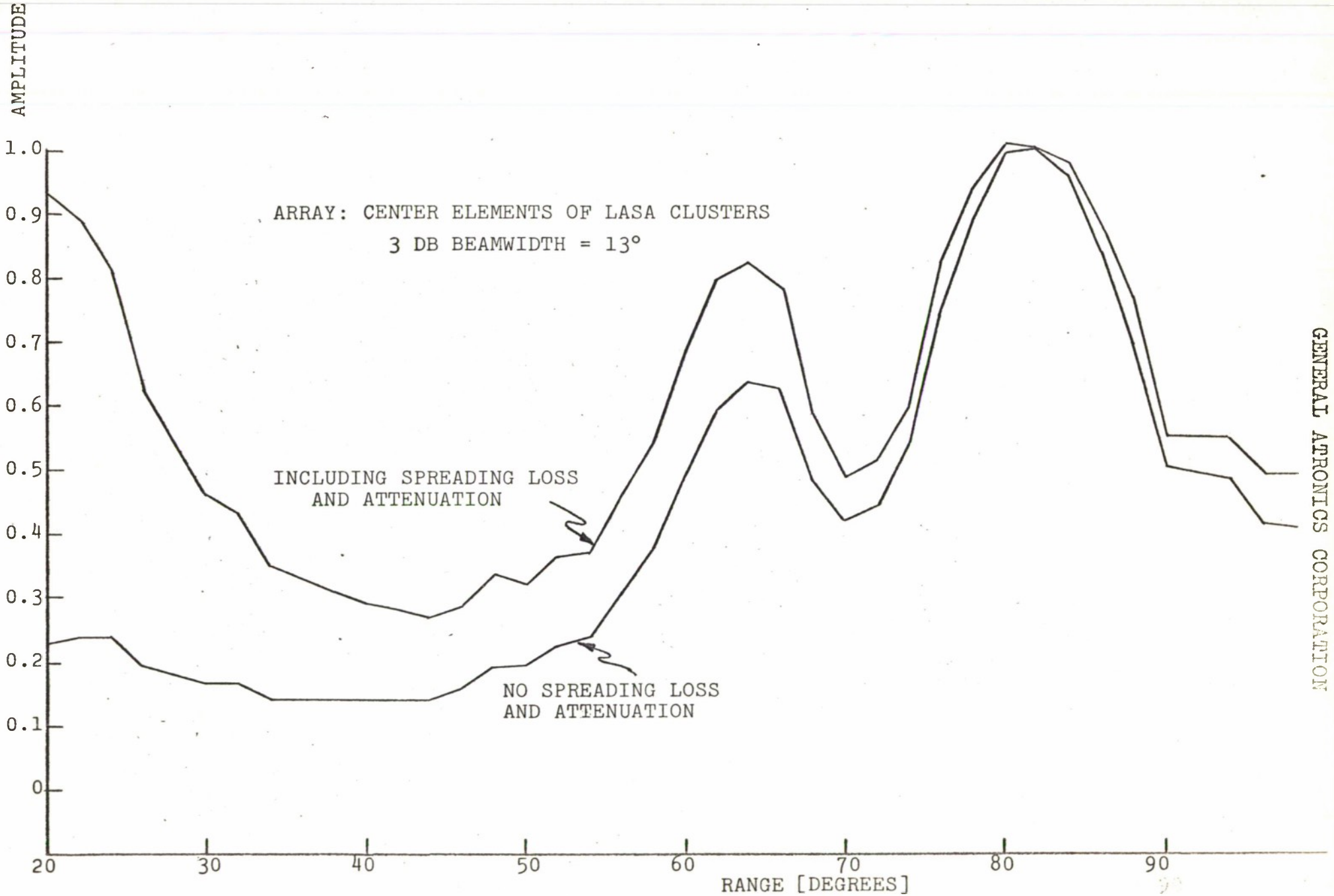

FIGURE 6 - LASA RADIAL PATTERN

FOCUS: Δ_o = 82°
AZ = 277°

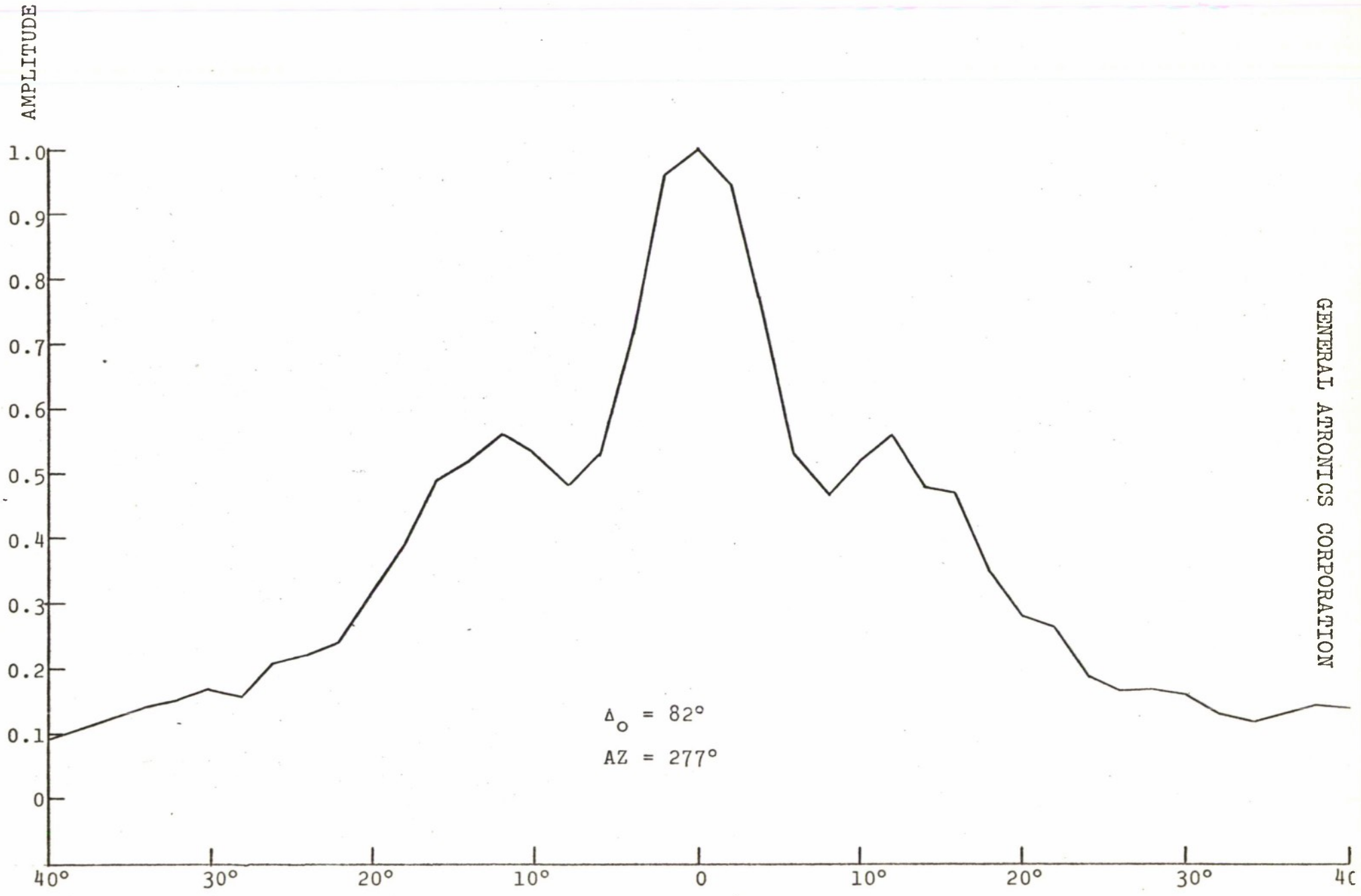

FIGURE 7 - TRAVERSE PATTERN

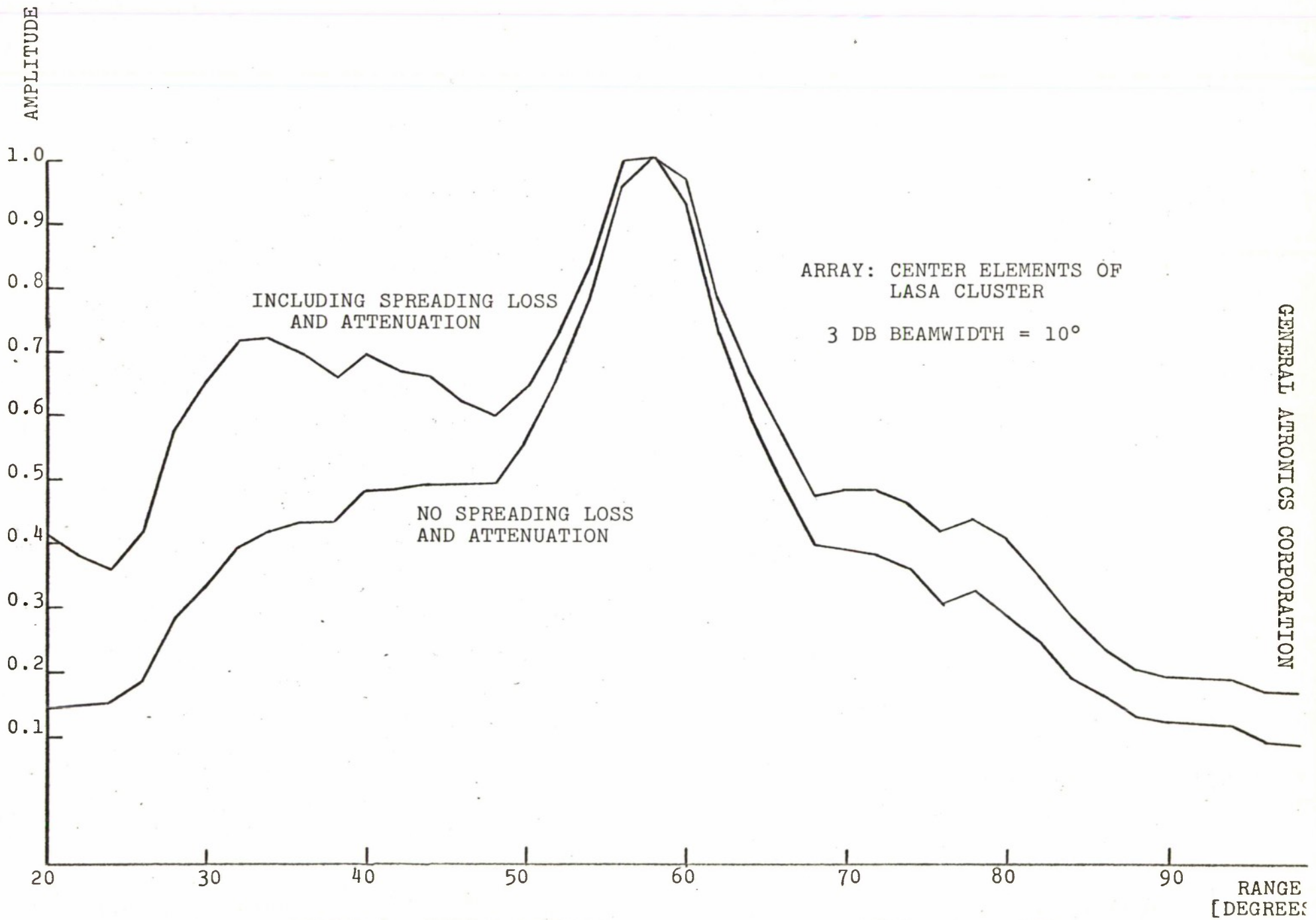

FIGURE 8 - RADIAL PATTERN

FOCUS: Δ_o = 58°
AZ = 264°

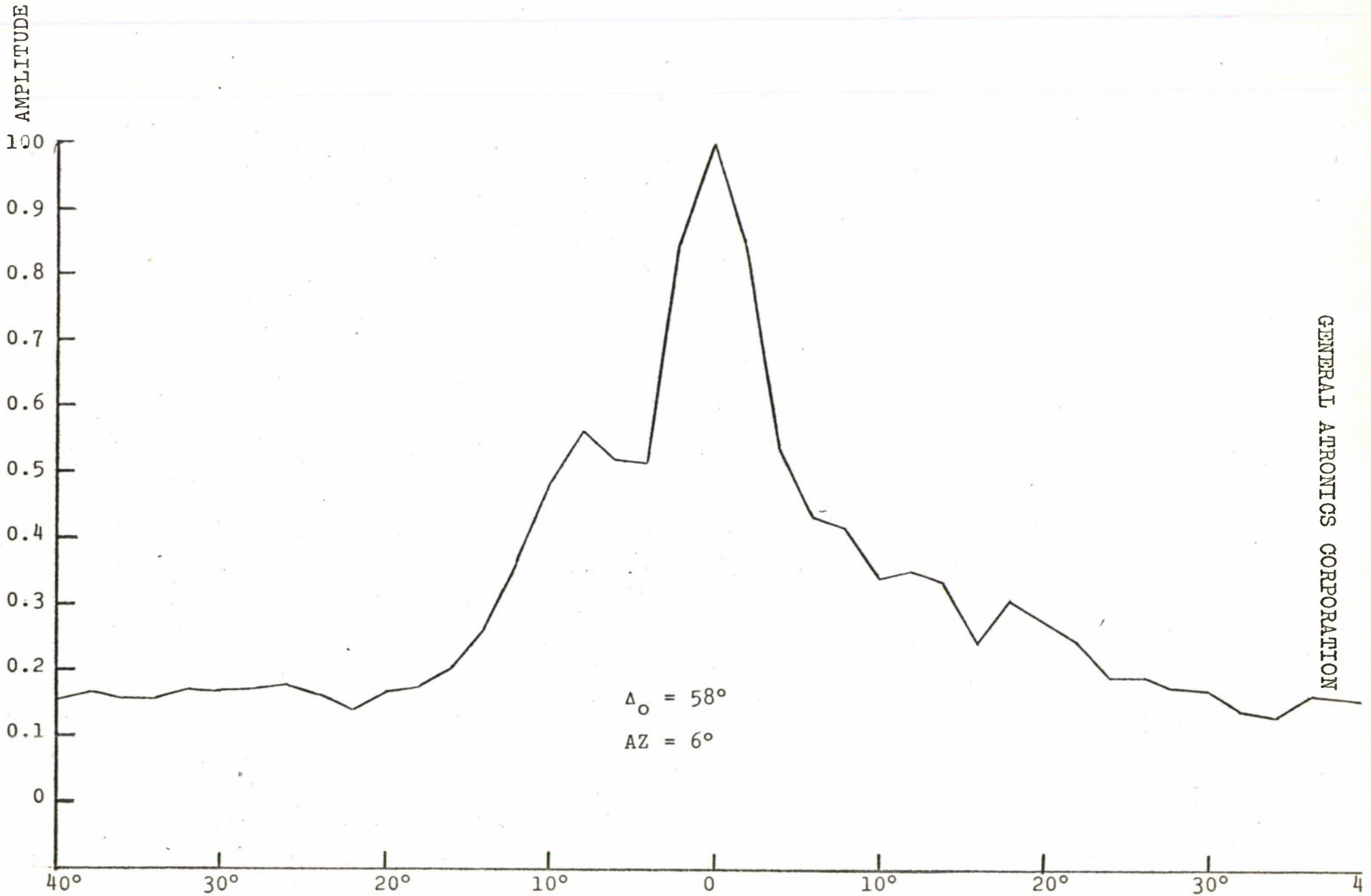

FIGURE 9 - TRANSVERSE PATTERN (KRESTOVAYA)

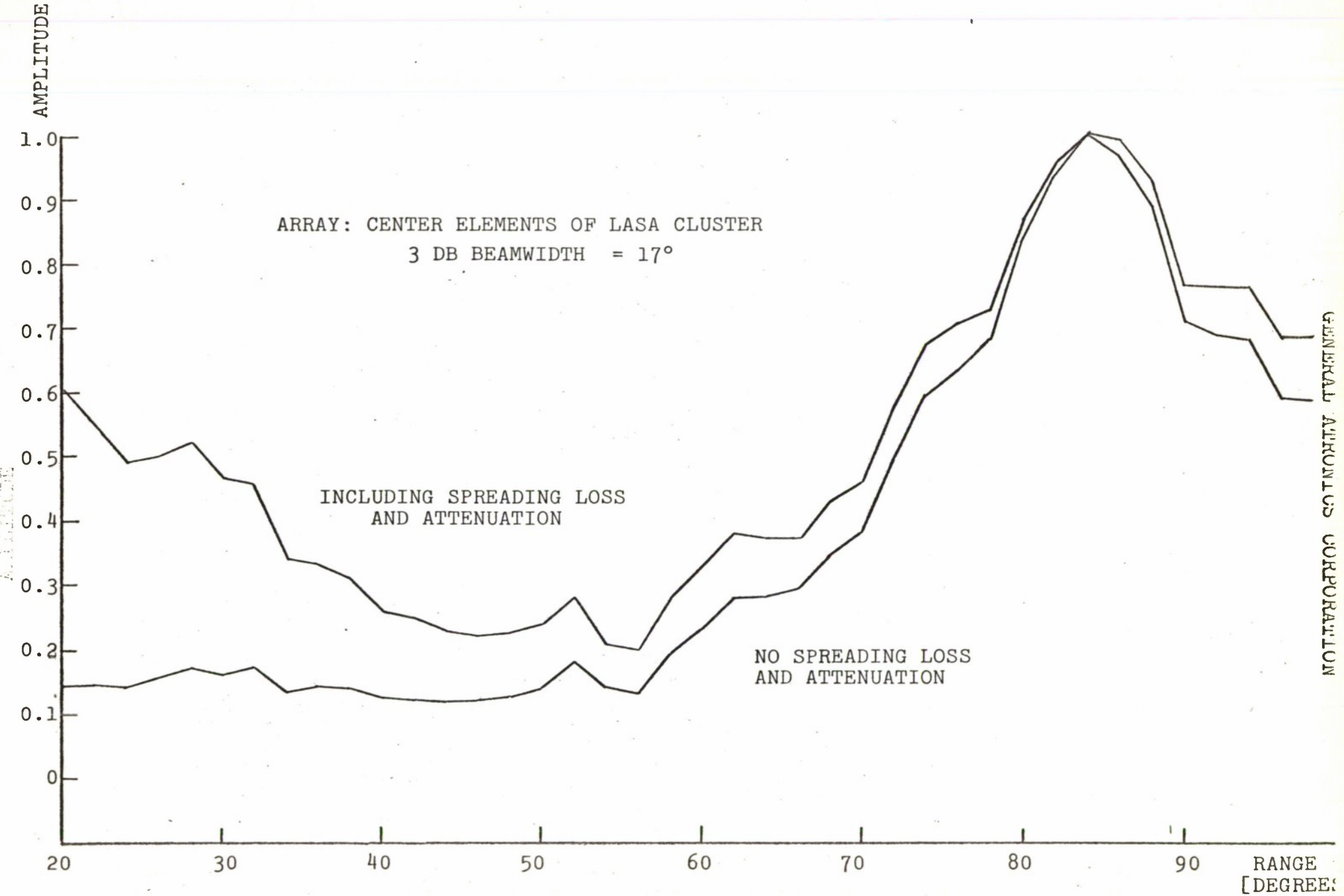

FIGURE 10 - LASA RADIAL PATTERN

FOCUS: Δ_o = 84°
AZ = 215°

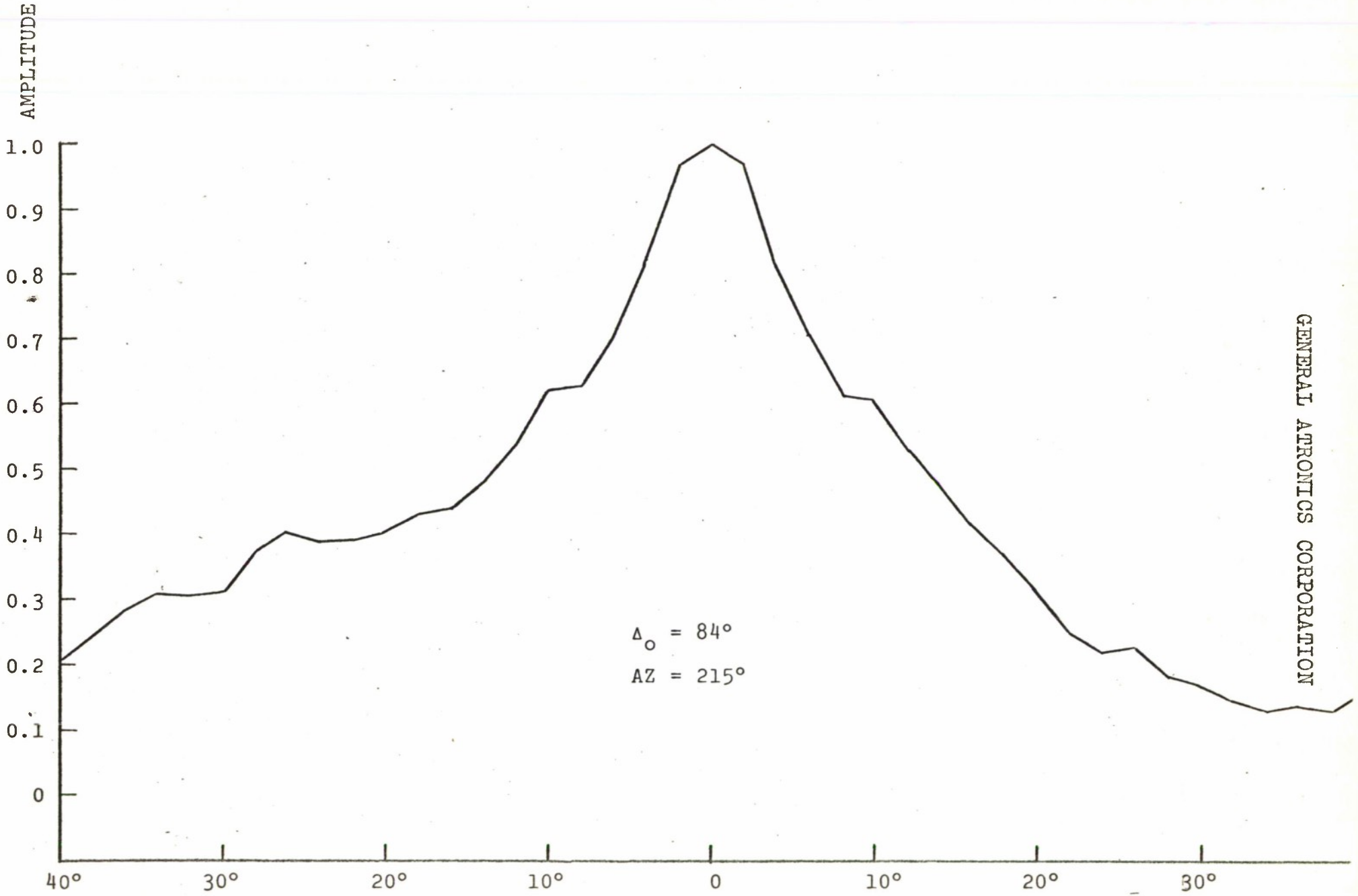

FIGURE 11 - TRANSVERSE PATTERN

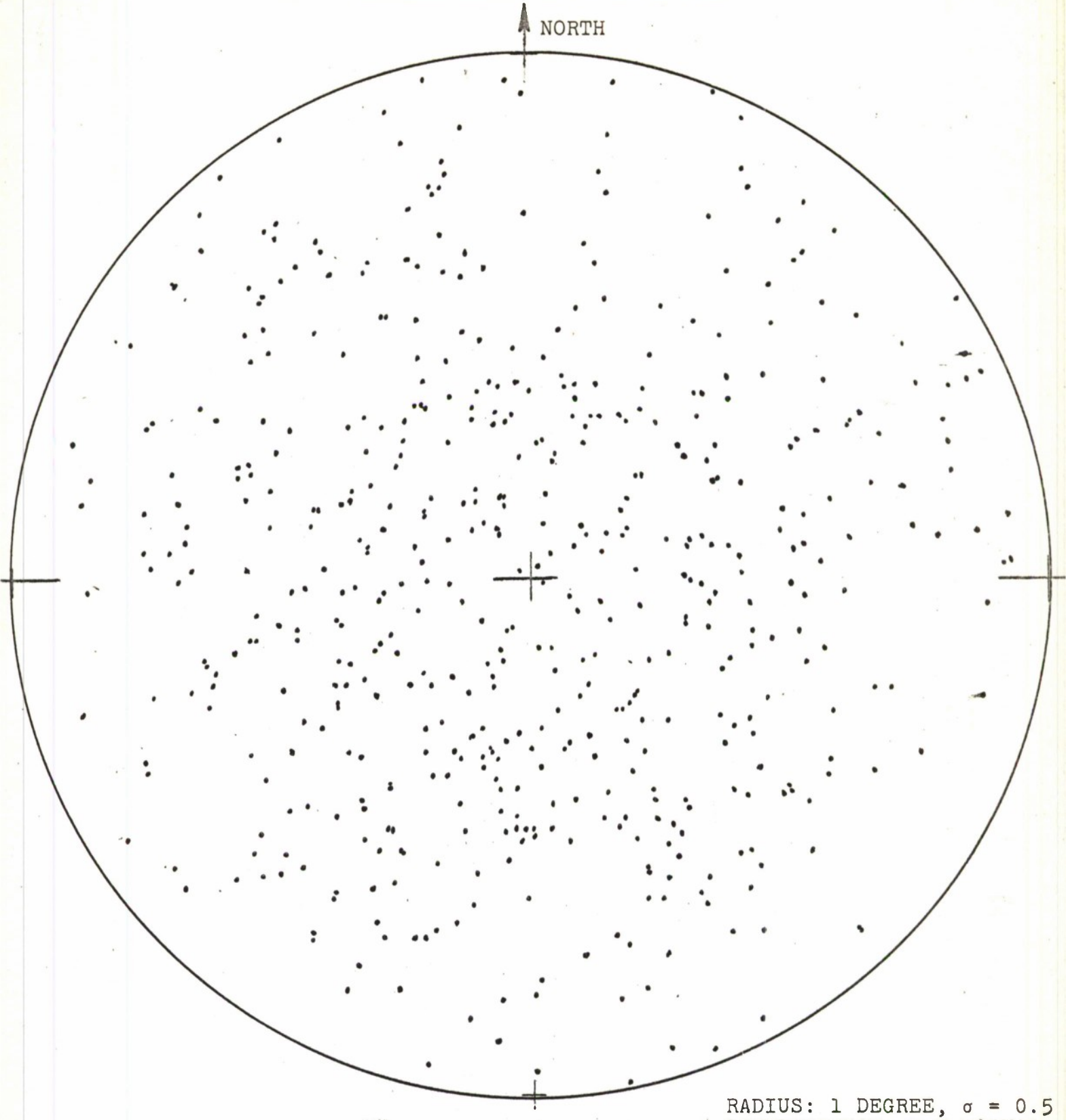

FIGURE 12 - SEISMIC ARRAY [525 ELEMENTS]

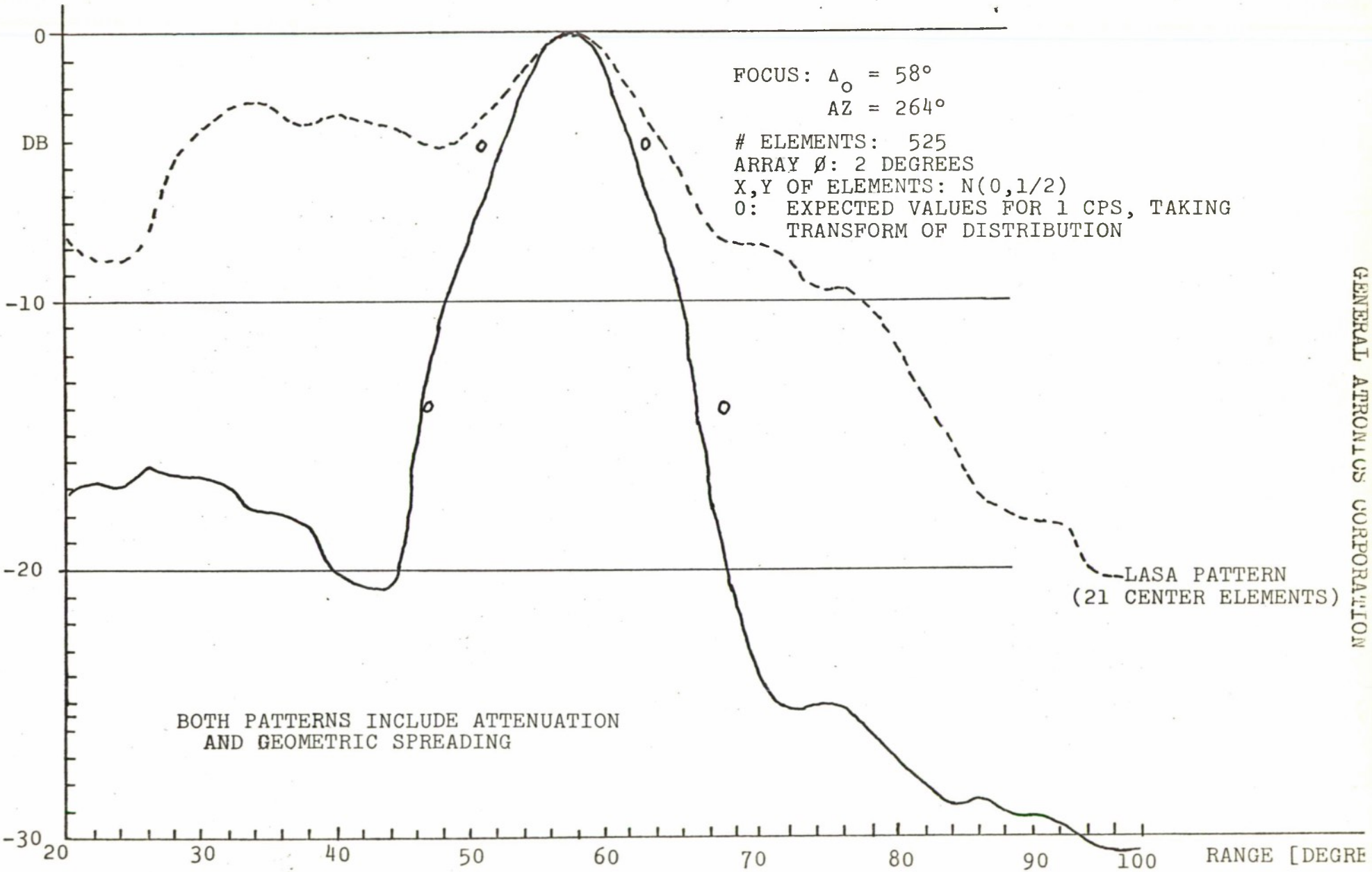

FIGURE 13 - RADIAL PATTERN (RANDOM ARRAY)

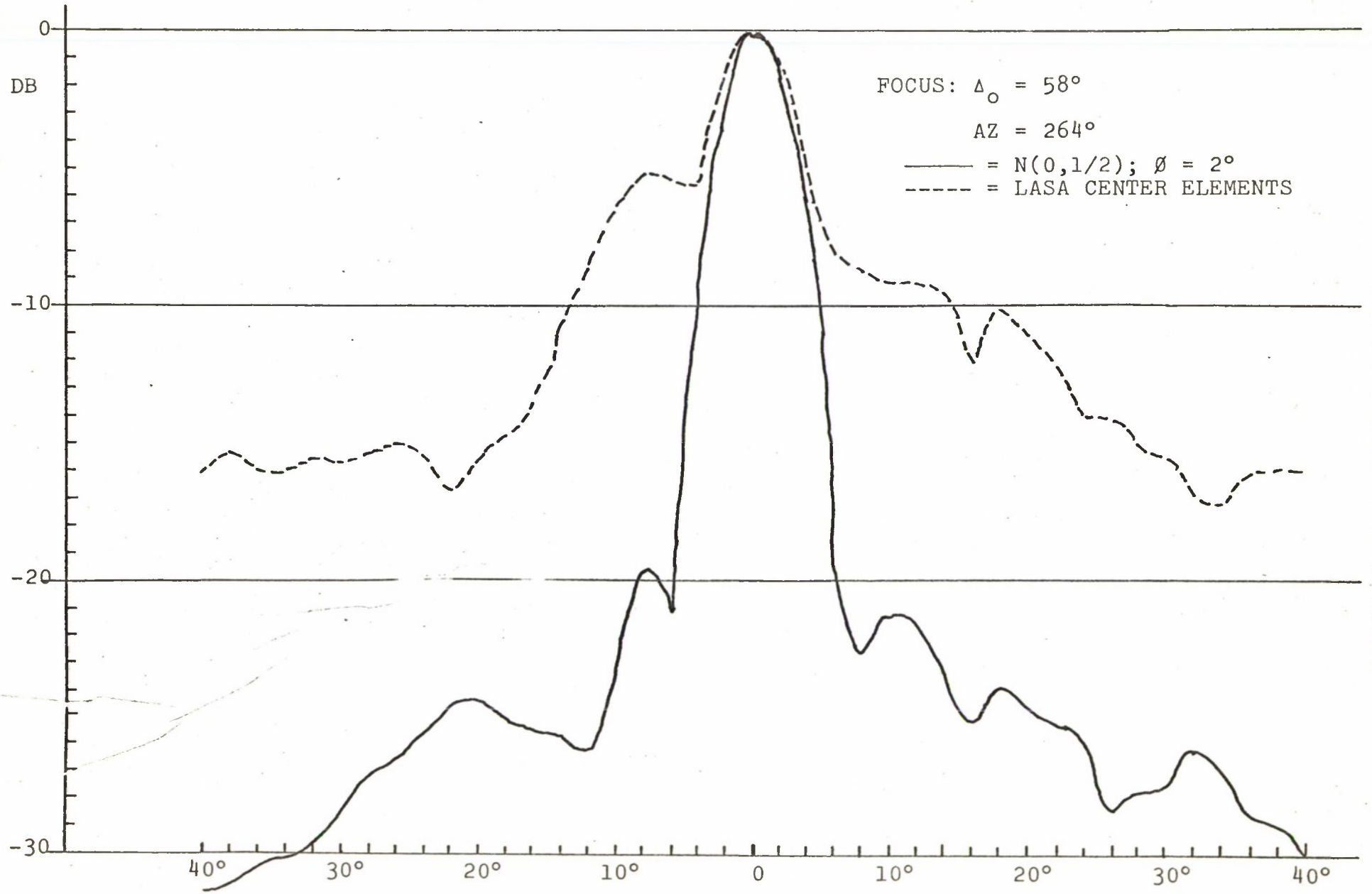

FIGURE 14 - TRANSVERSE PATTERN (RANDOM ARRAY)

Section II-C DIMUS Array Processing

Many investigators have treated the case of clipped (use of zero crossing information only) processing of signals in the presence of noise. Anderson of Scripps Oceanographic Institute coined the name of DIMUS (digital, multiple steered) array processing for additive arrays using clipper amplifiers and shift registers for delay compensation. Anderson concluded that the loss in array processing for the DIMUS is 1.95 dB [5], while authors have shown that this loss may be higher or lower depending on the character of the interfering noise [6], [7]. These losses in processing gain are for the case of low signal-to-noise ratio at each of the individual sensors which make up the array. For higher input signal-to-noise ratios, this loss can become much more severe. This may readily be seen from the fact that the DIMUS output is constrained to lie somewhere between positive and negative limits equal to the number of sensors in the array. Where the problem is the detection of weak signals in noise, a loss in output signal-to-noise ratio of some two dB or less in considered insignificant for seismic work. This is because of the tremendous variability of seismic measurements. What does appear significant, however, is the distortion introduced for large input signal-to-noise ratios (S/N>1). In this case, discrimination between earthquakes and underground explosions on the basis of the received waveforms might be severly curtailed. Hence, a study of DIMUS processing must be undertaken from two distinct points of view; detection, and identification.

Before proceeding further with a discussion of DIMUS processing itself, let us first mention several reasons why such processing might have distinct advantages for a large aperture seismic array. Most obvious is the reduction in the amount of data which must be handled and/or stored. Since in DIMUS each sample conveys one bit of information, there is available an immediate reduction of some 15 to 1 in the data handled over

that necessary in the current design of the Montana LASA system. Further, if we might limit our attention to seismic frequencies below two cycles per second, the sampling rate itself could be reduced to some four or five samples per second rather than the twenty samples per second for LASA Montana. The net result of such changes would be a data rate some sixty times less than current practice. One result of such a reduction in data rate would be the possibility of storing the entire output of a LASA on only two ten inch recording tapes each day. Perhaps more important, for a 500 seismometer array, the total output data rate (taking each seismometer separately) would be approximately 2.5 kilobits per second. Such a rate is clearly low enough to permit the transmission of the total raw data from such a site to a central data processing facility over a single telephone circuit in real time. Similar dramatic reductions in beamforming equipment are also easy to propose. Finally, if such a drastic reduction in data rate from individual instruments proves completely satisfactory, it may be realistic to consider arrays where the seismometers need not be clumped. Rather, each instrument could be self powered by a fuel cell or solar battery, and the instrument output relayed to the array center by means of very simple communications equipments located at the instrument sites. So much for the potential advantages of DIMUS processing itself. As stated above, we will consider such processing from two standpoints; detection and identification.

Detection Aspects of DIMUS Beamforming for LASA

As stated earlier in this section, previous studies of the detection capabilities of DIMUS beamforming systems have predicted a one to two dB loss in processing gain for such systems when compared to analog systems, depending on the characteristics of the interfering noise. While microseismic noise is admittedly non-white and non-stationary in the long run, it has been hypothesized that at least for short intervals of time, this noise is

Gaussian (see Section II-D for example). For this kind of noise, one would expect that the DIMUS processing would be two dB poorer than analog processing given low input signal-to-noise ratios. To test this hypothesis, a continental size seismic array was formed using the five continental U.S. array stations and NPNT as clusters. Each of the clusters was summed without delay, and the phased sum taken of these clusters. The event taken for the experiment was a surface focus event of magnitude 4.6, with epicenter located in Algeria. Differential delays for the clusters were determined from another, larger, surface focus event located in the same general vicinity.

Figure 15 is the record from a single seismometer located in the WMO "cluster". This record is typical of those for each instrument in the large array. From this figure, it is easy to see that the criterion of low signal-to-noise ratio at each seismometer was met for this test. Figure 16 shows both the analog sum of the seismometers for the array focussed at the event under study, the sum of the hardlimited seismometer outputs, and also the same two signals after band pass filtering (0.75 to 1.5 cps). This filter served the dual purposes of removing out of band interference and harmonic distortion introduced by the limiting process. The event in question is clearly visable on each of these four traces, however, the final signal-to-noise ratio leaves something to be desired.

Since the peak outputs of both kinds of array processing have been normalized in the traces shown, it was easy to compute the rms value of the noise for both array outputs immediately preceding the arrival of the event. The ratio of clipped noise to unclipped noise was found to be 2.1 or about the expected loss in DIMUS processing. While the length of the noise record available for analysis on each of these records was small (approximately 15 seconds), and only one experiment was performed, the results agree so well with theoretical expectations that one may assume that the detection performance of DIMUS beamformers can be predicted.

Before leaving the detection aspects of the DIMUS, it is interesting to note that such beamformers make possible CFAR (constant false alarm rate) automatic detectors without the usual problems of automatic gain controlled amplifiers. To see how this is so, first consider that the noise imputs to each of the seismometers are independent and have zero means. Then, the sum of N hard limited instrument outputs will range from -N to +N and possesses a binominal probability distribution with zero mean - no matter what the strength of the noise at each of the seismometers. It is easy to see, then, that a constant threshold set at the array output will give a constant and predictable false alarm rate.

To determine the probability of detection for such a system, first consider a constant signal at the input to each seismometer. Then in the absence of noise, all of the hard limiters following the seismometers would have the same polarity, and the magnitude of the output of the summer of the system would be exactly N. When sufficient noise is present at the inputs to the seismometers, not all of the hard limited outputs will be of the same polarity. Here the magnitude of the output of the array summer can take values less than N, the exact value being a function of the signal-to-noise ratio at the inputs to the individual seismometers.

Figure 17 illustrates how it is possible to determine the probability distribution of the magnitude of the summer output as a function of the input signal-to-noise ratio. The figure shows the distribution of signal plus noise at the input to a single sensor as a normal distribution with mean value E_s, the signal voltage. This results from the assumption that the noise is normally distributed with zero mean. From the figure, it is easy to see that the probability that noise will cause the limiter output to be of different polarity than would be true in the noiseless case is simply the area of the distribution for negative values of the variable. Thus, given the

input signal-to-noise ratio at the individual seismometers, it is possible to compute the probability of noise producing an incorrect polarity for a single seismometer output. One can in fact compute what this signal-to-noise ratio must be for a given probability that no more than m of the N outputs will be so reversed. If the threshold is set at a value N-m, this probability will be the probability of detection. Figure 18 give several illustrations of the detection performance (probability of detection versus input signal-to-noise ratio for a given false alarm rate) for a DIMUS CFAR detector. The illustrations are for a 21 element array and a 49 element array, the first chosen to illustrate what LASA performance would be if hard limiting takes place after analog summation of the individual seismometers of the clusters. As can be seen from the figure, the 21 element CFAR possess too large a false alarm rate for most purposes. Increasing the number of elements by a factor of approximately two improves the false alarm rate by two orders of magnitude to a value more consistant with good system operation ($P_{fa} \approx 10^{-6}$).

Identification With A DIMUS Array Processor

As stated at the beginning of this section, the DIMUS beamformer is inherently a nonlinear device. A recent paper by Remley[7], presents the first derivation of the transfer function for such a processor. This transfer function is given in Figure 19, where the output signal voltage is given as a function of the input signal-to-noise ratio at each limiter. As can be seen from the figure, when the signal-to-noise ratio is on the order of unity or less, the output signal waveform is expected to be linearly related to the input waveform. Where the number of elements in the array is large, not only will the output signal be a faithful representation of the input signal, but the output signal-to-nosie ratio may also be large - even for low input signal-to-noise ratios. Here, the DIMUS output may be used exactly as the analog output is in the determination of the source of the seismic signals. Of course

the signal-to-noise ratio for the DIMUS will be somewhat less (2 dB) than for the conventional array, however, no distortion of the waveshape will have been introduced by the nonlinear processing.

When the input signal-to-noise ratio is high, however, considerable distortion of the seismic waveform may take place. This would be true for magnitude 5 events, for example. To discover the magnitude of such effects, the records of some 13 teleseismic events (both earthquakes and underground explosions) were processed with both conventional and DIMUS techniques. At least 10 widely spaced seismometers were used to form beams focused at each event. The signal-to-noise ratio was high in all cases. Thus the differential time delays could be picked by eye from the individual seismograms. The measure chosen to determine the similarity between the analog and DIMUS outputs was the zero offset correlation coefficient for the P-coda signals of these events. Here P-coda was taken to be that portion of the seismogram from three to thirteen seconds following the onset of the P-phase. The choice of this measure was based on the hypothesis that the identification of source mechanism would be based mainly on the waveforms found in this time interval of the seismogram, although it was recognized that most complexity criteria employed to date required a measurement of the ratio of main P energy to energy in specific portions of the P-coda. Undoubtably this choice of hypothesis was strongly affected by the interesting results of study of the P-coda correlation coefficient as a discriminant (see Section III).

Results of these computations were much as expected. P-coda was emphasized with respect to main P, and the general noise level increased. These two effects are illustrated by Figure 20, which shows the filtered (0.75 to 1.50 cps) analog and DIMUS beam outputs (14 seismometers) for a typical earthquake. What is somewhat unexpected is the remarkable similarity of the coda waveforms for the two signals. In fact, the coda correlation

coefficient is 0.96. Of the 13 events studied, this coda correlation coefficient ranged from 0.97 to 0.59, with only two events showing correlation coefficients lower than 0.76. With this high correlation, it is hypothesized that the coda correlation discriminant discussed in Section III could be satisfactorily employed with conventional DIMUS processing. There are, however, a number of ways by which the nonlinear transfer function of the conventional DIMUS may be linearized.

To date, one test of the simplest modification of DIMUS processing has been made. Recognizing that only events with large signal-to-noise ratio will be distorted by the conventional DIMUS, it was hypothesized that the output of a single seismometer of the array should be a good estimate of the desired output signal - particularly for the largest portions of the record. Thus, in addition to the hard limited outputs of the individual seismometers, one analog channel was used to estimate the output of a conventional analog array. The modified array output was then computed in the following manner. At the first point in time that all hard limited signals possess the same polarity (presumably that time for which the input signal entered the region of severe distortion in the transfer function), the corresponding value of the single analog channel was noted. The analog channel was then normalized so that its value at the noted point was equal to the number of seismometers making up the array (21 for the case studied). Then, for those values of the sum of the hard limited channels was equal to the number of channels, the hard limited sum was replaced by the corresponding value of the normalized analog channel.

Results of this simple "fix" are illustrated in Figure 21. Shown in the figure are the analog beam output, the modified DIMUS beam output, and the conventional DIMUS beam output. From the figure, it is easy to see that even this simple "fix" eliminated nearly all of the distortion introduced by straight DIMUS processing. Some minor distortion still exits for the main P arrival and the first second of the coda, however, the

remaining portion of the modified array output is as nearly identical with the corresponding portion of the analog processor as could be desired. In addition, it can be seen from the figure that the level of the noise in the modified record is reduced over that for the conventional DIMUS. This is to be expected, as it will be the ratio of low energy coda to noise which is expected to remain unchanged by this processing technique. As a result, when the coda level is reduced to its proper relationship with respect to main P, the noise should also shrink with respect to P. Other, more sophistocated modifications of the DIMUS technique are currently under study with the view of correction of the distortion in the first three seconds noted above. Even without such further modifications, the work to date strongly suggests that the inclusion of a single analog channel with a DIMUS processor can provide all of the information possible with an analog array, and it can do so with far greater simplicity.

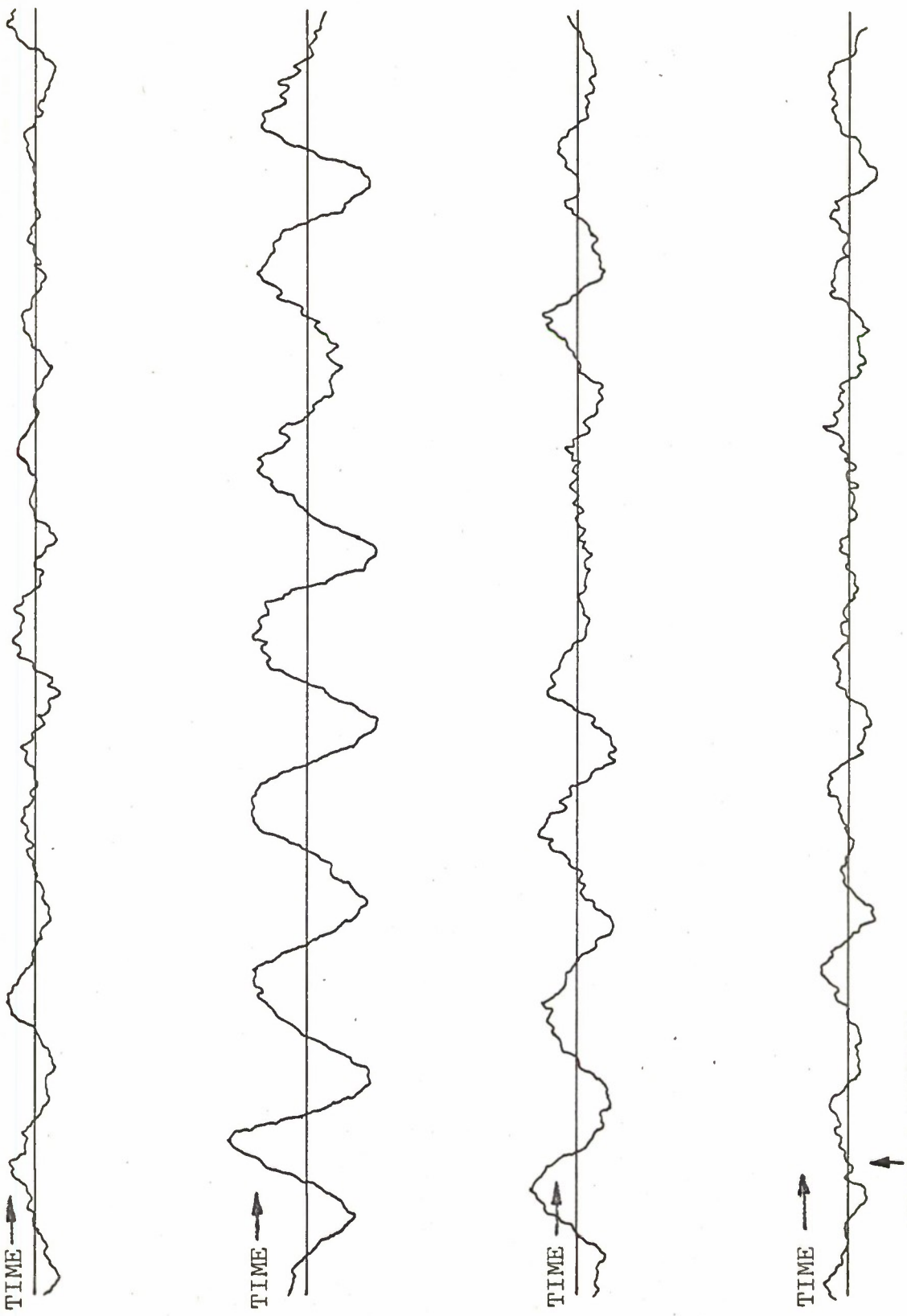

FIGURE 15 - ALGERIAN EVENT - SINGLE SEISMOMETER WMO

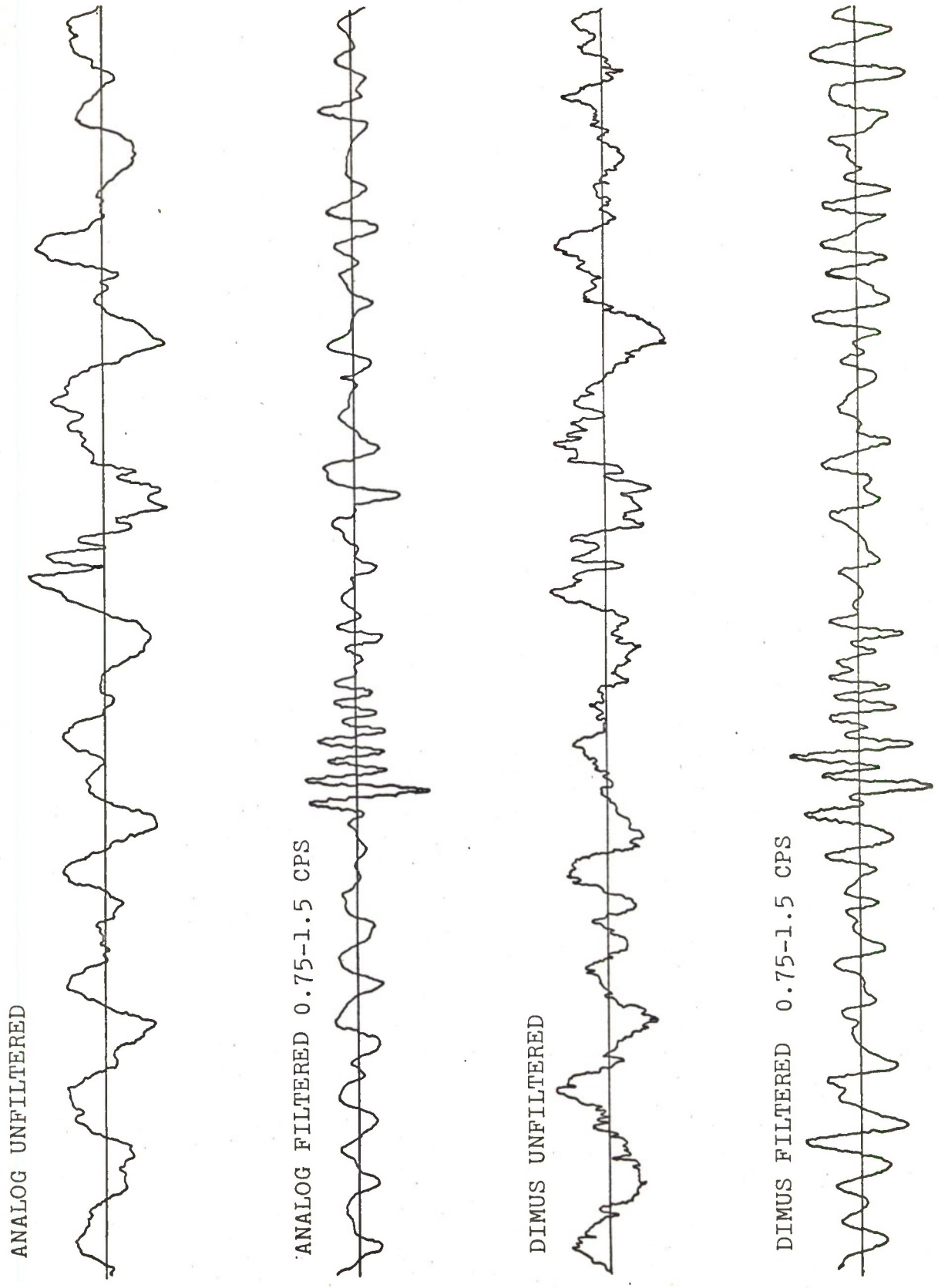

FIGURE 16 - ANALOG AND DIMUS BEAMS

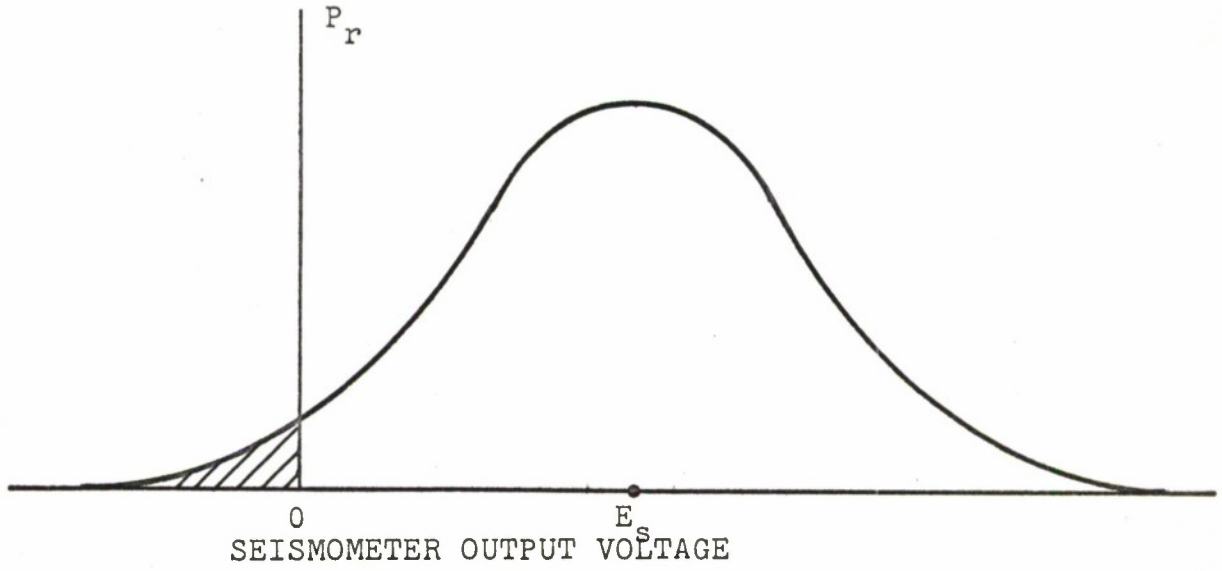

FIGURE 17 - PROBABILITY DISTRIBUTION FOR SIGNAL PLUS NOISE

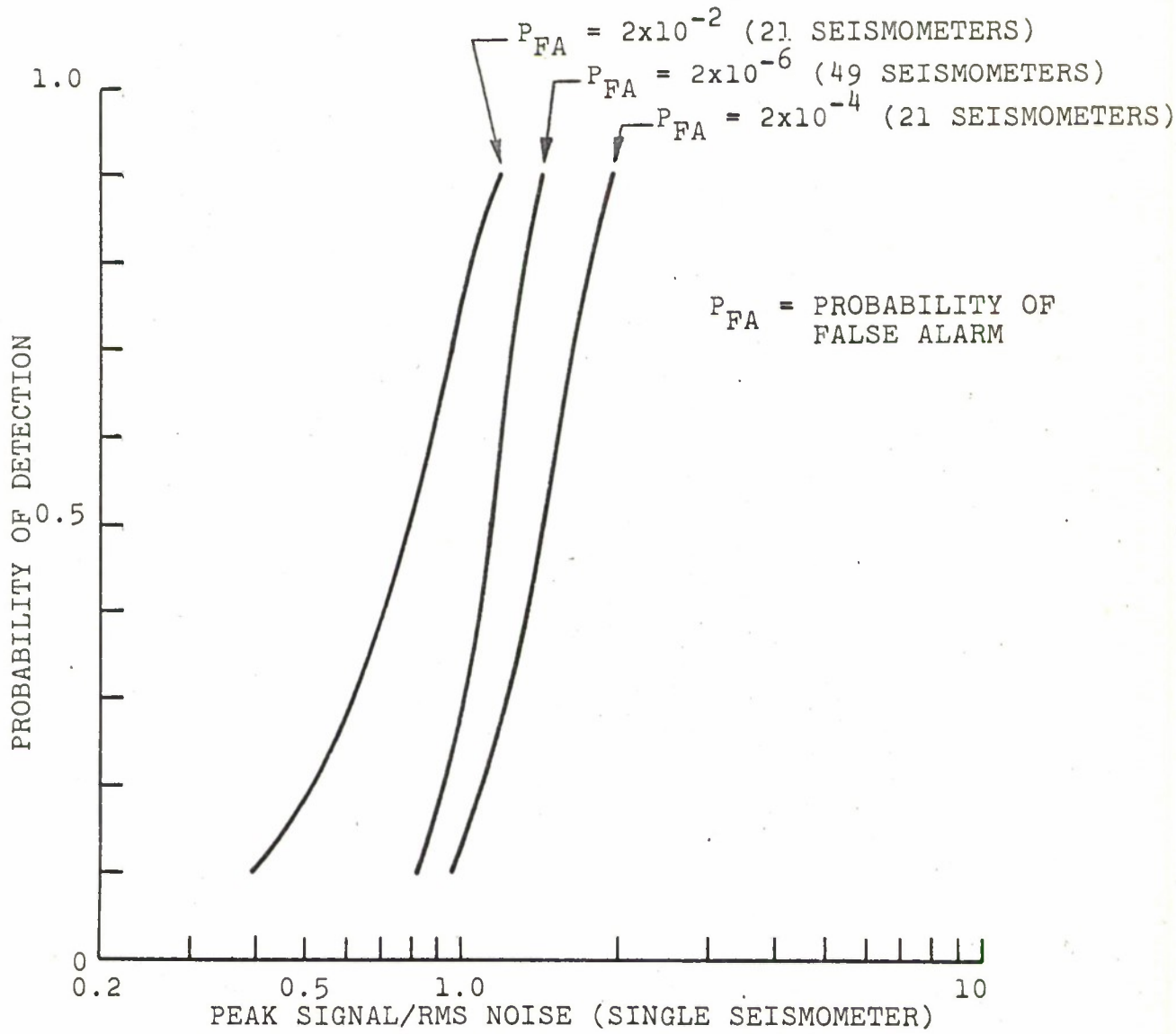

FIGURE 18 - REPRESENTATIVE DIMUS DETECTION CAPABILITY

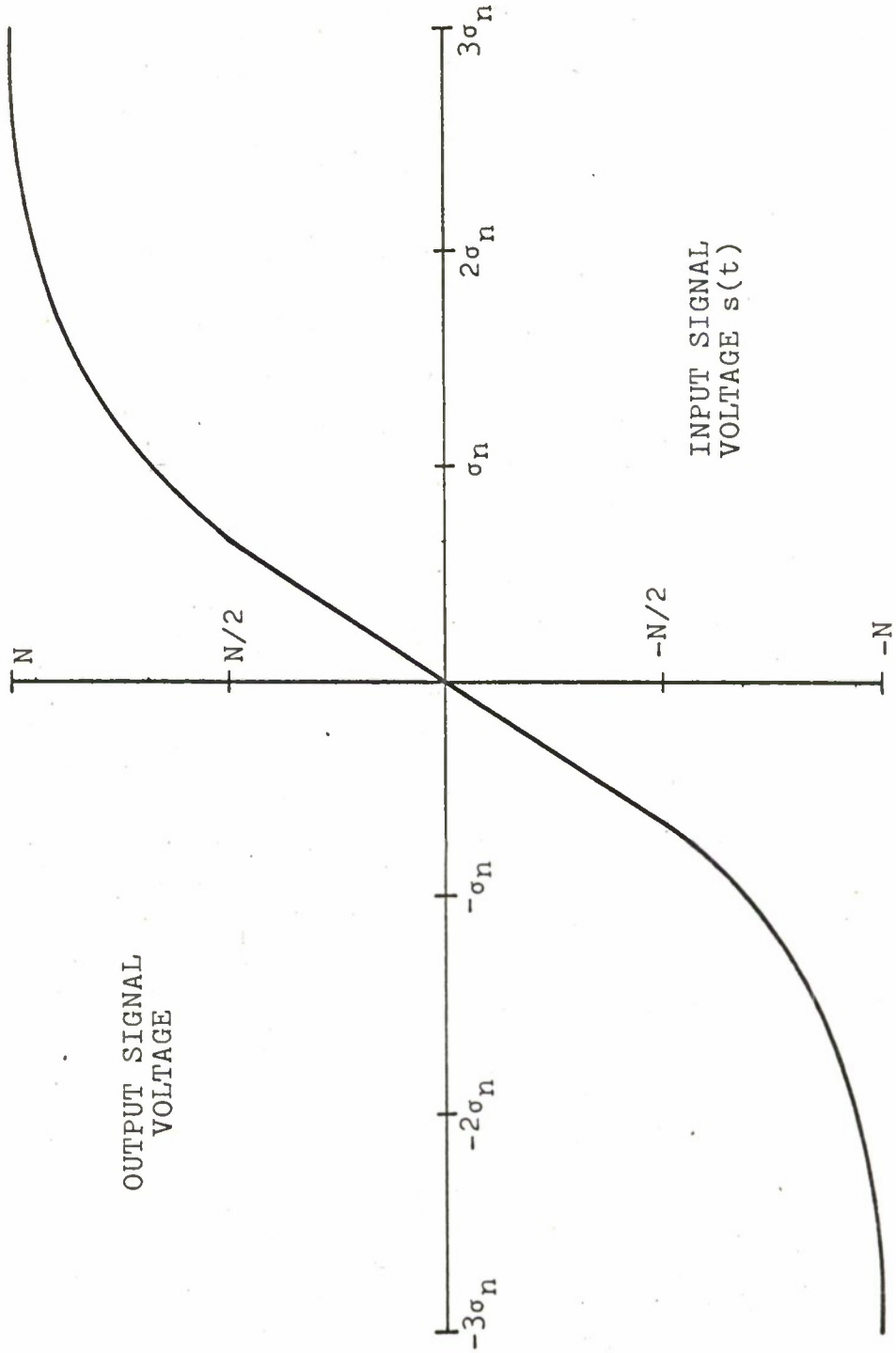

FIGURE 19 - STATISTICAL EQUIVALENT OF DIMUS FOR GAUSSIAN NOISE WITH RMS σ_n

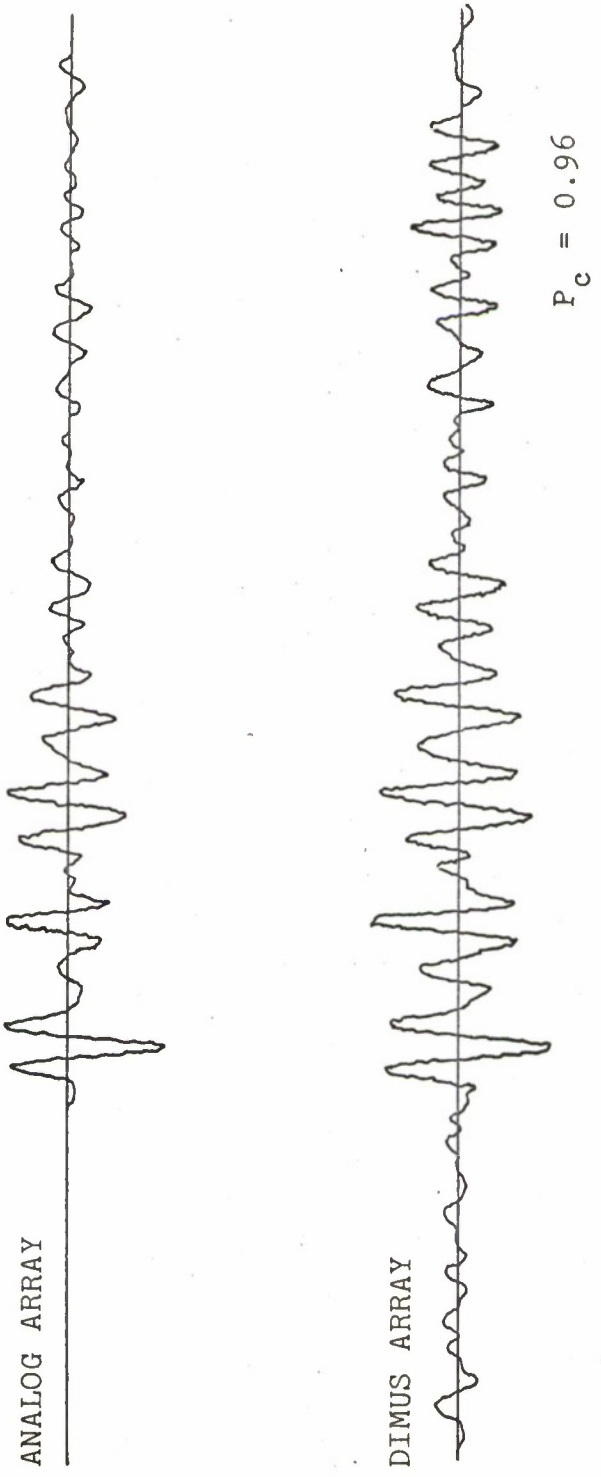

FIGURE 20 - COMPARISON OF ANALOG AND DIMUS PROCESSING

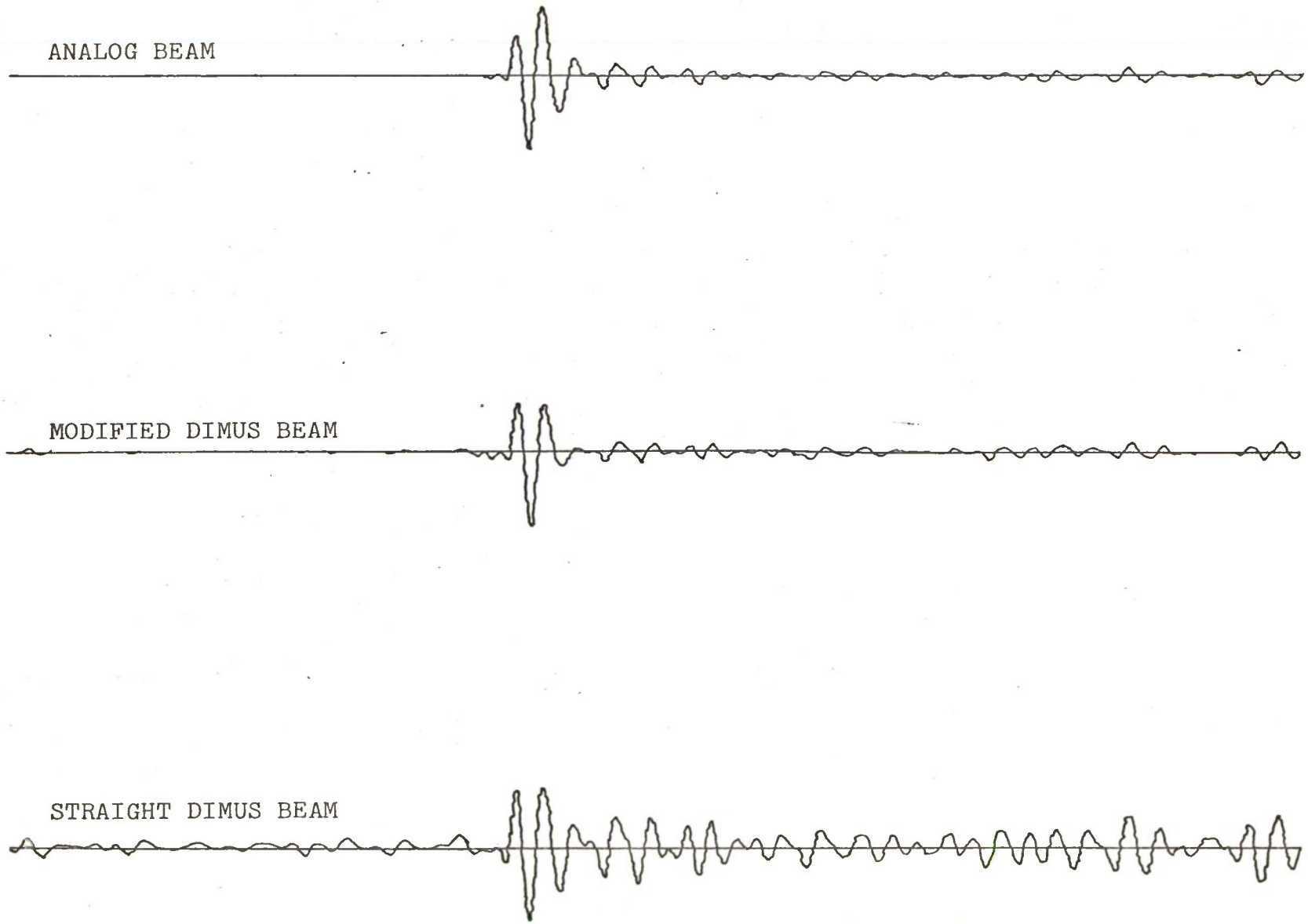

FIGURE 21 - COMPARISON OF BEAM PROCESSING TECHNIQUES

SECTION II-D. Spatial Correlations Observed Across LASA from LONGSHOT

Section III presents preliminary measurements on P-coda correlation between seismograms spaced 1000 to 7000 km for a small group of earthquakes (12) and nuclear explosions (11). Although the number of events was much too small to form conclusions, the data separated in such a way as to suggest that P-coda correlation measurements may possibly form the basis for a powerful classification procedure. Many more events are now being prepared to test the hypothesis of that note.

(Briefly stated, the mean value of the cross-correlation of P-coda for the explosions fell close to zero, grouped around 0.3 to 0.4 for shallow earthquakes(defined here as above the Moho) and fell in between for earthquakes deeper than the Moho. Since it is the shallow earthquake which it is most difficult to separate from a surface event, the large separation between the measured parameter for the two classes, i.e., explosions and shallow earthquakes, is very encouraging.)

It has been suggested by Mr. L. H. Orpin of MITRE that a similar experiment be conducted over a region of LASA dimensions (200 km), as the results may conceivably bear on LASA array design. This work has been started and the first numerical results are presented here. The LASA array in Montana has been used as the test bed and LONGSHOT used as the source. The distance from the center of the array to the source was about 5250 km.

In addition to P-coda correlation measurements the spatial cross-correlation of the main P wave and of noise just prior to the event also have been measured. The latter quantities are pertinent to prediction of array processing gain relative to the detection of the P wave in noise.[8] The coda portion used in

the experiment was 3 to 13 seconds following P-onset, typically after main P died out but before pP from a source below the Moho would arrive. The section of P wave used in the calculation was 1 second in duration centered at the first well-defined zero crossing of the P wave. Noise was 10 seconds in duration from 12 seconds to 2 seconds prior to main P.

Our cross-correlation program can accommodate 20 seismograms. We selected the central seismogram of each cluster except the central cluster. Thus each of the four subarrays in the B, C, D, E, and F rings contributed one sensor. The number of different cross-correlation coefficients computable from N instruments is $(N^2-N)/2$, which is 190 for N=20. The results follow.

P-Coda Correlation

The mean and standard deviation of the 190 correlation measurements are 0.24 and 0.25. The distribution of P-coda correlation clearly exhibits distance dependence, however. Figure 22 shows the mean values in the 10 km intervals. Table I lists the means, standard deviations and the number of correlation coefficients in each interval.

Although the variation with separation between the elements is erratic, a general diminution with separation is apparent. The mean correlation drops toward zero in the neighborhood of 100-150 km. The separation or distance dependence becomes clearer in Figure 23, in which the range scale is made logarithmic. Here the same data are replotted with the distance interval one decade in size. The decrease in the erratic nature (compare with Figure 22) is due to the larger number of sample points in each interval.

TABLE I

MEANS, STANDARD DEVIATIONS, AND NUMBER OF SAMPLES FOR FIGURES 1 AND 2

DISTANCE INTERVAL (km)	ρ_c	σ	N
8-	.47	.26	2
10-	.37	.24	18
20-	.39	.21	24
30-	.40	.15	20
40-	.29	.24	14
50-	.26	.16	14
60-	.25	.19	16
70-	.24	.20	16
80-	.04	.19	11
90-	.05	.33	14
100-	.13	.20	9
110-	.12	.19	10
120-	.01	.04	3
130-	.03	.21	4
140-	.16	.17	5
150-	-.13	.27	3
160-	.10	--	1
8-15	.40	.26	11
16-31	.37	.19	35
32-63	.31	.19	52
64-127	.14	.24	76
128-210	.03	.22	14

On the assumptions that:

i. the coda correlation test suggested in Section III may prove useful, and

ii. the distance dependence measured on LONGSHOT is somewhat typical,

it is pertinent to examine the distribution of subarrays in LASA so as to estimate the number of instruments which are adequately spaced to be useful for the test. Such examination shows that the A_0 subarray and the four subarrays in the F-ring are mutually far enough part. Thus from a single LASA a five-station test could be expected. Our experience last year in measuring the mean coda correlation indicates that about twice this number is wanted. Hence it is not likely that a single LASA would suffice; two would be needed to conduct the test with reasonable confidence, or one LASA plus five other array stations, such as the U.S. or Canadian observatories.

It is planned to test the latter possibility.

Signal

The cross-correlation of main-P is large. The mean value is 0.97 and the standard deviation is 0.04. The large correlation is not surprising in view of the fact that main P correlation was very large in the earlier reported work where the distances between elements were thousands of kilometers.[9,10]

No distance dependence is observed in the data contrary to the expected tendency for correlation to fall off with separation between seismograms. The smallest cross-correlation coefficient, which is 0.72, is obtained from seismometers in C_3 and D_4, which are only about 40 to 45 kilometers part. All C_3 values are low compared to the rest of the cross-correlation matrix. The mean correlation of C_3 with all the rest is 0.87, possibly due to error

in picking event arrival time. Dropping C_3 on this assumption raises the mean to 0.98 and reduces the standard deviation to 0.02.

The distribution of the correlation coefficient (minus C_3) is plotted in Figure 24.

Noise

In the earlier work where the distances between seismometers were thousands of kilometers, the mean noise cross-correlation appeared unbiased and reasonably symmetrical. It was of interest to determine if the same was true when the distance between elements shrank drastically. Across LASA the minimum spacing is about 8 km. The noise on the seismic records just prior to the LONGSHOT event permitted such a test. Figure 25 shows the cumulative distribution plotted on probability paper (dashed curve). The mean and standard deviation are 0.009 and 0.35.

A test for independence of the noise between elements may be made by comparing this distribution with the theoretical cumulative distribution for the cross-correlation coefficient between two independent Gaussian sources when the sample size is comparable to the estimated number of independent samples in the noise records from the seismograms. This quantity is

$$N = 2TW$$

where T is the length of the noise record and W is the noise bandwidth. The length of the record T = 10 seconds. From other spectral measurements of other records,[11]

$$1/4 < W < 1 \text{ cps.}$$

Thus the estimated number of independent noise samples in each record is about 5 to 20 samples.

Shown in Figure 25 are the theoretical curves for the cross-correlation coefficient between two independent Gaussian sources for a range of sample size which brackets the estimated number of independent samples in each record.[12] It is apparent that the measured distribution is consistent with N ≈ 9, except at the tail, where it deviates markedly. It is believed that this wild departure is attributable to the limited number of correlation coefficients from which the distribution was made up. That is, the experimental distribution had a very small number of extreme values. If this is true, a more extensive test will eliminate the seemingly abrupt truncation.

These results are consistent with the hypothesis that the noise at each cluster is independent of that of every other cluster.

Comment on Detection Efficiency

It was indicated in Reference 2 that the gain in signal-to-noise power ratio for a teleseismic array is a first order function of three quantities. These are the number of elements N, the mean spatial correlation of signal $\bar{\rho}_s$, and the mean spatial cross-correlation of noise $\bar{\rho}_n$. The relation is

$$G = \frac{\bar{\rho}_s(N-1)+1}{\bar{\rho}_n(N-1)+1}$$

In this expression N is the number of clusters or subarrays rather than the total number of seismometers. This is because the dimension of each subarray is only the order of a wavelength.

The ideal asymptotic enhancement is obtainable when $\bar{\rho}_s = 1$ and $\bar{\rho}_n = 0$. The limiting gain in this case is N, the number of subarray clusters.

It is to be expected that as the separation between elements increases, both mean correlations $\bar{\rho}_s$ and $\bar{\rho}_n$ will decrease. Thus to maximize detection efficiency an optimum array size is one which is not so large that $\bar{\rho}_s$ departs greatly from unity, while it is large enough so that $\bar{\rho}_n$ is near zero. The LONGSHOT experiment reported above suggests that the LASA dimension may be large enough to accomplish the latter while not so large as to cause significant degradation in the signal correlation. Thus for detection of main P in microseismic noise, 200 kilometers may well be within the broad optimum array size range.

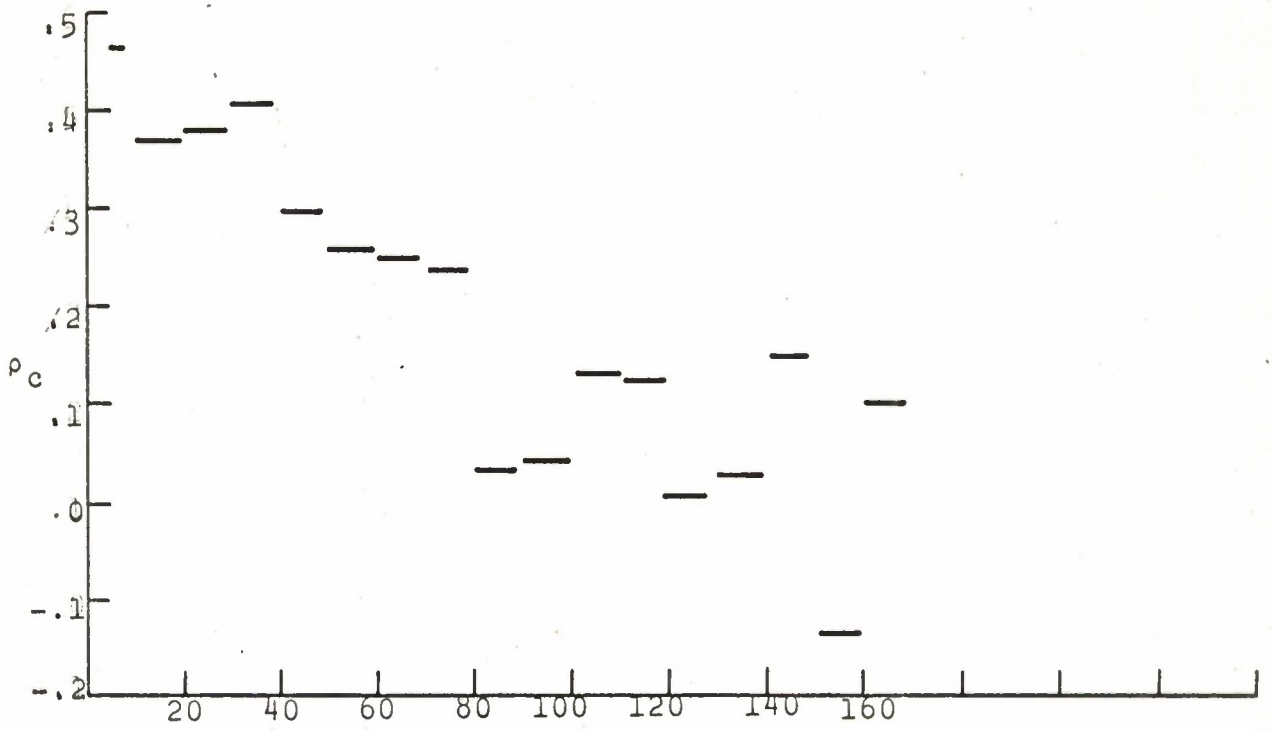

FIGURE 22 - SEPARATION BETWEEN ELEMENTS (KM)

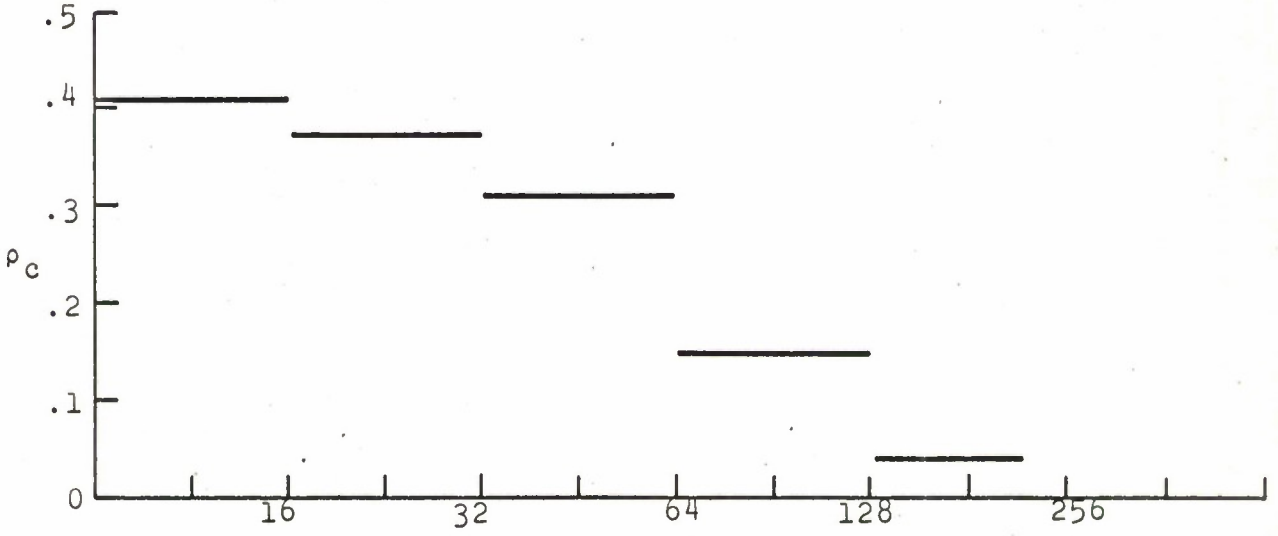

FIGURE 23 - SEPARATION BETWEEN ELEMENTS (KM)

MEAN SPATIAL CORRELATION OF LONGSHOT CODA AS A FUNCTION OF THE DISTANCE BETWEEN SEISMOMETERS. LENGTH OF CODA IS 10 SECONDS BEGINNING 3 SECOND AFTER P-ONSET

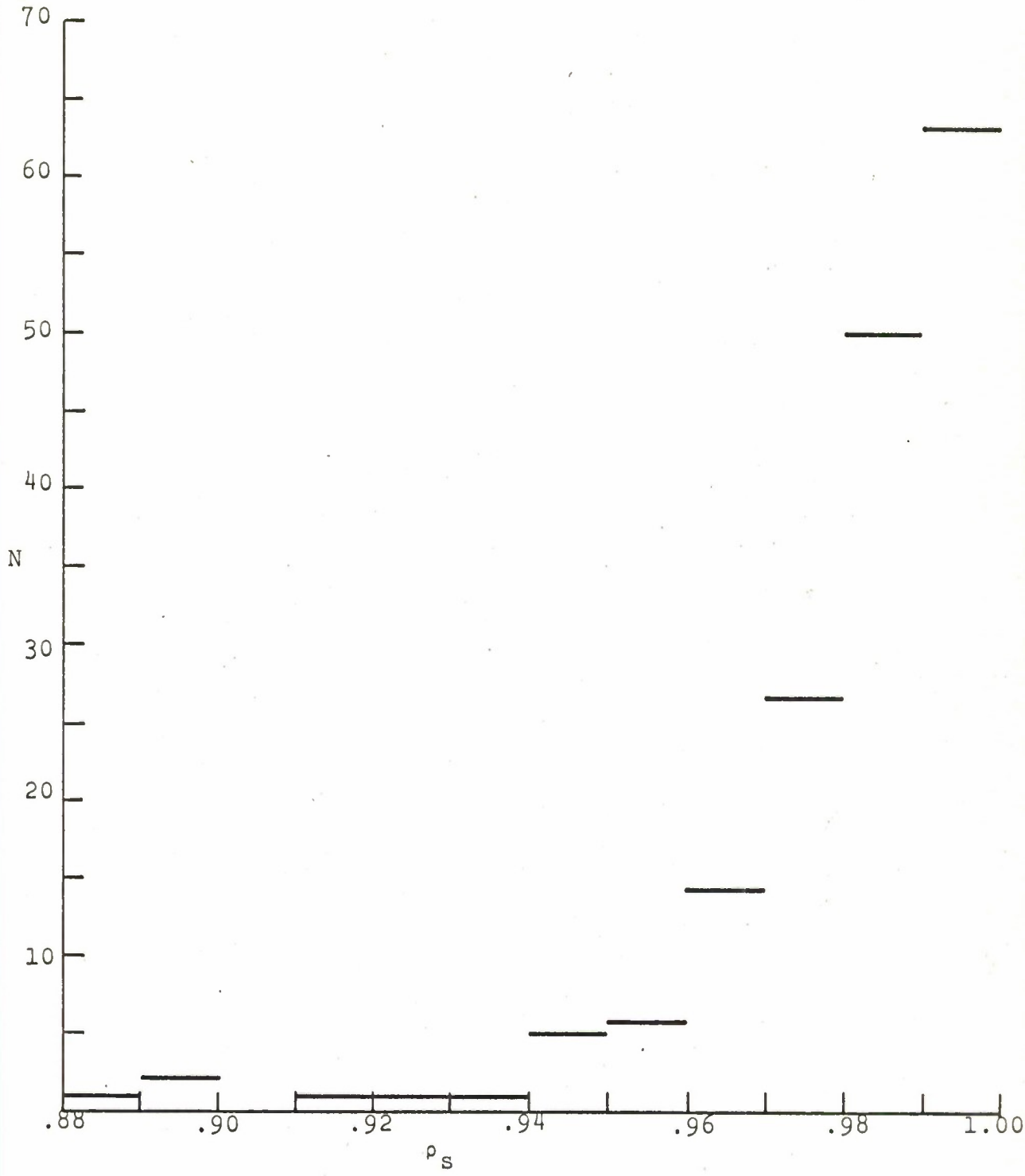

FIGURE 24 – DISTRIBUTION OF THE SPATIAL CORRELATION ACROSS LASA OF FIRST SECOND OF LONGSHOT P-WAVE

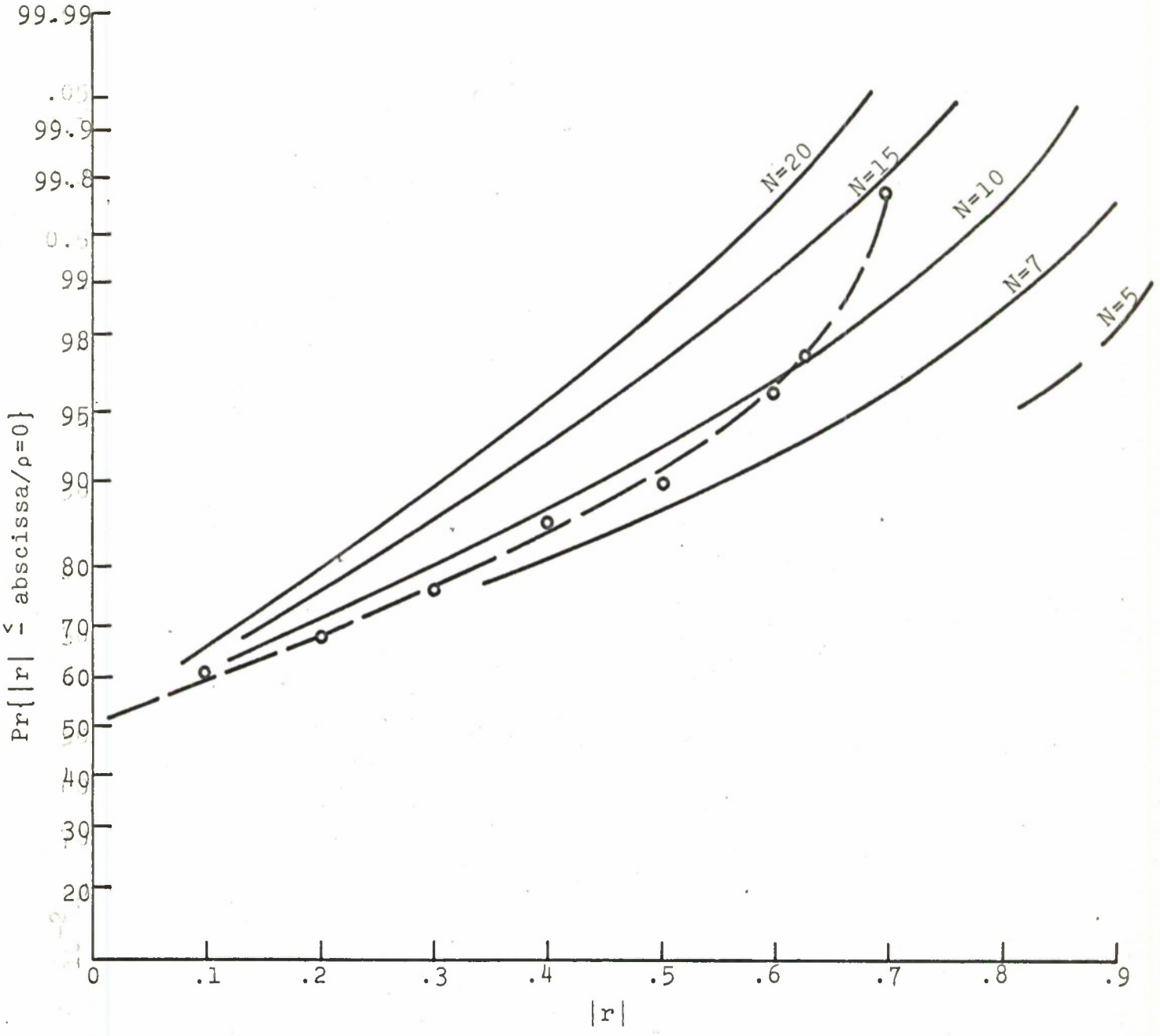

FIGURE 25 - CUMULATIVE DISTRIBUTION OF THE SPATIAL CROSS-CORRELATION ACROSS LASA OF 10 SECONDS OF NOISE PRIOR TO LONGSHOT. SOLID CURVES ARE THEORETICAL DISTRIBUTIONS FOR INDEPENDENT NORMAL SOURCES. N = NUMBER OF INDEPENDENT SAMPLES IN EACH RECORD

Section III Coda Correlation as a Discriminant

For several months General Atronics has been studying the average cross-correlation coefficient between seismograms from widely separated stations in response to common events. This has been done for microseismic noise, P wave onset, P-coda, and, where possible, pP. All seismograms were time aligned by eye. The separation between stations ran up to about 7000 kilometers.

The purpose of forming these mean correlation coefficients was to determine the extent to which signal enhancement would be achieved by beam formation from arrays of enormous extent. For the detection problem the signal was considered to be the P wave in the neighborhood of onset and the noise was considered to be microseismic; for the classification problem the signal was considered to be pP and the noise or background interference was considered to be P-coda.

Array theory indicates that it is the mean cross-correlation between appropriate portions of the seismogram which dominates the amount of signal enhancement relative to background interference provided by a large array. Consequently, the mean values of the four cross-correlation coefficients were obtained.

Still speaking historically, it was found that the mean cross-correlation coefficients for the P wave were reasonably close to unity, while those for microseismic noise were very close to zero. Consequently, excellent signal-to-noise enhancements could be obtained for the detection problem. For the classification problem, however, the data were much less conclusive. It appeared that the correlation for P-coda between stations separated by thousands of kilometers was much too high to achieve useful enhancement of pP in P-coda. However, the data were too fragmentary to form such a firm conclusion. Consequently, more events are now being prepared for inclusion in the study.

Even though the number of events was not large, the larger-than-expected coda correlation demanded examination of the data in any ways which might disclose consistencies, peculiarities, etc. One such examination did disclose a potentially important discriminator between shallow earthquakes and surface events. This is the subject of this section of the report.

A total of 23 events, 12 earthquakes and 11 surface events have been studied to date. The stations were widely distributed and were in no sense special. The section of coda used is 3 to 13 seconds after P onset. This interval is beyond the main P wave but before interaction with the Moho occurs. It thus includes pP for the range of earthquake depths in which we are most interested.

The 10 second P-coda interval contains 200 samples per record. An average of about 10 stations each recorded each event; hence each event is represented by about 2000 data samples. Each set of 10 records provided 45 $[(N^2-N)/2]$ correlation coefficients. The average of these 45 numbers is the statistical variate of interest. It is designated $\overline{\rho}_c$.

The total number of samples is deceptively large, being about 2000 samples for each of 20 events, or 40,000 samples. More important to remember is that they represent only 20 events, which is an inadequate number of permit conclusions to be drawn. The data, however, force the creation of a hypothesis which is worthy of testing, and for which testing is now underway.

Figure 26 is a plot of the fraction of events having a mean coda correlation less than the abscissa. It is plotted for each of the two classes. The points for the 23 events are shown. Also shown on the figure are the general locations of the surface events, the depth of the earthquakes, and the magnitudes for both classes of events. As can be seen from the figure, no particular location dependence can be observed in the data. Neither can a magnitude dependence be discovered. There

can be observed, however, a definite relationship between the earthquakes of differing depth. More will be said about this later.

The coordinates for Figure 26 are those of probability paper. A Gaussian distribution plots as a straight line on this paper. The number of events is very small in each of the two cases; however, if we assume that these small numbers of events typify the real world distributions, a powerful discriminant test becomes available. This is better seen in Figures 27 and 28. The curves of Figure 27 are the derivatives of the smoothed cumulative distributions of Figure 26. Therefore, to the extent that the 12 earthquakes typify the earthquake population, and the 11 surface events typify their population, the curves of Figure 27 may be taken as a first estimate of the probability density distributions of the mean cross-correlation of P-coda for earthquakes and for explosions.*

The surface event distribution (h=0) offers no surprises. However, the earthquake distribution is unusual. When double-humped distributions of this kind appear in nature, it is often the result of two separate phenomena operating. It is tempting, therefore, to break the distribution of Figure 27 into two roughly symmetrical distributions as shown by the dashed lines. It is further tempting to ask if the events associated with the left-hand part of the earthquake distribution are in some way distinguishable from those associated with the right-hand part of the distribution. We find that the left-hand distribution includes all the earthquakes deeper than the Moho while the right-hand distribution represents all the earthquakes shallower than the Moho.

.....

*Here it is necessary to caution that the smallest earthquake studied had a magnitude of 4.7.

This, of course, is very attractive, as earthquakes deeper than the Moho can, with reasonable confidence, be distinguished from surface events by other means. It is the shallow quakes which constitute the problem, and in Figure 27 their distribution appears separable from the surface event distribution.

On the assumption that the deeper earthquakes can be identified by other means, the data of Figure 26 has been replotted as Figure 28, where only those earthquakes shallower than 40 kilometers have been retained. The results are striking. Both the surface events and the shallow earthquakes follow Gaussian distributions as closely as could be desired. Further, the separation between these two distributions is large. In conventional signal processing terms, the signal-to-noise ratio is 16 dB.

It is hardly necessary to urge caution in expressing one's optimism at this point. The foregoing discussion is predicated on too many if's to be taken seriously. Consequently, considerable effort is being made at the present time to increase the size of the earthquake population manyfold. Nevertheless, one more if is worth observing; namely, if Figure 28 turns out to be a reasonable approximation to the real world distributions of the coda correlation for shallow earthquakes, then an extremely powerful discriminant is immediately available.

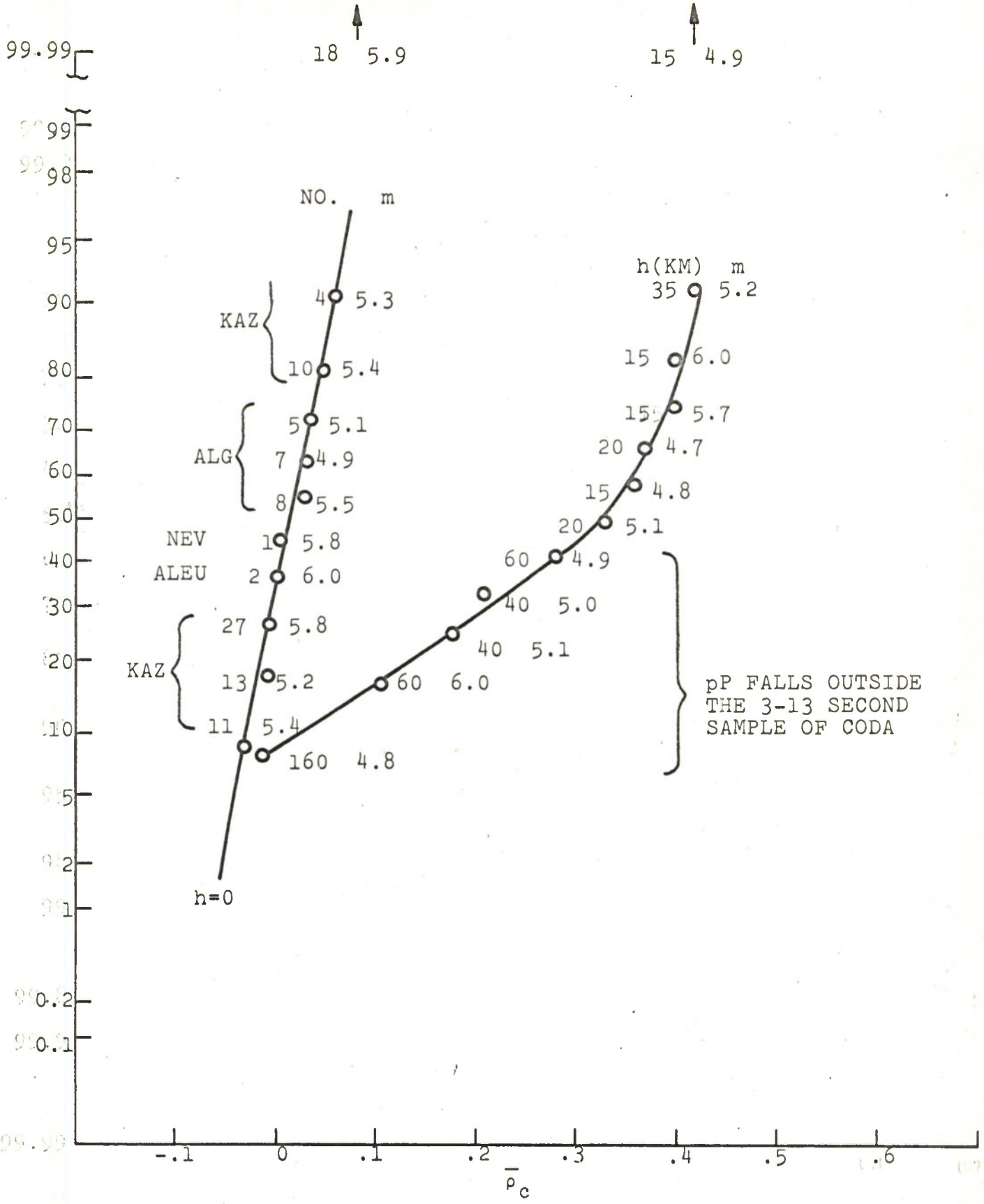

FIGURE 26 - FRACTION OF EVENTS HAVING MEAN CODA CORRELATION $\bar{\rho}_c$ OR GREATER

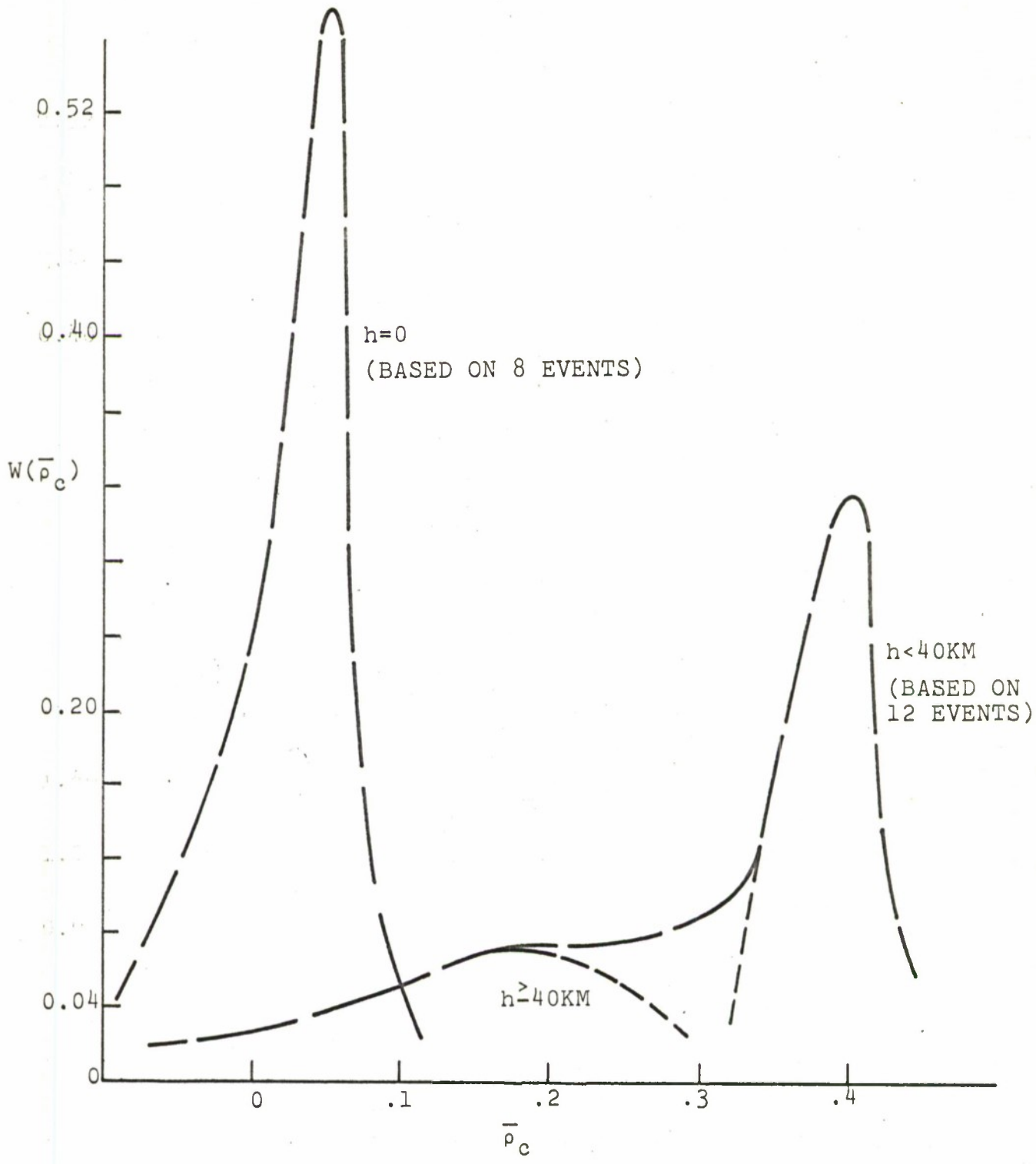

FIGURE 27 - ESTIMATES OF THE FIRST PROBABILITY DENSITY DISTRIBUTIONS OF MEAN P-CODA CORRELATION OF SURFACE EVENTS AND EARTHQUAKES

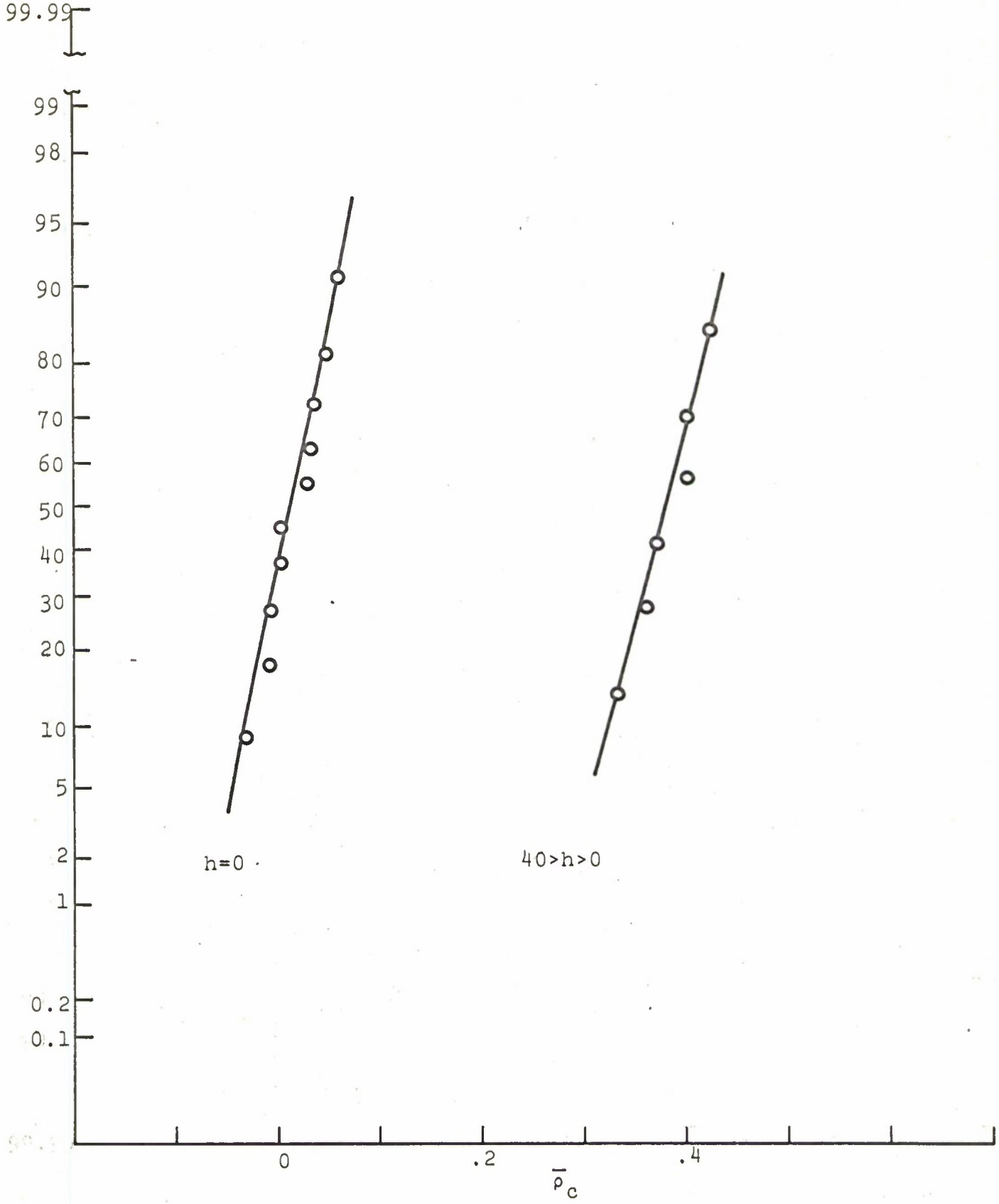

FIGURE 28 - FRACTION OF EVENTS HAVING MEAN CODA CORRELATION $\bar{\rho}_c$ OR GREATER

Section IV Attenuation of Seismic Waves in the Earth's Upper Mantle

General

A suggestion by Dr. Eugene Herrin that the large discrepancies in the measured spectra from LONGSHOT might result from low Q regions in the earth's upper mantle prompted a brief study to discover whether it is possible to determine the existence of such layers using the spectra of the P and pP phases of deep earthquakes. This section describes the results obtained to date.

The absorption strength of a medium can be measured by the fractional energy absorbed per cycle = Q. Experiments point toward a Q constant with frequency for the earth. A comparison of the frequency content of two phases of the same deep event, pP and P, makes it possible to find the average value of Q in the upper mantle at the epicenter region. Three events from the Fiji Islands region were analyzed. These events yield measurements of Q of the order of 200, indicating that the attenuation is one order of magnitude larger than expected from previous measurements.[12]

A method is suggested to extend the study to treat the upper mantle of aseismic regions.

Description of the Experiment

The attenuation suffered by a wave traveling through a medium is characterized by the dimensionless factor Q, defined as

$$\frac{2\pi}{Q} = \frac{\Delta E}{E} = \text{fractional energy absorbed per cycle.}$$

In general Q is a function of frequency. A large number of observations of absorption indicated a constant energy absorption per cycle.[13] Since no linear relation between stress and strain will produce a Q constant with frequency, effect other than simple absorption must contribute to the empirical results obtained by Howell. This fact will not prevent measurement of attenuation on the upper mantle.

For a given range, a constant factor Q implies stronger attenuation for high frequencies than low frequencies. The

attenuation function (energy) for a monochromatic wave can be considered as

$$A(\Delta,\omega) = e^{-2\alpha(\omega)\Delta}$$

Δ = length of the path

$\alpha(\omega)$ = absorption coefficient

To find the attenuation function that corresponds to a constant Q, let

$\Delta = \lambda$ (wave length)

$$\frac{\Delta E}{E} = 1 - e^{-2\alpha\lambda} = \frac{2\pi}{Q}$$

$$1 - 1 + 2\alpha\lambda - 4\alpha^2\lambda^2 + \ldots = \frac{2\pi}{Q}$$

for $\alpha\lambda \ll 1$: $\alpha = \frac{\pi}{\lambda Q} = \frac{\omega}{2cQ}$

where c = group velocity

$$A(\Delta,\omega) = e^{-\frac{\omega}{cQ}\Delta}$$ = attenuation function (energy)

In studying attenuation in the upper mantle the phases pP and P are of particular importance. The path of pP is greater than the path of P. This additional travel is composed of two crossings of the upper mantle and the crust in the region of the epicenter. This fact allows us to determine the attenuation characteristics of the upper mantle, since the ratio of the energy spectra of P and pP is determined by the attenuation suffered during this extra path.

For the purpose of this study, the following model will be used for the earth.

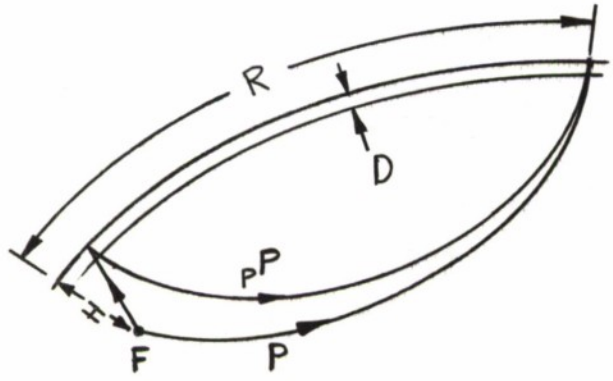

F: Focus
D: Crust thickness
H: Focal depth
R: Range to the receiver

The attenuation functions will be given by the following approximate expressions:

a) $A_{pP}(R,\omega) = e^{-\frac{\omega}{c}\left(\sum \frac{\Delta_i}{Q_i}\right)}$

Δ_i = length of path in region i, Q_i = Q value in region i

$\frac{\Delta_i}{Q_i} = 2\left(\frac{H-D}{Q}\right) + \frac{2D}{Qc}$ + (Terms including attenuation in the lower mantle and the crossing of the upper mantle and crust at the receiver = T)

$$A_{pP}(R,\omega) = e^{-\frac{\omega}{c}\left(2\left(\frac{H-D}{Q}\right) + \frac{2D}{Qc} + T\right)}$$

b) $A_P(R,\omega) = e^{-\frac{\omega}{c}T}$

These are the square of the moduli of the transfer functions of the earth as a filter, for both cases, and therefore relate the energy spectra, at the receiver, with the energy spectrum at the focus.

For the following two cases it is assumed that the source spectrum for P and pP are identical:

a) Spherically symetric radiation pattern (explosive type of source mechanisms)

b) Plane fault as the source mechanism, P and pP leaving the source approximately in the same direction and opposite sense.

$$\frac{E_P(\omega,R)}{E_{pP}(\omega,R)} = \frac{A_P(\omega,R)}{A_{pP}(\omega,R)} = e^{+\frac{\omega}{c}\left(2\left(\frac{H-D}{Q}\right) + \frac{2D}{Qc}\right)}$$

where E_P and E_{pP} are the energy spectra. This means that we expect to find more attenuation in pP because it crossed the crust and the upper mantle two additional times.

Since the thickness of the crust is small (25-40 km), the effect of the attenuation in the crust (assuming a Q of 200 for both crust and upper mantle) is very small compared with the effect of the upper mantle crossing.

$$\frac{2D}{Qc} = \frac{80}{200} = 0.4 \text{ with } D = 40 \text{ km}$$

$$\text{the term } 2\left(\frac{H-D}{Q}\right) = 5.0 \text{ for } H-D = 500 \text{ and } Q = 200$$

As a result, should the average Q show a low value, this phenomenon must be related to the upper mantle and not the crust.

For an earth without high attenuation in the upper mantle, the ratio of the energy spectra should have the following expression:

$$\frac{E_P(\omega,R)}{E_{pP}(\omega,R)} = e^{\frac{\omega}{c}\left(\frac{2h}{\bar{Q}} + \frac{2D}{Qc}\right)}$$

where h = focal depth
$\bar{Q}$ = average Q over ray path = 2000

$$\frac{2h}{\bar{Q}} = \frac{1000}{2000} = .5$$

$$\frac{2D}{Qc} = 0.4$$

In this case the attenuation in the crust could not be neglected; however, interpretation of the results would be difficult should the upper mantle have an intermediate Q, (approximately 800). It was the purpose of this investigation to seek only existence of very low Q's in some regions of the upper mantle. Hence, we can side step this problem.

Experimental Results

Three deep earthquakes in the Fiji Island region were chosen to test the hypothesis of a low Q layer for the upper mantle in this part of the earth. (See Figure 29) These events were:

1) E.Q. Fiji Islands Region 7 Oct 63 13:14:24.6z
23.6°S 179.9°E d = 550 km. M = 5.7

2) E.Q. Fiji Islands Region 7 Dec 63 04:07:52.8z
22.1°S 179.4°W d = 546 km. M = 5.5

3) E.Q. Fiji Islands Region 26 April 64 14:52:07.6z
20.6°S 178.0°W d = 490 km. M = 5.1

The energy spectra for both the P and pP phases were computed for each of these events, and the ratio of the spectra of the two phases was then compared with the modeled functions for a layer with high Q and one with low Q. The experimental data together with the theoretical expressions are shown in Figures 30 through 32 The abscissa is frequency in cps. The ordinate is the logarithm of the ratio of the energy spectra normalized to the value at .5 cps. Hence all curves cross the abscissa at 0.5 cps. From these curves the following data may be summarized. The measured, average Q of the upper mantle for the three events studied was 458, 218, 272. As can be seen from Figure 1, the earthquake leading to the highest measured value of Q is the only one of the three which lies on the Fiji Ridge. This fact might explain the difference in the observed values of attenuation. The experimental data obtained are shown in more detail in Figures 30 through 32. These values show a tendency to have a smaller spread with respect to the least square fit as we increase the record length.

The least square fitted curves are summarized for each event in Figures 30through 32.

Extension of the Method to Analyze Non-Seismic Regions

Some seismic stations have shown a greater high frequency content in their records than others. This could mean that the attenuation characteristics of the upper mantle are regionally dependent. To analyze this hypothesis, the following method is suggested.

Let us assume that we are interested in studying the attenuation characteristics of the upper mantle of a certain region

where there are no deep earthquakes. Let us call that area region S. We must first study some other region which possesses both deep earthquakes and a seismic station. Let us call this region A. Records obtained at A and a station in S may then be compared, taking the ratio of the energy spectra of the P arrivals. The ratio of the energy spectra of the P phase recorded at A and S enables us to learn about the attenuation characteristics of the upper mantle in the region S. It is important to note that in following this procedure care must be taken to include any frequency dependent radiation pattern effects which will result from geometry of the measurement.

FIGURE 29 - EPICENTER LOCATIONS

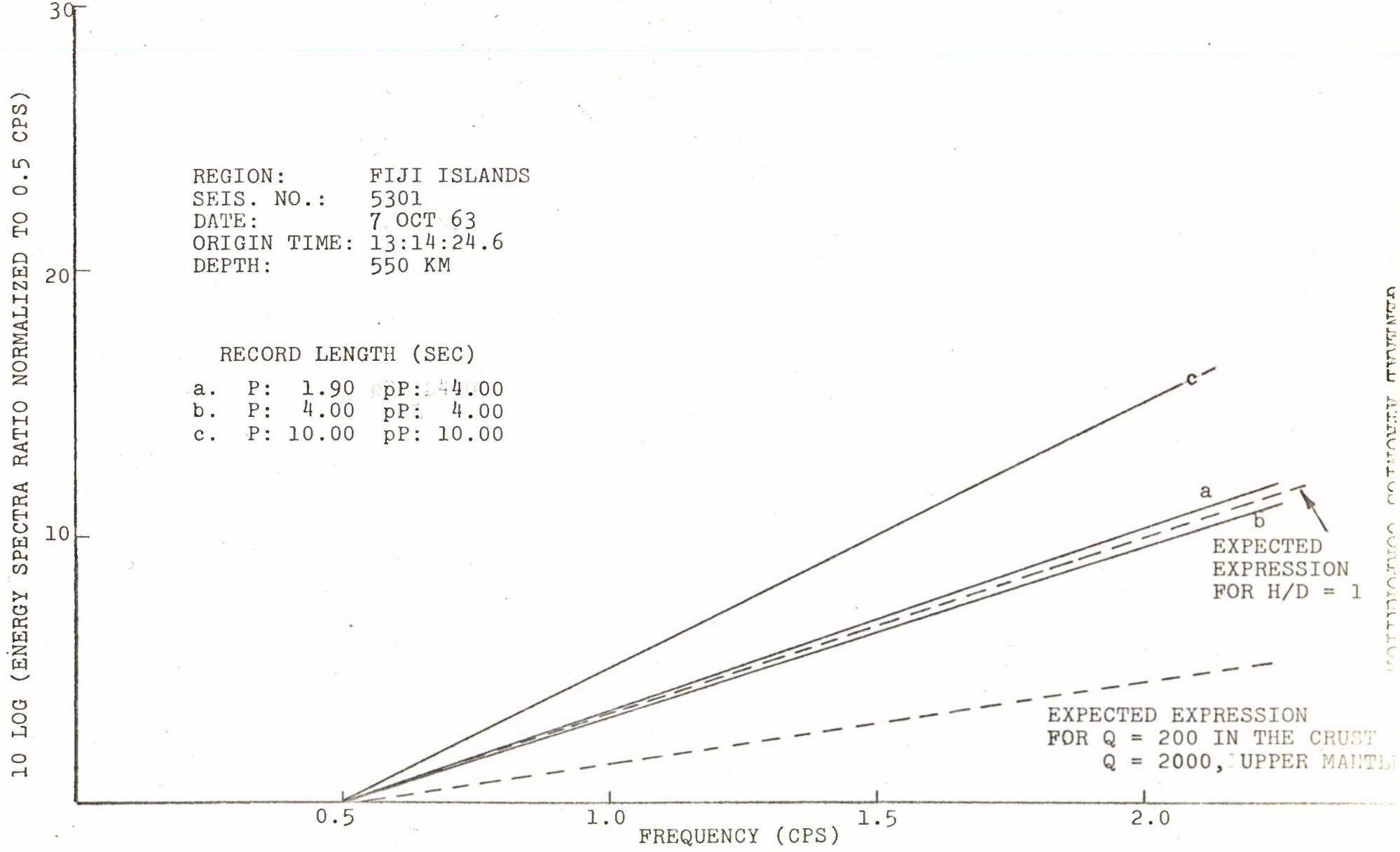

FIGURE 30 - LEAST SQUARES FITS TO THE EXPERIMENTAL RATIO OF ENERGY SPECTRA (SUMMARY)

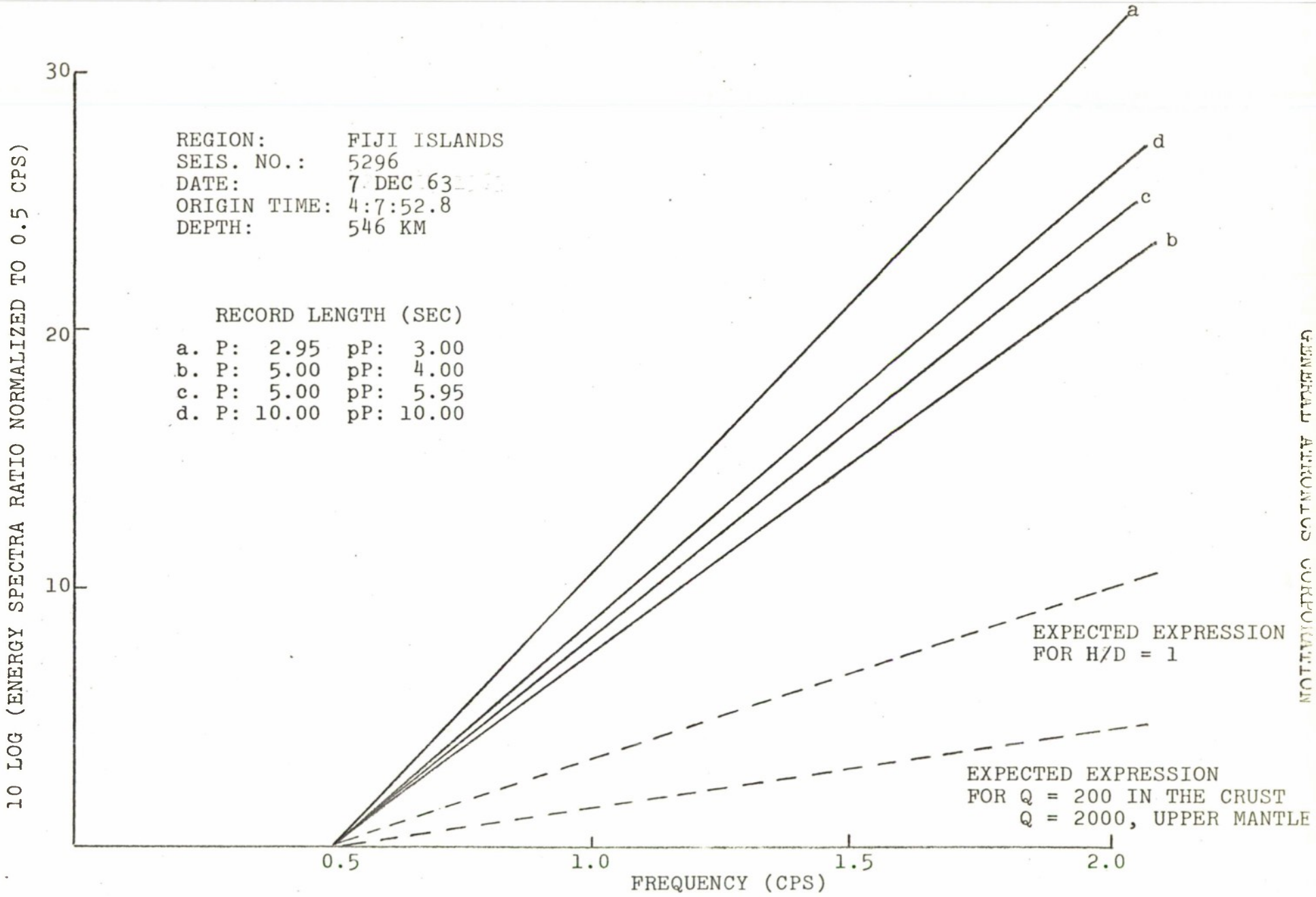

FIGURE 31 - LEAST SQUARES FITS TO THE EXPERIMENTAL RATIO OF ENERGY SPECTRA (SUMMARY)

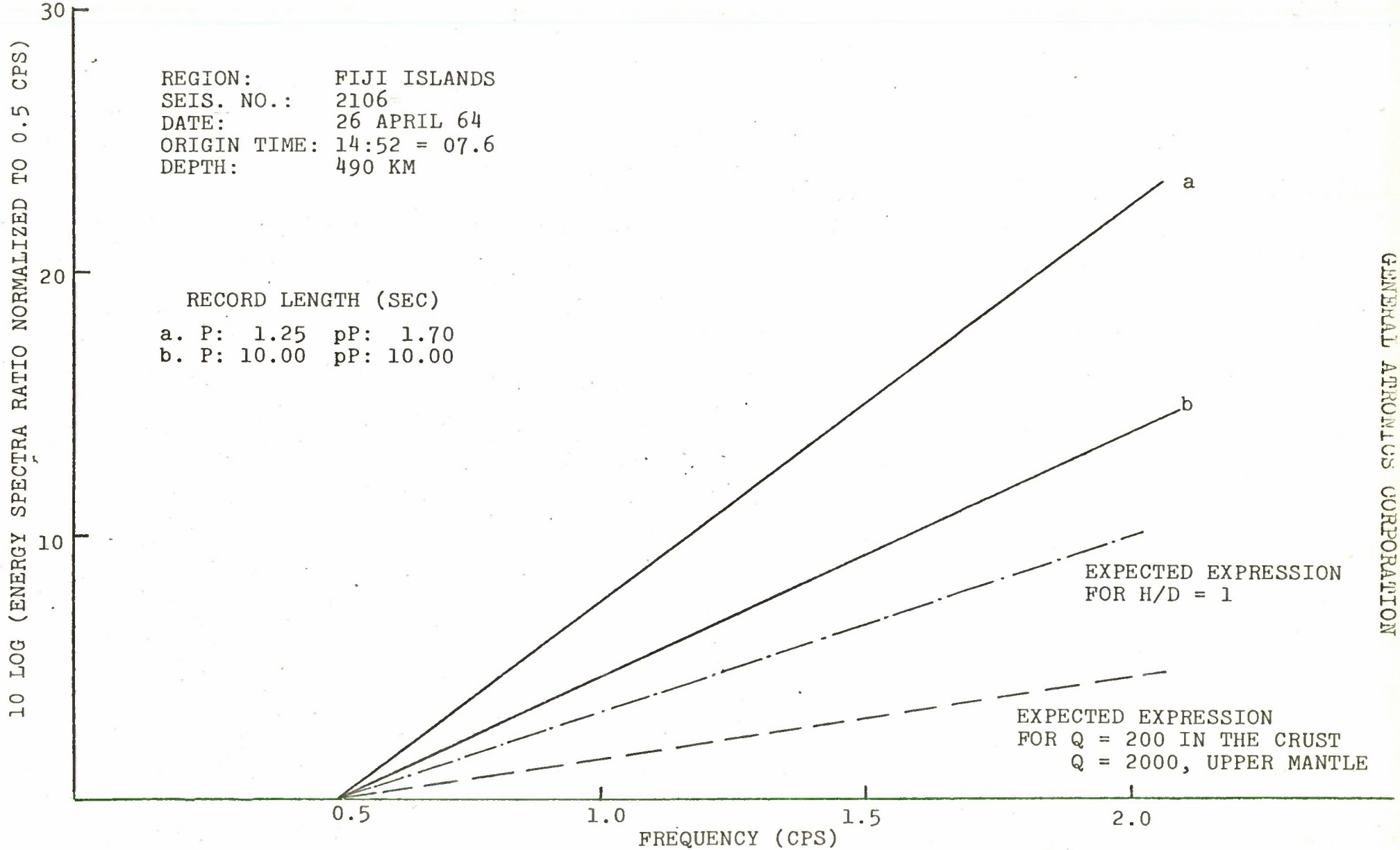

FIGURE 32 - LEAST SQUARES FITS TO THE EXPERIMENTAL RATIO OF ENERGY SPECTRA (SUMMARY)

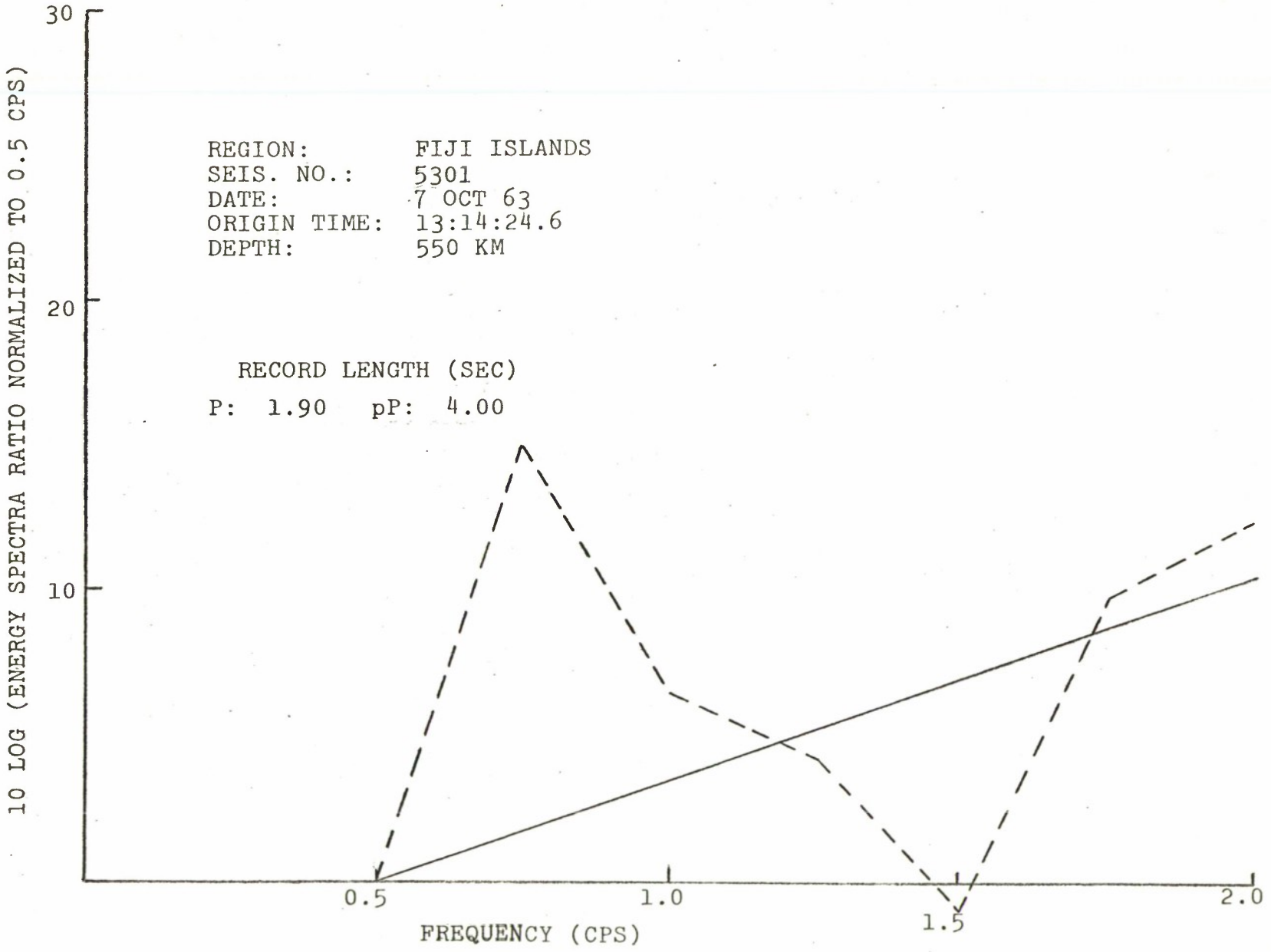

FIGURE 33 - ENERGY SPECTRA RATIO - EXPERIMENTAL DATA AND LEAST SQUARES FIT

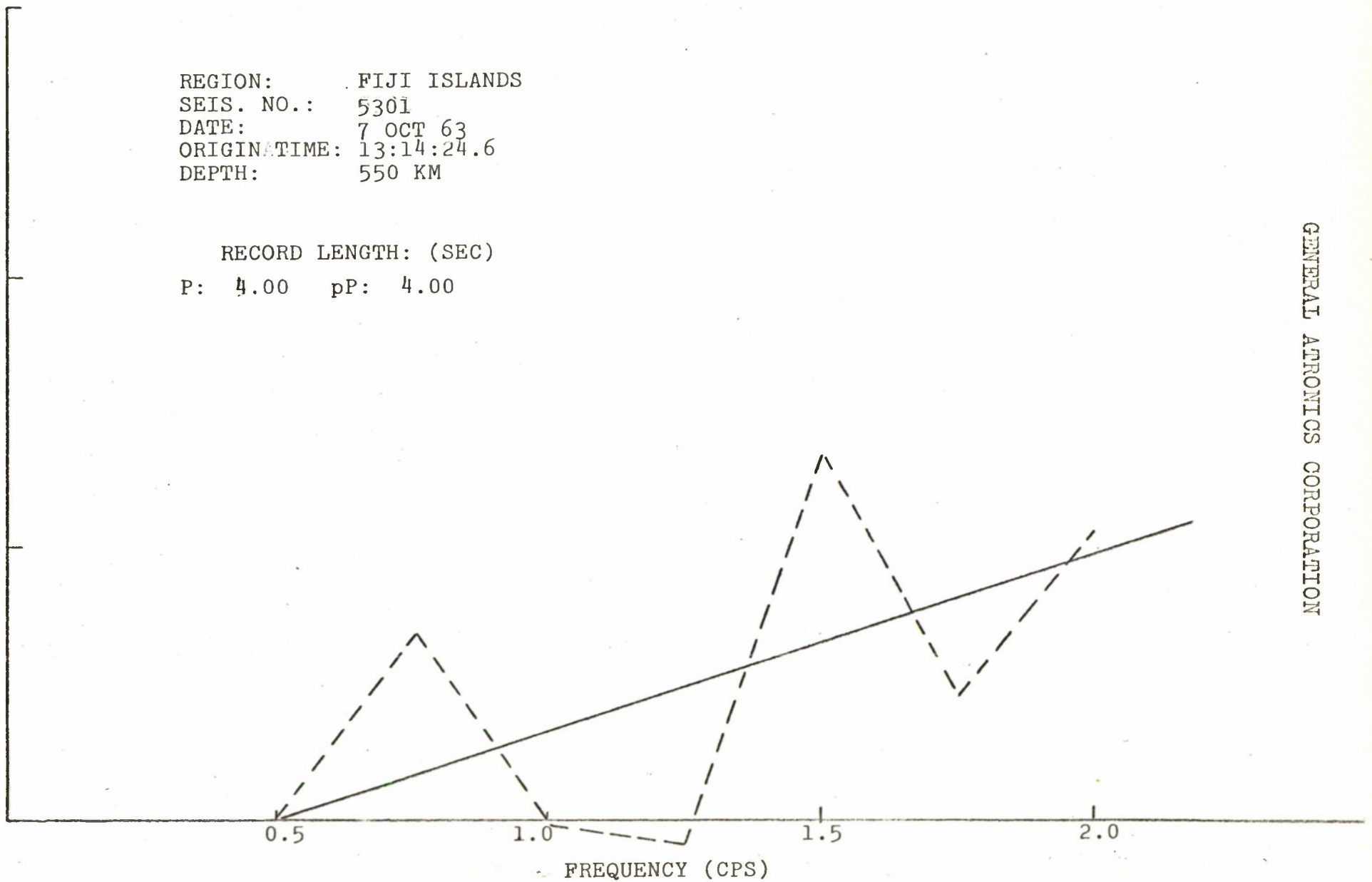

FIGURE 34 - ENERGY SPECTRA RATIO - EXPERIMENTAL DATA AND LEAST SQUARES FIT

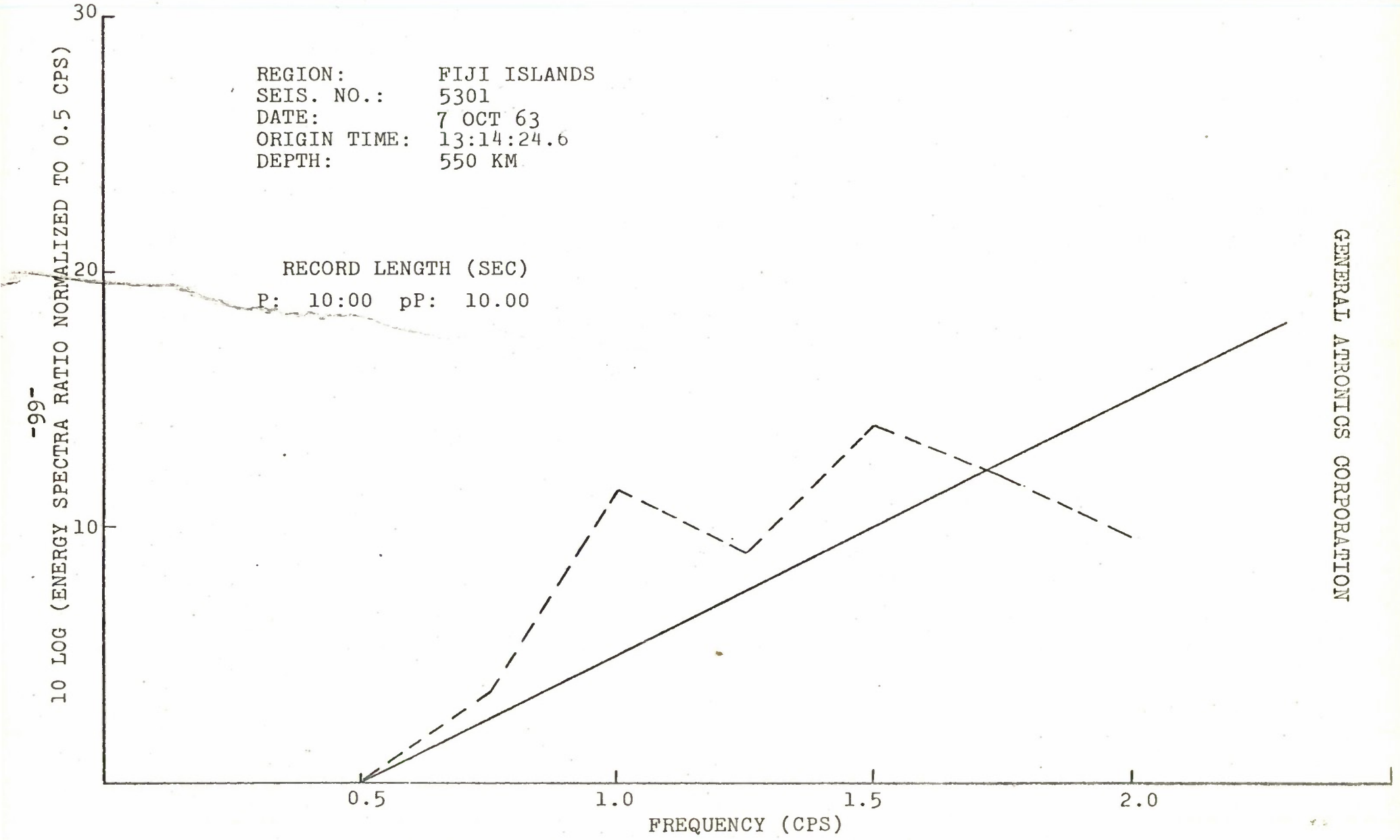

FIGURE 35 - ENERGY SPECTRA RATIO - EXPERIMENTAL DATA AND LEAST SQUARES FIT

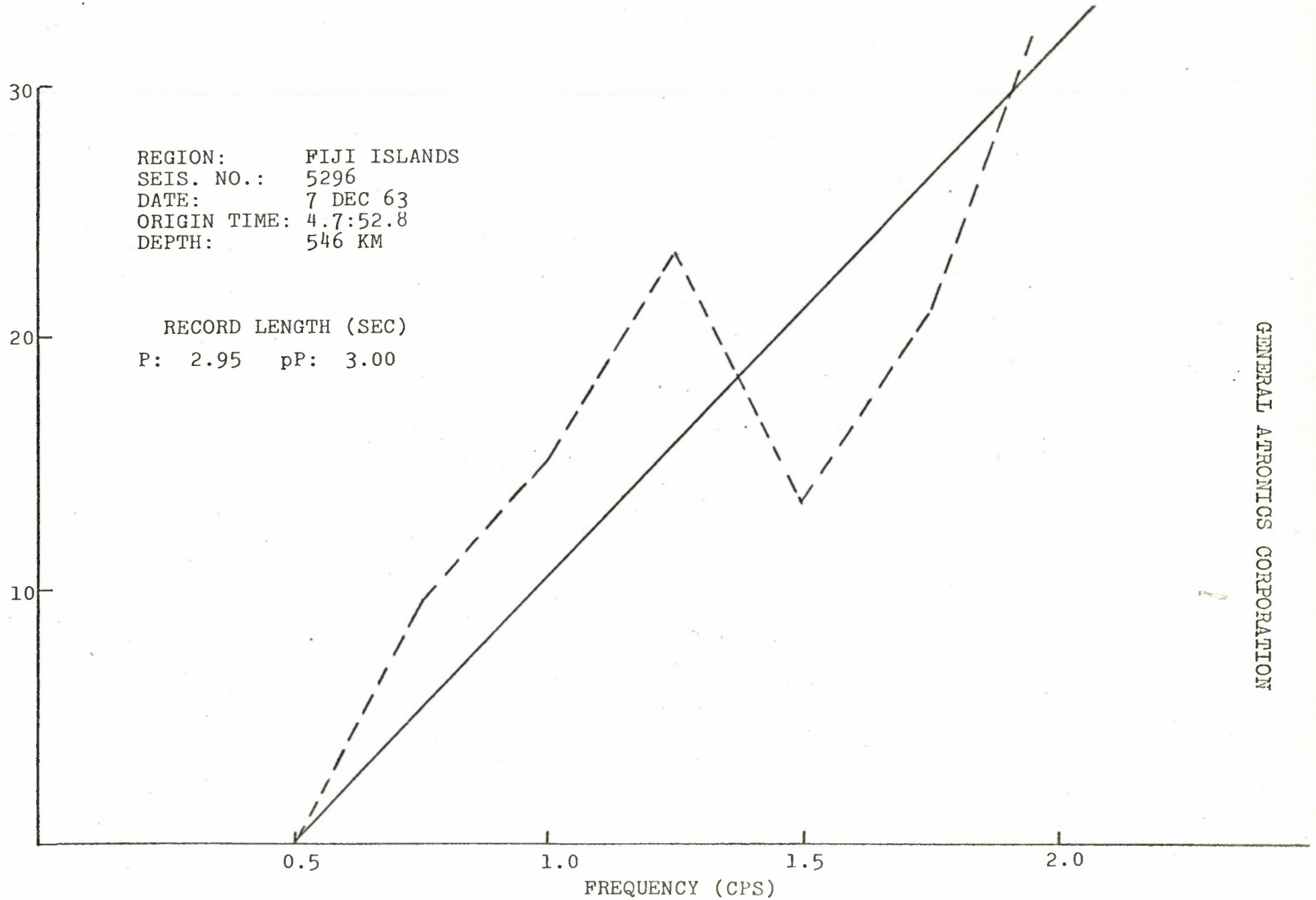

FIGURE 36 - ENERGY SPECTRA RATIO-- EXPERIMENTAL DATA AND LEAST SQUARES FIT

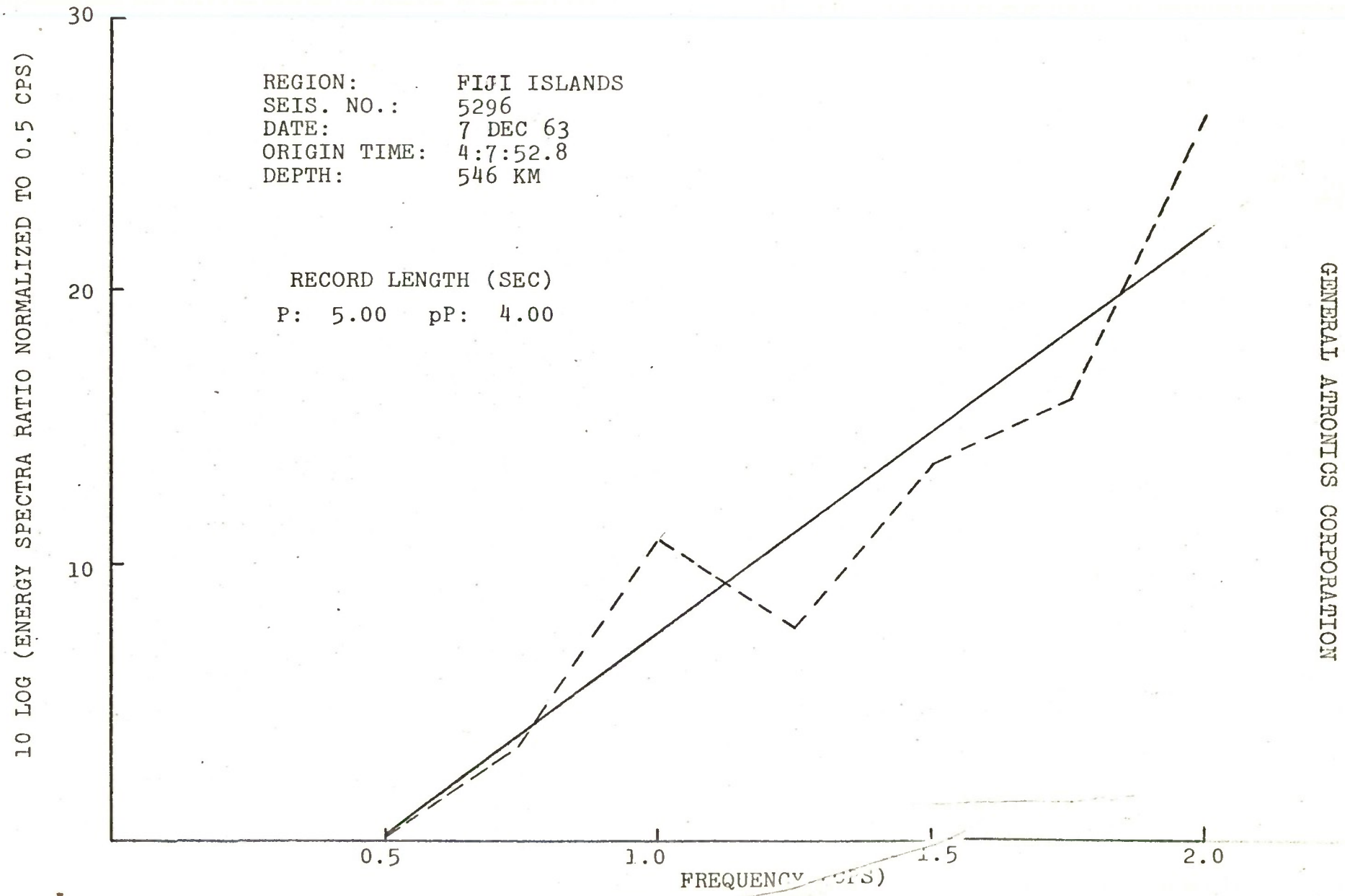

FIGURE 37 - ENERGY SPECTRA RATIO - EXPERIMENTAL DATA AND LEAST SQUARES FIT

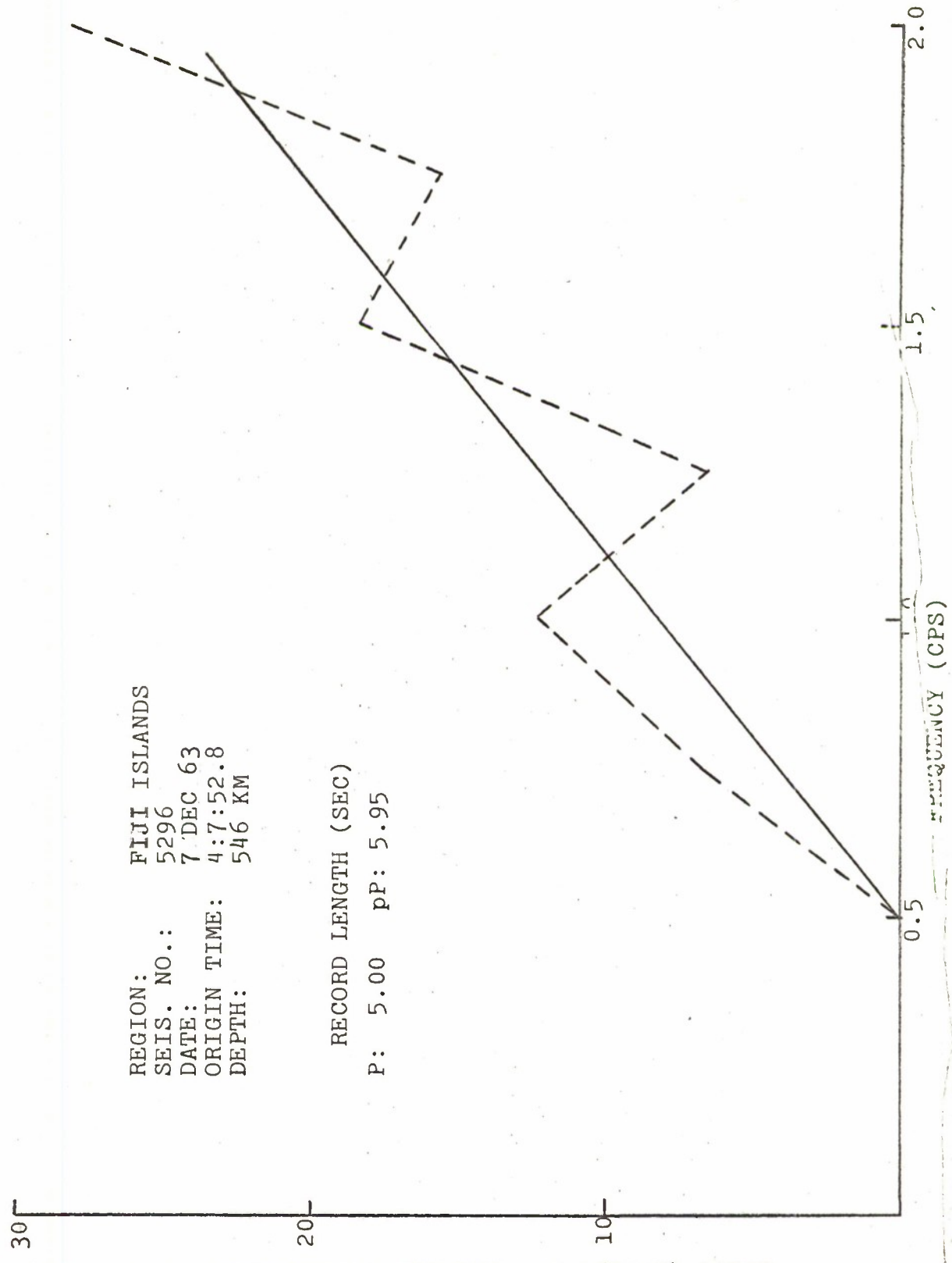

FIGURE 38 - ENERGY SPECTRA RATIO - EXPERIMENTAL DATA AND LEAST SQUARES FIT

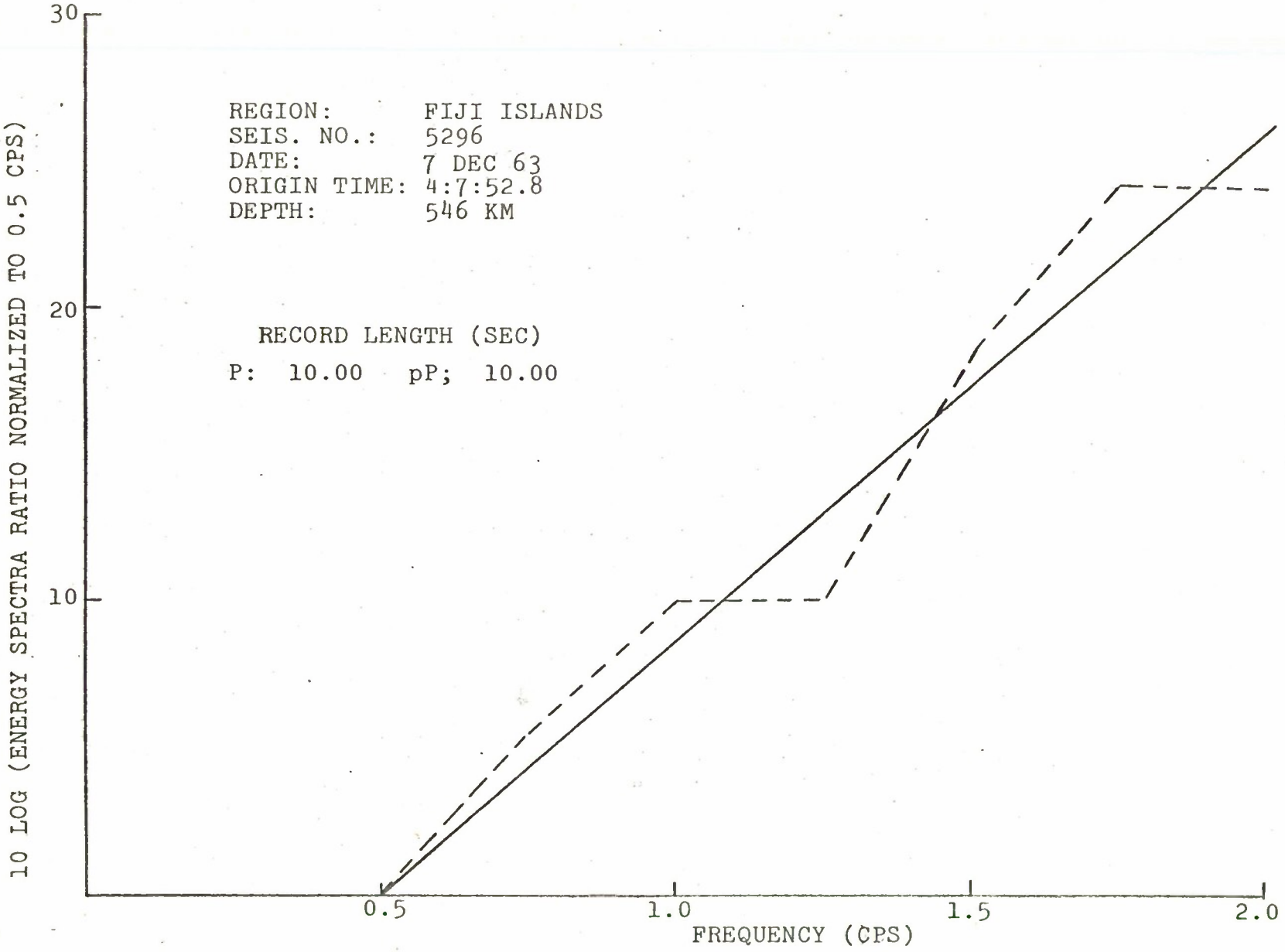

FIGURE 39 - ENERGY SPECTRA RATIO - EXPERIMENTAL DATA AND LEAST SQUARES FIT

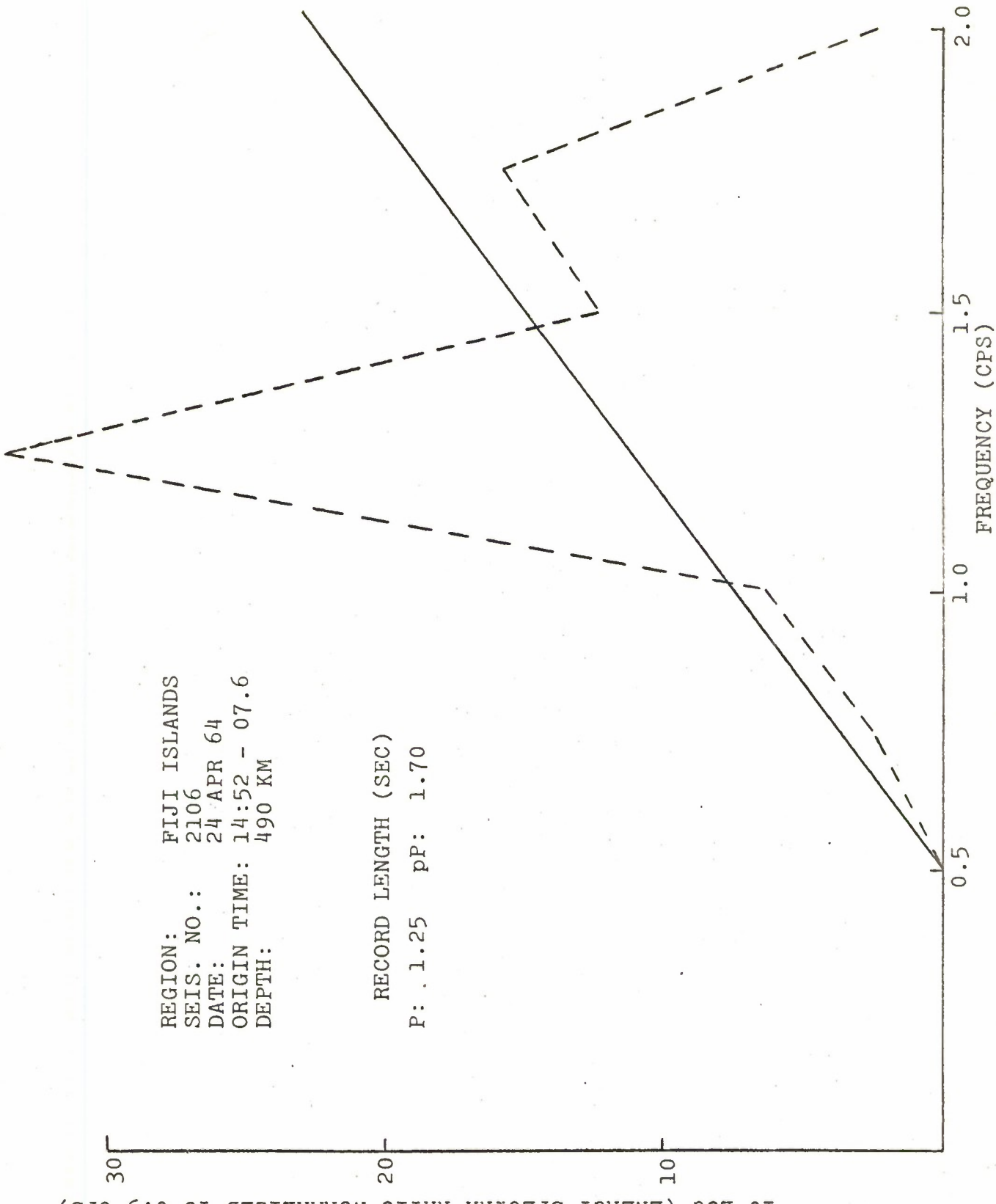

FIGURE 40 - ENERGY SPECTRA RATIO - EXPERIMENTAL DATA AND LEAST SQUARES FIT

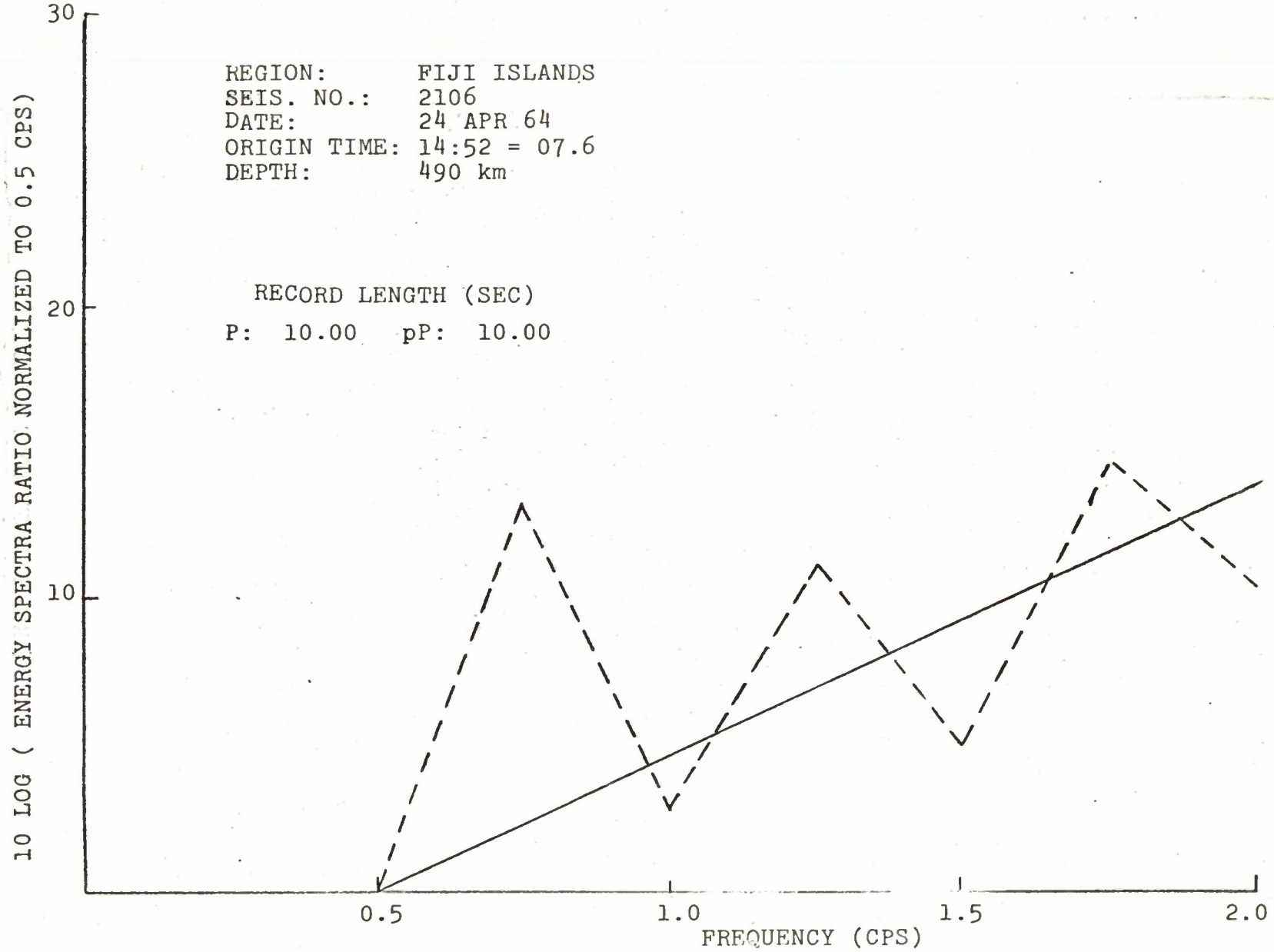

FIGURE 41 - ENERGY SPECTRA RATIO - EXPERIMENTAL DATA AND LEAST SQUARES FIT

REFERENCES

1. B.D. Steinberg. "Large Aperture Teleseismic Array Theory". First LASA Systems Evaluation Conference Proceedings. Chapter 15, p. 140, 14-16 September 1965
2. General Atronics Corporation. "Final Study Report on Systems Aspects of Seismic Detection and Identification of Nuclear Explosions". GAC Report 1456-2026-9, Contract SD-283, January 1966.
3. Jeffreys, H. and Bullen, K.E. Seismological Tables. Office of the British Association, London, 1958.
4. Toshi Asada, Kei Takano. "The Attenuation of Short Period P Waves in the Mantle". LAKEWOOD CONFERENCE PROCEEDINGS: The University of Michigan, April 1964. Page 41 ($Q \approx 2000$-4000).
5. V.C. Anderson, J. Acoust. Soc. Am. 32, 867-870 (1960).
6. Banta, Edwin D. "Far Field Properties of Wide Band Planar Arrays with Nonlinear Processing". IRE International Convention Record, 1961.
7. Remley, Winslow R. "Some Effects of Clipping in Array Processing". Marine Systems Department, Federal Systems Division, International Business Machines Corporation. March 1965.
8. "Seismic Detection and Classification Techniques". General Atronics Report 1400-2026-1, April 1965, pp. 35-37.
9. B.D. Steinberg. "Large Aperture Teleseismic Array Theory". Proc of First LASA System Evaluation Conference. ARPA, September 1965, p. 149.
10. "Systems Aspects of Seismic Detection and Identification of Nuclear Explosions". General Atronics Report 1456-2026-9, January 1966, p. IV-7.
11. A.M. Rubenstein, J. Aein, J.T. Beardwood. "High Frequency Content in Seismic Events". Proc of First LASA System Evaluation Conference. ARPA, September 1965, pp. 230-231.
12. Handbook of Tables for Probability and Statistics. Chemical Rubber Company, 1966, p. 299.

REFERENCES (Cont.)

13. Toshi Asada, Kei Takano,. loc. cit.
14. B.F. Howell, Jr. "Absorption of Seismic Waves". The University of Michigan, May 1963.